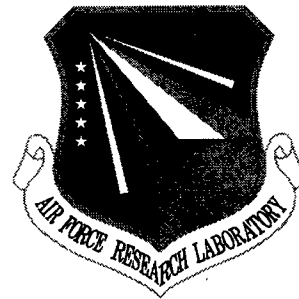AFRL-IF-RS-TR-1998-186
Final Technical Report
October 1998

SPATIAL ADAPTIVE PRE-SUPPRESSION OF WIDEBAND JAMMERS IN CONJUNCTION WITH STAP

Research Associates for Defense Conversion, Inc.

Sponsored by
Defense Advanced Research Projects Agency
DARPA Order No. C242

APPROVED FOR PUBLIC RELEASE; DISTRIBUTION UNLIMITED.

19981229 006

The views and conclusions contained in this document are those of the authors and should not be interpreted as necessarily representing the official policies, either expressed or implied, of the Defense Advanced Research Projects Agency or the U.S. Government.

AIR FORCE RESEARCH LABORATORY
INFORMATION DIRECTORATE
ROME RESEARCH SITE
ROME, NEW YORK

This report has been reviewed by the Air Force Research Laboratory, Information Directorate, Public Affairs Office (IFOIPA) and is releasable to the National Technical Information Service (NTIS). At NTIS it will be releasable to the general public, including foreign nations.

AFRL-IF-RS-TR-1998-186 has been reviewed and is approved for publication.

APPROVED:

DAVID D. FERRIS, JR.
Project Engineer

FOR THE DIRECTOR:

JOSEPH CAMERA, Deputy Chief
Information & Intelligence Exploitation Division
Information Directorate

If your address has changed or if you wish to be removed from the Air Force Research Laboratory Rome Research Site mailing list, or if the addressee is no longer employed by your organization, please notify AFRL/IFEA, 32 Brooks Road, Rome, NY 13441-4114. This will assist us in maintaining a current mailing list.

Do not return copies of this report unless contractual obligations or notices on a specific document require that it be returned.

SPATIAL ADAPTIVE PRE-SUPPRESSION OF WIDEBAND JAMMERS IN CONJUNCTION WITH STAP

P. Rivkin
Y. Zhang
H. Wang

REPORT DOCUMENTATION PAGE

Form Approved
OMB No. 0704-0188

1. AGENCY USE ONLY *(Leave blank)*	2. REPORT DATE	3. REPORT TYPE AND DATES COVERED	
	October 1998	Final	Dec 96 - Jun 97

4. TITLE AND SUBTITLE

SPATIAL ADAPTIVE PRE-SUPPRESSION OF WIDEBAND JAMMERS IN CONJUNCTION WITH STAP

6. AUTHOR(S)

P. Rivkin, Y. Zhang, and H. Wang

5. FUNDING NUMBERS

C   - F30602--95-C-0121
PE - 63226E
PR - MSEF
TA - 05
WU - 09

7. PERFORMING ORGANIZATION NAME(S) AND ADDRESS(ES)

Research Associates for Defense Conversion, Inc.
10002 Hillside Terrace
Marcy NY 13441-4514

8. PERFORMING ORGANIZATION REPORT NUMBER

N/A

9. SPONSORING/MONITORING AGENCY NAME(S) AND ADDRESS(ES)

Defense Advanced Research Projects Agency   AFRL/IFEA
3701 North Fairfax Drive   32 Brooks Road
Arlington VA 22203-1714   Rome NY 13441-4114

10. SPONSORING/MONITORING AGENCY REPORT NUMBER

AFRL-IF-RS-TR-1998-186

11. SUPPLEMENTARY NOTES

AFRL Project Engineer: David Ferris/IFEA/(315) 330-4408

12a. DISTRIBUTION AVAILABILITY STATEMENT

Approved for public release; distribution unlimited.

12b. DISTRIBUTION CODE

13. ABSTRACT *(Maximum 200 words)*

     This report extends the original work described by Klemm and Marshall, pertaining to the cascaded (or two-step nulling) pre-suppression of WNJ's (Wideband Noise Jammers) in STAP based radar system. Two aspects of the cascaded SPATIAL ADAPTIVE PRE-SUPPRESSION (SAP)/STAP approach are addressed.

     (1) System architecture and its impact on detection performance, and (2) ASP algorithm development and the acquisition of clutter-free jammer secondary data. Several cascaded architectures have been proposed as an implementation of the SAPS concept. The performance results for these cascaded favorably with the simultaneous of the WNJ pre-suppression concept is the acquisition of jammer-only secondary data. The sideband technique described has the unique advantage over other techniques in that it allows collection of secondary data during any portion of an RPI. Sideband compensation methods were proposed and analyzed showing that ample jammer suppression can be achieved in the mainband while using the sideband secondary data for weight calculation.

14. SUBJECT TERMS
SPATIAL ADAPTIVE PRE-SUPPRESSION
Adaptive Signal Processing
Secondary Data

15. NUMBER OF PAGES
104

16. PRICE CODE

17. SECURITY CLASSIFICATION OF REPORT	18. SECURITY CLASSIFICATION OF THIS PAGE	19. SECURITY CLASSIFICATION OF ABSTRACT	20. LIMITATION OF ABSTRACT
UNCLASSIFIED	UNCLASSIFIED	UNCLASSIFIED	UL

Table of Contents

List of Figures

List of Tables

1 Introduction

1.1 Objectives

In theory, a Space-Time Adaptive Processor (STAP) based radar system can be used to simultaneously suppress clutter and wideband noise jammers (WNJ). Simultaneous suppression typically involves the estimation of a joint space-time covariance matrix which can be quite large even for moderately sized radar systems required to handle a number of WNJ. Since the statistics of the interference sources generally must be estimated, this approach may be suboptimal in terms of both performance and cost. The size of the secondary data set required to adequately estimate the covariance matrix may be unattainable, particularly in a nonhomogenous interference environment. Additionally, since WNJ have temporally white spectrums, Doppler processing of WNJ is ineffective and causes an unnecessary inflation of the size of the space-time covariance matrix to be estimated. An approach to the problem of handling combined clutter and WNJ interference is to partition the adaptive processor so that clutter and WNJ can be handled separately. A promising approach already addressed in the literature, which provides the desired partition, makes use of the concept of jammer pre-suppression followed by a clutter rejection filter.

This report addresses the topic of Spatial Adaptive Pre-Suppression (SAPS) of WNJ in conjunction with STAP. Specifically, system architectures which cascade an Adaptive Spatial Pre-Processor (ASP) for WNJ suppression with STAP are investigated. The objective of this study is to evaluate these cascaded systems as alternatives to simultaneous suppression, for the case when the available secondary data set is limited, and to elucidate some of the key issues in determining the most suitable approach.

1.2 Overview

This report extends the original work described by Klemm in [2], and later on from a slightly different perspective by Marshall in [3], pertaining to the cascaded (or two-step nulling) pre-suppression of WNJ's in STAP based radar systems. Two aspects of the cascaded ASP / STAP approach are addressed: (1) system architecture and it's impact on detection performance, and (2) ASP algorithm development and the acquisition of clutter-free jammer secondary data.

The underlying theme behind the SAPS approach (i.e. reduction in the size of the statistical estimation problem) is also one motivation behind the partially adaptive techniques which have been under inves-

tigation since the 1970's in the case of *partially adaptive arrays* and since the late 1980's in the case of *partially adaptive STAP*. The benefits of degree-of-freedom (DOF) reduction in terms of detection performance and/or system affordability can be substantial. As a result, the cascade architectures proposed herein are a combination of partially adaptive array techniques and a high performance partially adaptive STAP approach. The idea of separating the WNJ and clutter suppression problems provides a new perspective in the general area of partially adaptive processing. By taking advantage of the inherent differences between the WNJ and clutter interference, a large covariance estimation problem is reduced to two much smaller ones. In Section 2, three cascaded architectures and a baseline ASP algorithm are proposed and compared with two simultaneous STAP approaches. Throughout this report, computer generated analytical results are used as a means for performance evaluation and comparison. Therefore, part of Section 2 is devoted to a description of the computer models used as well as the performance metrics. Section 2 results are generated assuming the availability of a sufficient number of jammer-only secondary data samples to accurately estimate the jammer covariance matrix. The problem of obtaining these secondaries is the subject of Section 3.

A key issue in applying the SAPS concept is the acquisition of the necessary jammer-only statistics for adaptive suppression, free from strong clutter contamination. Common acquisition methods include the use of clutter-free range gates for low pulse-repetition-frequency (PRF) systems, clutter-free Doppler bins for high PRF systems, or receive-only mode between two coherent processing intervals (CPI). All of these techniques require jammer data to be collected within a restricted region of the available space-time domain, and may not always be able to generate sufficient jammer-only data. Moreover, fast-changing jamming environments and large-scale PRF hopping can also make these techniques unsuitable. In Section 3, a new technique is presented which makes use of a carrier frequency sideband, close to but disjoint from the radar's mainband, to estimate the jammer-only covariance matrix. Such an idea can be applied to a system with any PRF, and the entire or any appropriate portion of the Range Processing Interval (RPI) could be used to collect jammer data. It should be noted that wideband jammers are designed to sufficiently cover the radar's mainband, making a sideband containing their energy always available. Since the ASP weights for jammer suppression are derived from data with a carrier frequency different from the radar signal, an important part of the successful implementation of the sideband approach involves the design of sideband compensation algorithms. These and other algorithms are investigated in Section 3.

2

2 Cascaded Space and Space-Time Adaptive Processing

The intent of the Cascaded Space and Space-Time Adaptive Processor (CS_STAP) is to separate the WNJ suppression function from the clutter suppression function, thereby replacing a large space-time covariance matrix estimation problem with the estimation of two smaller covariance matrices. Some of the potential benefits of this approach, relative to a system employing STAP to simultaneously reject jammers and clutter, are (1) improved detection performance in an environment of WNJ's and nonhomogenous clutter, (2) reduced susceptibility to false detections by discretes in the same range cell, and (3) a more cost-efficient/practical system architecture.

2.1 Fundamental System Models

In the following, a system model is established which is commonly used for airborne surveillance pulsed-Doppler radars. For a well organized description of a pulsed-Doppler radar system model see for example [9]. An abbreviated development of the models pertinent to this study are given in Section 2.1.1 thru Section 2.1.6. The data models of interest here will be complex sampled data vector descriptions of the received radar signals along with their 1st and 2nd order statistics. This will be sufficient to establish the key performance metrics (e.g. probability of detection, P_d, at a specified probability of false alarm, P_f) for the case when the data is Gaussian distributed.

2.1.1 Radar System

The radar system considered here employs a phased-array antenna which provides N_c column sensor outputs whose phase centers correspond to a uniformly spaced line array along the y-axis. The coordinate system used is depicted in Figure 2-1. A unit vector, r, pointing in the (ϕ,θ) direction is given by

$$r = \cos\phi\cos\theta \cdot x + \sin\phi\cos\theta \cdot y + \sin\theta \cdot z \qquad (2\text{-}1)$$

where x, y, and z are unit vectors. Vectors corresponding to physical quantities (i.e. direction, velocity, etc.) will be distinguished from data vectors by using italics. The array is situated so that the first element resides at the origin of the x-y plane and along the z-axis at the platform altitude. The first element serves as the phase reference for the entire array. The x-y plane is tangent to the earth's surface directly below the array.
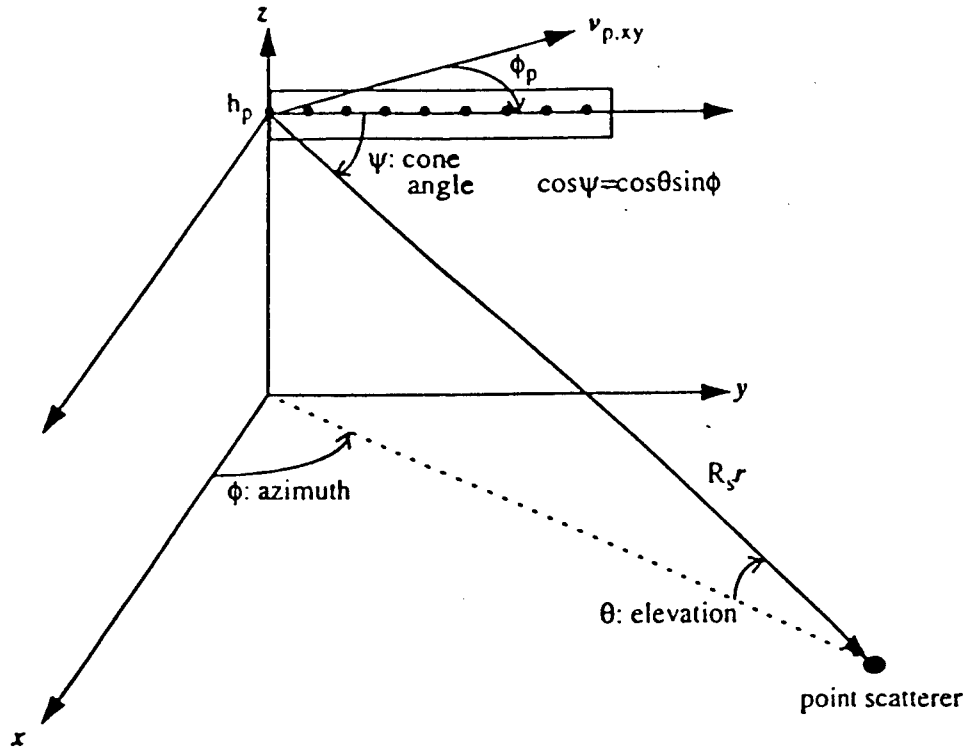
Figure 2-1: Radar Platform Geometry

The nth sensor position is described by it's position vector, d_n, relative to the first sensor. For the case considered here in Figure 2-1 we have

$$d(n_s) = n_s \cdot d \cdot y .$$

(2-2)

The angle directions are defined as follows: (1) positive azimuth, ϕ, is a counter-clockwise rotation from the x-axis to the y-axis, (2) positive elevation, θ, is from the horizontal xy-plane down towards the negative z-axis, and (3) positive platform velocity azimuth misalignment angle, ϕ_p, is a clockwise rotation from the y-axis to the x-axis. The platform velocity azimuth misalignment angle, ϕ_p, is the angle from the y-axis to the projection of the platform velocity vector onto the xy-plane. The *numerical results* generated in this report will always have the platform velocity vector residing in the xy-plane as indicated in Figure 2-1, so that only ϕ_p is necessary to define the velocity direction. Although the results presented are for horizontal platform motion, the formulas involving the platform velocity, v_p, are for a general vector. The line array is

4

of great practical interest in radar engineering and will be sufficient in this investigation to establish the desired results. The reader interested in a detailed treatment of an array with arbitrary sensor positions is referred to [10].

A top-level block diagram of the radar system considered is given in Figure 2-2. For convenience,
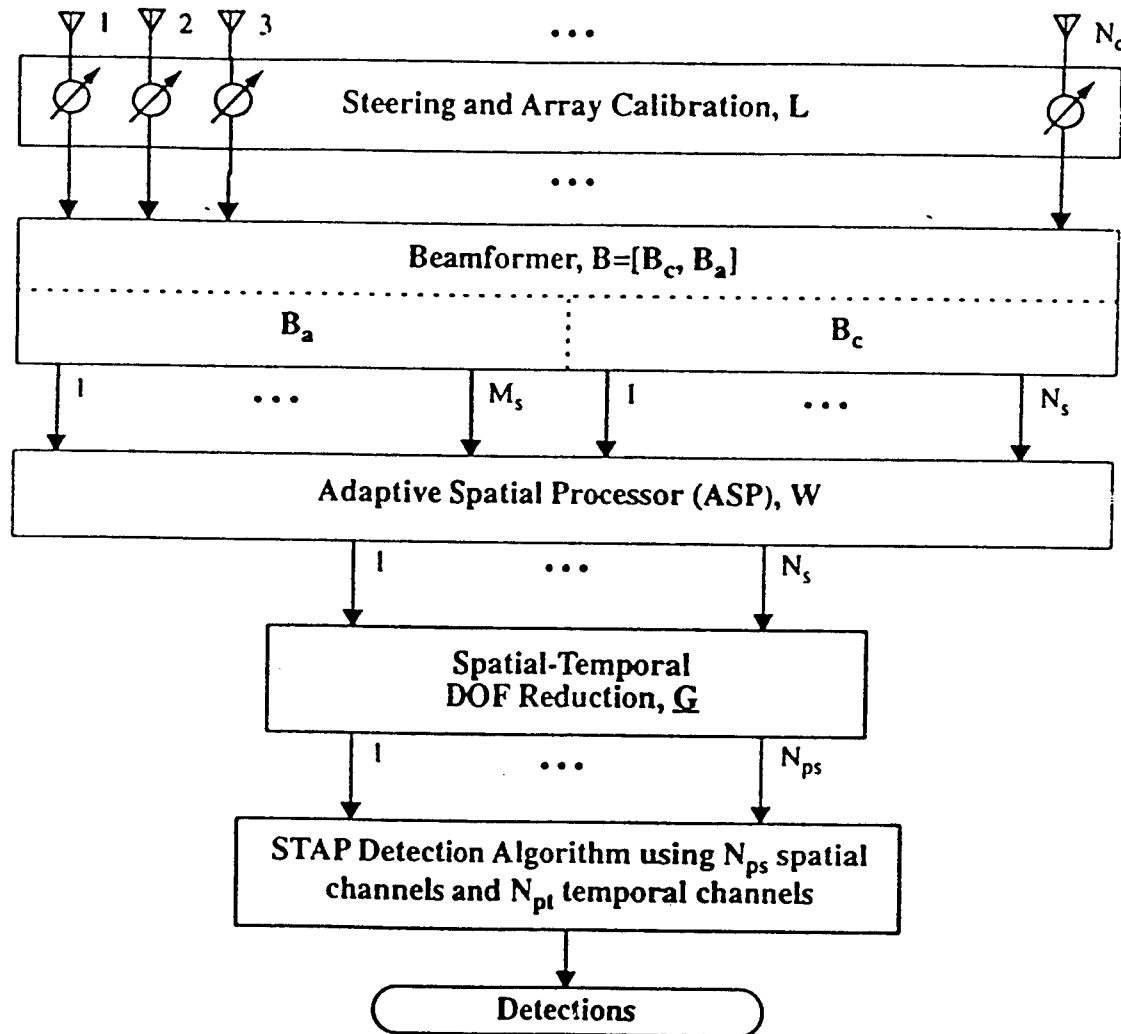
Figure 2-2: Radar Signal Processor Top-Level Block Diagram

the receiver (i.e. down-conversion to baseband, waveform matched filter, and sampling and digitization via A/D conversion) portion of the radar system is imbedded in the Adaptive Spatial Processor (ASP) block. Different spatial processing architectures can have different receiver schemes in order to minimize system cost and control channel errors. Therefore, the receiver structure for each will be described separately as needed. Narrowband signals are considered in this paper, unless stated otherwise, and therefore the analog

signals prior to matched filtering will also be treated as narrowband. In addition, unless stated otherwise, the analog components will be assumed to have a uniform response over the system bandwidth. The pertinent Radar system parameters are defined in Table 2-2.

In general, the sampled data obtained from the column sensors will be represented as $N_c \times 1$ spatial snapshot vectors, x. When space-time processing is intended, the spatial snapshots, sampled from PRI-to-PRI, are stacked into $(N_c \cdot N_t) \times 1$ space-time snapshots, $\underline{x}$. A space-time vector is created by stacking (or rasterizing) spatial snapshot vectors, separated in time by integer multiples of a PRI. Double-domain matrices (i.e. rasterized vector and it's corresponding covariance matrix corresponding to two different processing domains) will be distinguished from single-domain matrices by using an underline. During a single PRI, different spatial snapshots correspond to different ranges and therefore will be referred to as range-domain spatial snapshots (or space-range vectors when stacked) in contrast with the temporal-domain snapshots (or space-time vectors). This study will be primarily concerned with space and space-time vectors.

The task of the signal processor is to ascertain if a target with a prespecified angle-of-arrival (AOA) and Doppler frequency is present in the data collected over a CPI for each range bin. Thus a binary hypothesis test is performed by the STAP algorithm block which then produces detection reports. Under the target-absent hypothesis, H_0, the data contains receiver noise and interference consisting of clutter and wideband noise jammers;

$$H_0 : \underline{x} = \underline{c} + \underline{j} + \underline{n} .$$
(2-3)

Under the target-present hypothesis, H_1, the data also contains the desired target;

$$H_1 : \underline{x} = \alpha \underline{s} + \underline{c} + \underline{j} + \underline{n}$$
(2-4)

where α is the target's unknown complex amplitude. The specific form of these data vectors for the various source types used in the numerical analysis/simulation results is the subject of Section 2.1.2 thru Section 2.1.6. A major goal of these sections is to establish 1st and 2nd order statistical models for each source type. The covariance matrix of the total space-time interference (i.e. clutter-plus-jammers-plus-noise) will be

6

denoted by $\underline{R}$.

2.1.2 Target Model

The development of the target model closely parallels that given in [9] and therefore, only a brief synopsis is given here. The received target signal is defined as the transmission echo from a moving point scatterer which is to be detected. It is characterized by it's range, angle, and velocity relative to the radar, and the normalized amplitude (i.e. relative to the 'rms' sensor noise) of the echo received at a sensor column output. The pre-envelope of the transmitted uniform train of coherent pulses corresponding to a coherent processing interval (CPI) is

$$\tilde{s} = a_t u(t) e^{i(2\pi f_0 + \varphi)} \text{ , where } u(t) = \sum_{n_t = 0}^{N_t - 1} u_p(t - n_t T_r) \quad . \tag{2-5}$$

The amplitude of a single pulse waveform, u_p, is normalized to unit energy. Thus the energy transmitted in a single pulse is $E_p = a_t^2$. The pre-envelope of the target echo received by the nth sensor is written as

$$\tilde{s}(n_s) = a_r u(t + \tau_s - \tau_r) e^{i2\pi (f_0 + f_d)(t + \tau_s - \tau_r)} e^{i\varphi} \text{ , where } f_d \equiv \frac{2v_t}{\lambda_0} \tag{2-6}$$

with received target amplitude and Doppler a_r and f_d respectively (v_t is the radial velocity of the target relative to the platform). The delay to the n_s^{th} sensor is composed of the round trip delay, τ_r, to the first sensor (i.e. the array reference) and the relative delay from the first sensor to the n_s^{th} sensor, τ_s, which are given by

$$\tau_r \equiv \frac{2R_t}{c} \quad \text{ and }$$

$$\tau_s(n_s) \equiv \frac{r(\phi_t, \theta_t) \cdot d(n_s)}{c} = n_s \cdot \frac{d}{c} \sin\phi \cos\theta \tag{2-7}$$

Since the transmitted signal is assumed narrowband, the relative sensor delay is presumed insignificant in

7

the complex envelope term of Equation 2-6. This is tantamount to making the following approximation,

$$u(t + \tau_s - \tau_r)e^{i2\pi f_d(t + \tau_s - \tau_r)} \approx u(t - \tau_r)e^{i2\pi f_d(t - \tau_r)}$$ (2-8)

which ignores the variation of the received pulse from sensor to sensor. The received signal pre-envelope for the n_s^{th} sensor then becomes

$$\bar{s}(n_s) = a_r e^{i\varphi} u(t - \tau_r)e^{i2\pi f_d(t - \tau_r)} e^{i2\pi f_0(t + \tau_s)}$$ (2-9)

where a constant phase term has been absorbed into the random phase, φ. It will be convenient to use the following definitions for 'normalized spatial frequency', f_s, and 'normalized Doppler frequency', f_t:

$$f_s \equiv \frac{f_0 \tau_s}{n_s} = \frac{d}{\lambda_0}\sin\phi\cos\theta \quad \text{and} \quad f_t \equiv \frac{2v_t T_r}{\lambda_0} = f_d T_r \quad .$$ (2-10)

After the signal has been processed by the receiver (i.e. down-conversion, matched filtering, and A/D conversion) the data can be represented in complex envelope form. Consider only those samples corresponding to the target range gate at times $t=\tau_r+n_t \cdot T_r$, where $n_t=0,...,N_t-1$. Then the complex target samples are given by

$$s(n_s, n_t) = \alpha(\phi, \theta, R_t, n_s, n_t)e^{i2\pi f_s n_s} e^{i2\pi f_t n_t} ; n_s = 0, ...; N_c - 1 \text{ and } n_t = 0, ..., N_t - 1$$ (2-11)

where the echo amplitude and unknown phase have been combined into the complex amplitude, α, and the following simplifying assumptions have been made; (1) the transmit waveform is insensitive to Doppler shift such that it's ambiguity function at zero delay is unity for all Doppler frequencies of interest, and (2) no target range ambiguities exist. A relation between the Radar system parameters and the signal-to-noise ratio (SNR) can be developed (e.g. see [9]), but in this paper SNR will be specified directly instead. It is

8

formally defined as

$$SNR \equiv \frac{E\{|\alpha|^2\}}{\sigma_n^2} = \frac{P_t T_p G_t(\phi, \theta)|g(\phi, \theta)|^2 \lambda_0^2 \sigma_{ot}}{(4\pi)^3 N_0 L_s R_t^4}$$

(2-12)

where σ_n^2 is the system noise power from one sensor channel. The second relation involving the Radar system parameters, defined in Table 2-2 which assumes identical sensors and a target cross-section which is fixed over a CPI, is included for reference. Next, it will be useful to define generic spatial and temporal steering vectors as

$$s_s(f_s) \equiv [1, e^{i2\pi f_s}, ..., e^{i2\pi f_s(N_c - 1)}]^T \text{ and }$$
$$s_t(f_t) \equiv [1, e^{i2\pi f_t}, ..., e^{i2\pi f_t(N_t - 1)}]^T$$

(2-13)

Note that for a given set of Radar parameters, the complex amplitude of Equation 2-11 is, in general, a function of azimuth, elevation and range. The case considered in this paper assumes each sensor has an identical radiation pattern so that for each sensor the complex amplitude is the same and, in addition, the amplitude is constant over a CPI. This allows the target data samples to be written as the product of a space-time vector, s, and a complex amplitude, α, using the steering vectors of Equation 2-13 as follows:

$$\left[s(n_s, n_t)\right] = \alpha(\phi, \theta, R)(s_{ts} \otimes s_{ss}) \equiv \alpha s(f_{ts}, f_{ss})$$

(2-14)

where '$\otimes$' is the matrix Kronecker product, s_{ss} represents a spatial steering vector with spatial frequency, f_{ss}, corresponding to the target's angular position, and s_{ts} is the temporal steering with normalized target Doppler, f_{ts}.

2.1.3 Receiver Noise

The predominant system noise component in a channel is assumed to be internally generated with

a level established by the sensor front-end RF components. The noise in each channel is assumed to be mutually uncorrelated, identically distributed, and be modeled as a zero-mean Gaussian random process. For the case of the space-time data vector (i.e. data collected for a particular range cell), the system bandwidth is presumed sufficiently larger than the PRF such that temporal samples are also uncorrelated. Under these conditions the correlation matrix of the system noise is given by

$$\underline{R}_n \equiv E\{\underline{n}\underline{n}^H\} = \sigma_n^2(I_{N_t} \otimes I_{N_s}) \quad . \tag{2-15}$$

For convenience, the channel noise power will be normalized to unity without loss of generality, since the results in this paper are characterized in terms of noise ratios (e.g. SNR, CNR, JNR, etc.). If desired, the noise power can be linked to the Radar system parameters by $\sigma_n^2=N_oB$. As previously noted, the system noise level is established in the sensor front-end, thus any subsequent linear operations on the data (e.g. beamforming, filtering, etc.) will not produce any significant change in the noise ratios (i.e. SNR, CNR, and JNR) specified at the sensor outputs.

2.1.4 Clutter Modeling

The main focus of this paper is the study of techniques to effectively handle jammers in a typical WAS radar interference environment. The intent of clutter modeling is to provide a representative clutter component so that the effects of jammer processing on STAP based clutter suppression can be assessed. For an airborne surveillance radar the predominant clutter return is from the earth and this will be the only clutter component used for numerical analysis (i.e. simulation results) in this paper. A thorough treatment of clutter modeling typically used in airborne radar is provided in [9]. Here, the primary aspects of the clutter model are reviewed. The radar/earth geometry is treated using the '4/3 effective radius spherical earth' model. Clutter from a specific range cell is represented as the sum of individual scatters all at the same range and uniformly spaced in azimuth. The total clutter component in a range gate is the sum of contributions from the unambiguous range cell and any ambiguous range cells. The signal model for the radar echo from a clutter patch is treated in a fashion similar to Section 2.1.2 for a target. The clutter amplitudes on each sensor from a single pulse are identical due to the assumption of identical sensor patterns and the nar-

rowband signal approximation. However, pulse-to-pulse fluctuations due to various system and environmental factors, typically referred to as intrinsic clutter motion (ICM), will be modeled as a wide-sense stationary random process with a Gaussian power spectrum. Using the spatial and temporal steering vectors from Equation 2-13, the composite space-time clutter vector can be written as

$$
\underline{c} = \sum_{l=1}^{N_r} \sum_{k=1}^{N_{ac}} [a_{lk} \bullet s_t(f_{tc})] \otimes s_s(f_{sc}) \qquad \text{where}
$$

$$
f_{sc} \equiv \frac{r(\phi_k, \theta_l) \cdot d}{\lambda_0} \qquad \text{and} \qquad f_{tc} \equiv \frac{2T_r r(\phi_k, \theta_l) \cdot v_p}{\lambda_0} \tag{2-16}
$$

with the spatial and temporal frequencies of the $(l,k)^{th}$ clutter patch given by f_{sc} and f_{tc}. The large product symbol, '$\bullet$' represents a Hadamard matrix product (i.e. element by element). The index 'l' enumerates the ambiguous range bins up to N_r and 'k' enumerates the azimuth patches up to N_{ac}. The vector of complex amplitudes, a_{lk}, represent the returns for each pulse in a CPI for the $(lk)^{th}$ clutter patch. The clutter patch amplitudes are modeled as wide-sense stationary zero-mean random variables which are uncorrelated from patch-to-patch and whose variance depends on various Radar system parameters (similar to a target as shown in Equation 2-12 as well as the clutter patch position and reflectivity, $\sigma_{oc}(\phi,\theta)$. For the simulations in this paper a reflectivity model proposed by Barton in [11] for various types of land clutter is used. The correlation matrix for the clutter space-time data vector can be written as

$$
\underline{R}_c \equiv E\{\underline{c}\underline{c}^H\} = \sum_{l=1}^{N_r} \sum_{k=1}^{N_{ac}} \left[E\{a_{lk}a_{lk}^H\} \bullet s_{tc}s_{tc}^H \right] \otimes s_{sc}s_{sc}^H \quad . \tag{2-17}
$$

As indicated previously, the temporal fluctuations of the clutter patch returns are modeled as having a Gaussian shaped power spectrum. Hence, the temporal autocorrelation function for a clutter patch is given by

$$r_c(n_t) = \exp\left[-2\left(\pi\sigma_{icm}n_t\right)^2\right] \tag{2-18}$$

where the clutter spectral spread parameter, σ_{icm}, is assumed to be the same for all clutter patches. The ICM standard deviation, σ_{icm}, is the rms clutter spectral spread normalized by the system PRF. The clutter patch temporal correlation matrix becomes

$$E\{a_{lk}a_{lk}^H\} = \sigma_{c,lk}^2 A_c \text{ where } A_c \equiv \text{Toeplitz}\left(\left[r_c(0), r_c(1), \ldots, r_c(N_t-1)\right]\right) \tag{2-19}$$

and $\sigma_{c,lk}^2$ is the power in the $(lk)^{th}$ clutter patch. The function Toeplitz() represents a Hermitian Toeplitz matrix whose first row is given in the parentheses.

The final step in the clutter modeling is to characterize the clutter power level. As previously noted, the clutter power level will be specified in terms of CNR. Define the average total clutter power per pulse per sensor[1], σ_c^2, and the CNR as

$$\sigma_c^2 \equiv \frac{\text{tr}[\underline{R}_c]}{N_s N_t} = \sum_{l=1}^{N_r} \sum_{k=1}^{N_{ac}} \sigma_{c,lk}^2 \text{ and CNR} \equiv \frac{\sigma_c^2}{\sigma_n^2} , \tag{2-20}$$

where tr[] denotes matrix trace. Using this definition of clutter power and a relationship given in [9] for the CNR of an individual clutter patch, the space-time correlation matrix can be written in a way which elucidates the dependence of the correlation structure on the antenna transmit pattern, the receive sensor patterns, and the ground reflectivity,

---

1. Since an ideal uniform linear array has been used along with an uncorrelated identically distributed clutter patch model, the correlation matrix is doubly block Toeplitz and an average is not needed, however to include the cases where the Toeplitz structure is not preserved this definition will be used.

12

$$\underline{R}_c = \sum_{l=1}^{N_r} \sum_{k=1}^{N_{ac}} \frac{\sigma_{c,lk}^2}{\sigma_c^2} [A_c \bullet s_{tc}s_{tc}^H] \otimes s_{sc}s_{sc}^H \quad \text{where}$$

$$\frac{\sigma_{c,lk}^2}{\sigma_c^2} = \frac{(G_t(\phi_k, \theta_l) |g(\phi_k, \theta_l)|^2 \sigma_{oc}(\phi_k, \theta_l) \sec \psi_l) / R_l^3}{\sum\limits_{a=1}^{N_r} \sum\limits_{e=1}^{N_{ac}} (G_t(\phi_a, \theta_e) |g(\phi_a, \theta_e)|^2 \sigma_{oc}(\phi_a, \theta_e) \sec \psi_e) / R_e^3} \qquad (2\text{-}21)$$

2.1.5 Wideband Noise Jammer (WNJ) Modeling

In this section, continuous wideband independent noise jammers are considered. By definition, the jammer spectrum is flat and encompasses the entire receiver bandwidth. In the literature (e.g. [9]), jammer space-time models for narrowband systems often assume that the data samples are uncorrelated pulse-to-pulse but perfectly correlated sensor-to-sensor (i.e. across the array). In this paper, jammer sample correlation will be modeled based on a Gaussian shaped receiver spectral characteristic. This will lead to a Gaussian shaped autocorrelation function similar to the clutter ICM model. The autocorrelation function, assuming wide-sense stationarity, is a function of the delay between samples, τ, and normalizing to unit power is given by

$$r_j(\tau) \equiv \exp\left[-4\pi (B \cdot \tau)^2\right], \qquad (2\text{-}22)$$

where the bandwidth, B, used here is the equivalent noise bandwidth. The pulse-to-pulse correlation for typical PRF and receiver bandwidth combinations (i.e. $B\tau$ products) will be negligible, and therefore, for space-time data vectors the jammers will be treated as temporally uncorrelated. In contrast, the spatial decorrelation in samples taken across the array will be large enough to cause a reduction in jammer cancellation and, hence, Equation 2-22 will be employed in the construction of the jammer spatial covariance matrix.

Begin by considering the combined spatial snapshot, j, for N_j jammers with coordinates (ϕ_k, θ_k, R_k) written as

13

$$j = \sum_{k=1}^{N_j} j_k \,, \text{ where } j_k \equiv a_{jk} \cdot s_{sjk} \quad , \tag{2-23}$$

a_{jk} is the vector of random amplitudes received across the array of sensors for the kth jammer, and s_{sjk} is the spatial steering vector for the kth jammer. For the case where the sensors are identical (i.e. the case studied here), the elements of the kth jammer amplitude vector, a_{jk}, are time delayed, filtered, and sampled versions of the kth jammer complex envelope waveform where the time delays are the sensor delays defined in Equation 2-7. Next, assuming that jammer sources are independent, the jammer spatial correlation matrix can be written as

$$\begin{aligned}
R_j &\equiv E\{jj^H\} = E\left\{ \sum_{k=1}^{N_j} [a_{jk} \cdot s_{sjk}][a_{jk} \cdot s_{sjk}]^H \right\} \\
&= \sum_{k=1}^{N_j} E\{a_{jk} a_{jk}^H\} \cdot s_{sjk} s_{sjk}^H = \sum_{k=1}^{N_j} \sigma_{jk}^2 A_{jk} \cdot s_{sjk} s_{sjk}^H
\end{aligned} \tag{2-24}$$

where the jammer spatial decorrelation is accounted for by the matrix

$$A_{jk} \equiv \text{Toeplitz}\{ \{r_j(\tau_{sk}(0)), r_j(\tau_{sk}(1)), ..., r_j(\tau_{sk}(N_t - 1))\} \} \quad , \tag{2-25}$$

σ_{jk}^2 is the power received from the kth jammer, and τ_{sk} is the sensor-to-sensor delay given by Equation 2-7 for the kth jammer. The power level for each jammer is specified independently in terms of jammer-to-noise ratio (JNR) per sensor per sample as

$$JNR_k \equiv \frac{\sigma_{jk}^2}{\sigma_n^2} = J_k |g(\phi_k, \theta_k)|^2 \quad . \tag{2-26}$$

14

The dependence of the JNR on sensor patterns has been included to illustrate how they affect the structure of the jammer correlation matrix. The constant 'J$_k$' depends on jammer power density impinging on the array and several fixed Radar system parameters, but will not be important in this study. Since the jammer samples are temporally uncorrelated, it is easy to see that the combined space-time correlation matrix for the N$_j$ jammers is given by

$$\underline{R}_j = I_{N_t} \otimes R_j = I_{N_t} \otimes \left[\sigma_n^2 \sum_{k=1}^{N_j} JNR_k A_{jk} \bullet s_{sjk} s_{sjk}^H \right] \quad . \tag{2-27}$$

2.1.6 Analog Beamformer Transformations

The analog beamformer transformation is an important aspect of the cascaded processor of Figure 2-2 and will have a significant impact on the Adaptive Space Processor. It represents a fixed spatial transformation from element (or sensor channel) space to a subspace with equal or lower dimension which will be referred to as beamspace, regardless of whether the transformation develops spatial 'beams' in the normal sense or not. In practice the beamformer acts on the analog RF or IF signals, however, in this paper only the effect on the digitized baseband signals are of concern. Unless otherwise stated, the beamformer will be assumed to be adequately represented by a full-rank matrix operation on the baseband data vectors as indicated in Figure 2-3. This implies that the beamformer's spectral response over the receiver band-

$$y = B^H x$$
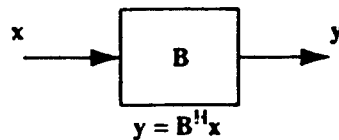
Figure 2-3: Analog Beamformer Transformation

width is a constant. For the narrowband (i.e. ≤1% of the carrier) systems under consideration this is a reasonable assumption. If any beamformers are frequency dependent they will be handled in a manner consistent with the situation at hand. Any non-full-rank beamformers would be wasteful from a system cost perspective and therefore will not be studied.

A specific type of analog beamformer will now be discussed, namely the Butler Matrix, since it will be fundamental to the discussion of the baseline system architectures as well as other architectures. The Butler matrix is essentially an analog implementation of a DFT. It is a well known method for generating a set of orthogonal beams from a uniform line array with uniform response over a reasonably wide bandwidth (see e.g. [13]). Consequently, the mathematical description of the Butler beamformer operating on baseband data is a DFT matrix.

2.2 Performance Criteria and Analysis Tools

2.2.1 Detection Performance

In this study, detection of a space-time target of known structure in additive interference is treated as a binary statistical hypothesis testing problem. The STAP detection algorithm block of Figure 2-2 utilizes a Neyman-Pearson approach (see e.g. [12]) where detection probability, P_d, is maximized for a specified probability of false alarm, P_f. The binary hypothesis test under consideration is expressed by Equation 2-3 and Equation 2-4. The target's complex amplitude will be treated as a zero-mean complex Gaussian random variable whose variance is determined by the specified SNR and whose value is fixed during a CPI but varies CPI-to-CPI. This amplitude model is similar to the well known Swerling Type I target model. Another model commonly used in the literature (see e.g. [7], [14], or [15]) treats the target amplitude as an unknown complex constant with a magnitude commensurate with the specified SNR. However, the choice of target model will not significantly affect the results of this investigation. Although the conclusions are based on comparisons of different system architectures and ASP's, the same detection algorithm is used in each system and the impact of target model on detection performance should have an approximately equal affect for each system studied. The random amplitude model is used here because it not only exhibits a more tractable theoretical detection characteristic, which will assist in further developments, but also is a reasonable way to account for amplitude fluctuations experienced by a surveillance radar which dwells on a target once per scan.

2.2.1.1 Optimal Detection

The optimal Neyman-Pearson detection statistic is given by the likelihood ratio (see e.g. [12]). It is straightforward to show that the optimal detector for the binary hypothesis test of Section 2.2.1 is the col-

ored-noise matched filter given by (see Appendix A)

$$\underline{w}_o = \frac{\underline{R}^{-1}\underline{s}}{\underline{s}^H\underline{R}^{-1}\underline{s}} ,$$ (2-28)

which has been normalized for unity variance under the target absent hypothesis. Evidently, this filter turns out to be the same filter for the case when the target amplitude is a constant or has constant magnitude with uniformly distributed phase (Brennan and Reed [14]). The optimal decision rule is given by

$$\eta \equiv \left|\underline{w}_o^H \underline{x}\right|^2 \underset{HO}{\overset{H1}{\gtrless}} \eta_o ,$$ (2-29)

and the corresponding probability of detection and false-alarm for the optimal detector are readily determined as (Park [16])

$$P_f = \exp\left[-\eta_o\right] \text{ and}$$

$$P_d = \exp\left[\frac{-\eta_o\underline{s}^H\underline{R}^{-1}\underline{s}}{(\underline{w}_o^H[\underline{R}+\sigma_s^2\underline{s}\underline{s}^H]\underline{w}_o)}\right] = \exp\left[\frac{-\eta_o}{(1+\beta_o)}\right].$$ (2-30)

$$\text{where } \sigma_s^2 = E\{|\alpha|^2\} \text{ and } \beta_o \equiv \sigma_s^2\underline{s}^H\underline{R}^{-1}\underline{s}$$

The detection performance is seen to be a function of a parameter which will be referred to as the generalized signal-to-interference-plus-noise ratio for the optimal processor ($SINR_o$ or β_o). It represents an upper bound on the SINR obtainable for the sensor data being processed.

2.2.1.2 Generalized Likelihood Ratio Algorithm (GLR)

The STAP detection algorithm block of Figure 2-2 will utilize a GLR test for all the systems analyzed. Kelly [15] developed the maximum-likelihood GLR algorithm and it's analytical detection performance for the case of detecting a signal of known structure with unknown constant complex amplitude embedded in zero-mean Gaussian interference. Kelly assumed that a set of independent identically distrib-

uted (i.i.d.) data vectors (i.e. secondary data) was available having the same statistics as target-absent data under test (i.e. primary data without a target). For the radar problem, the secondary data is normally obtained from range cells in the vicinity of but different from the primary data. Wang and Cai [7] extended the results to the case where the data is first processed by a linear transformation (i.e the JDL-GLR). Park [16] adapted these results for the case of random complex-normal target amplitude which is the case of interest in this study. The results for a receiver using Kelly's maximum-likelihood GLR, with a general full-rank linear pre-transformation applied to the data, and employing a random target amplitude model, are summarized below.

The GLR decision rule for data which has been transformed by a full-rank linear transformation, $\underline{T}$, is

$$\eta_{glr} = \frac{\left| \underline{s}_T^H \hat{\underline{R}}_T^{-1} \underline{x}_T \right|^2}{\underline{s}_T^H \hat{\underline{R}}_T^{-1} \underline{s}_T \left(1 + \underline{x}_T^H \hat{\underline{R}}_T^{-1} \underline{x}_T \right)} \underset{H0}{\overset{H1}{\gtrless}} \eta_{oT} \tag{2-31}$$

where the transform domain data vectors are related to the sensor data by

$$\underline{x}_T = \underline{T}^H \underline{x} \text{ and } \underline{s}_T = \underline{T}^H \underline{s} . \tag{2-32}$$

The unnormalized estimate of the covariance matrix is the sum of "K" outer-products of i.i.d. secondary data, $\underline{y}_T$.

$$\hat{\underline{R}}_T = \sum_{k=1}^{K} \underline{y}_T(k) \underline{y}_T^H(k) = \underline{T}^H \hat{\underline{R}} \underline{T} . \tag{2-33}$$

Multivariate normally distributed data remains multivariate normal under a full-rank transformation with a straight-forward alteration of the mean vector and covariance matrix (Result 4.3 in [17]). Thus the modification of Kelly's analytical detection results for transformed data is straightforward. The transformation $\underline{T}$

used here represents the combination of the linear processing blocks in Figure 2-2 preceding the STAP Detection Algorithm block (i.e. the beamformer, the ASP, and the spatial-temporal DOF reduction block) all of which are treated as fixed for the purposes of analyzing detection performance. The combined transformation can be written in terms of the response matrices of it's component blocks as

$$\underline{T} \equiv [I_{N_t} \otimes (LBW)] \underline{G} \tag{2-34}$$

which emphasizes that the spatial processing blocks (i.e. L, B, and W) are fixed during a CPI. In this paper, the space-time DOF reduction transformation, $\underline{G}$, performs temporal reduction only using a partial DFT matrix as discussed in Section 2.3.1. In this case, $\underline{G}$ is the kronecker product of selected columns of a DFT matrix and an identity matrix of size N_s.

From [7], the probability of false alarm is given by

$$P_f = (1 - \eta_{oT})^{K - N_T + 1} \tag{2-35}$$

where N_T is the dimension of the transformed data vectors, and the "T" subscript denotes dependence on the transformation. From [16], the probability of detection for the random target amplitude case is calculated as

$$P_d = \int_0^1 P_{d|\rho} f_\rho(\rho) d\rho. \tag{2-36}$$

where

$$P_{d|\rho} = 1 - \frac{P_f}{\beta_T} \cdot \sum_{j=1}^{K - N_T + 1} \binom{K - N_T + 1}{j} \left(\frac{\eta_{oT}}{1 - \eta_{oT}}\right)^j \cdot \sum_{m=0}^{j-1} \frac{[\rho(1 - \eta_{oT})]^m}{[\rho(1 - \eta_{oT}) + 1/\beta_T]^{m+1}}. \tag{2-37}$$

ρ is a Beta distributed random variable with probability density function

$$f_\rho(\rho) = \frac{K!}{(K - N_T + 1)!(N_T - 2)!} \rho^{K - N_T + 1} (1 - \rho)^{N_T - 2},$$ (2-38)

and the SINR parameter for transformed data is

$$\beta_T \equiv \sigma_s^2 s_T^H \underline{R}_T^{-1} s_T.$$ (2-39)

The detection threshold is seen to be a function of the specified false alarm probability, the number of secondary data vectors, K, and the dimension of the transformed data vectors, N_T. Using the transformation to reduce the data dimension results in a smaller threshold for the same P_f thereby improving P_d. The probability of detection is a function of the specified false-alarm probability, P_f, the transformed SINR, β_T, the number of secondary data vectors and the transformed data dimension. In order to more readily see the effects that the transformation has on P_d thru $P_{d|\rho}$, Equation 2-37 is simplified in Appendix B with the result

$$P_{d|\rho} = \left[\frac{\rho\beta_T + 1}{\rho\beta_T + (1/P_f)^{1/(K - N_T + 1)}} \right]^{K - N_T + 1}.$$ (2-40)

Since $P_f < 1$ and for $0 < \rho < 1$ and $(K - N_T + 1) > 0$, it follows that $P_{d|\rho}$ is a monotonically increasing function of β_T and therefore so is P_d since $f_\rho(\rho) > 0$ and is not a function of β_T. With substantially more work, it can also be demonstrated that $P_{d|\rho}$ and P_d are monotonically decreasing functions of N_T and monotonically increasing functions of K. This is not proved here because it is not essential to this study. The point is that detection performance can be improved by using a linear transformation to reduce the data vector dimension. However, the transformed SINR, β_T, may consequently be reduced by the transformation thereby degrading detection. Hence, it is desired to design the transformation so as maximize SINR for a given transform-domain dimension and to select the transformed data dimension which results in the maximum improvement in P_d. Thus, in the design of the signal processor there are two main objectives as far as detection performance is concerned, (1) maximizing SINR for a given N_T and (2) determining the N_T which maximizes

P_d by providing the best balance between SINR loss and estimation loss.

2.2.1.3 Detection Probability Based Performance Metrics

In order to determine how different systems compare in their detection capability, three interrelated performance metrics will be discussed. The first metric is based on the SINR parameter which may be plotted directly using a normalized version of Equation 2-39 (i.e. normalized with respect to SNR), or may be plotted using the "SINR Loss" relative to the optimal SINR (β_o given in Equation 2-30) defined as

$$\text{SINR Loss} \equiv \beta_o / \beta_T . \qquad (2\text{-}41)$$

The SINR Loss is a measure of the degradation of the detection capability (via the SINR parameter) due to preprocessing the data (i.e. processing raw sensor data prior to generating the detection test statistic). The SINR metric is useful for comparing systems which have the same transformed data dimension, but it does not include other factors influencing detection, such as the loss incurred due to having to estimate the interference covariance matrix which is primarily a function of K and N_T.

A second detection-based performance metric, referred to as "Detection Loss", which will include all model-based effects on detection performance (i.e. SINR Loss and Estimation Loss) is defined as the additional SNR required by the system-under-test in order to achieve the same detection probability as the optimal Neyman-Pearson detector of Section 2.2.1.1. Numerical evaluation of Detection Loss proceeds by determining the ratio

$$\text{Detection Loss} \equiv \frac{\text{SNR}\big|_{P_{d,glr} = P_{d,spec}}}{\text{SNR}\big|_{P_{d,opt} = P_{d,spec}}} = \frac{\sigma_s^2(\underline{R}, \underline{s}, P_d, P_f, \underline{T}, K, N_T)\big|_{P_{d,glr} = P_{d,spec}}}{\sigma_s^2(\underline{R}, \underline{s}, P_d, P_f)\big|_{P_{d,opt} = P_{d,spec}}}, \qquad (2\text{-}42)$$

where the dependence on the target structure, interference covariance matrix, specified detection and false-alarm probabilities, data transformation, number of secondary data vectors (i.e. K) and data vector dimension (i.e. N_T) is indicated. The difference in Detection Loss(dB) between two systems represents the relative SNR(dB) requirement to detect a target of a given structure embedded in interference with specified

21

covariance matrix. It can be directly related to the size of a target (i.e. the target radar cross-section) that one system can detect relative to the other. It can also be indirectly related to detection range and system resources (such as transmit power, noise figure, transmit sidelobe levels, etc.) and as such represents an important way to asses the impact on practical system issues.

The third detection-based performance metric, referred to as "Estimation Loss", is based on a convenient factorization of the Detection Loss. Using P_d formulas from Equation 2-30, Equation 2-36, and Equation 2-40 the SINR *required* to achieve a specified P_d can be obtained. Then rewriting Equation 2-42 in terms of this *required* SINR by making use of the SINR relations in Equation 2-30, Equation 2-39, and Equation 2-41, the Detection Loss can be written as

$$\text{Detection Loss} = \text{Estimation Loss}(P_{d, \, spec}, P_f, K, N_T) \cdot \text{SINR Loss}(\underline{R}, \underline{s}, \underline{T})$$

$$\text{where} \qquad \text{Estimation Loss} \equiv \frac{\text{SINR}|_{P_{d, \, glr} = P_{d, \, spec}}}{\text{SINR}|_{P_{d, \, opt} = P_{d, \, spec}}} \qquad (2\text{-}43)$$

This factorization effectively separates the dependent variables into two (almost) disjoint groups. The qualifier 'almost' is used here because the data dimension, N_T, implicitly influences the SINR Loss through $\underline{T}$. The Estimation Loss is a measure of the degradation of the detection capability for a specified P_d and P_f as a consequence of having to estimate the interference statistics for data with dimension N_T using K i.i.d. sample vectors. These performance metrics are power ratios and are conveniently calculated in decibel units resulting in

$$\text{Detection Loss (dB)} = \text{SINR Loss (dB)} + \text{Estimation Loss (dB)}. \qquad (2\text{-}44)$$

It should be noted that the *required* SNR and SINR of Equation 2-42 and Equation 2-43 are implicit functions of the modeling assumptions and detection algorithms used. That is why the P_d subscripts contain 'opt' for optimum and 'glr' for the GLR algorithm.

2.2.2 Jammer-to-Noise Ratio (JNR) Improvement

The primary function of the ASP within the cascaded system architectures, which incidentally are

the focus of this study, is to suppress jammer signals, thereby relieving the STAP of this task. How well the ASP performs this task is certainly not the only determining factor in the systems overall performance, but oftentimes particularly good or bad detection performance can be attributed to ASP jammer rejection capability. Thus, as a figure-of-merit for the ASP, either the JNR at the ASP output or the ASP jammer cancellation ratio (JCR) will be used. The JNR at the input of the ASP is defined as the total jammer power to noise power ratio,

$$JNR_{in} \equiv \frac{tr[(LB)^H R_j (LB)]}{tr[(LB)^H R_n (LB)]},$$

(2-45)

where the system spatial noise covariance matrix, R_n, is the identity matrix for these analyses. The JNR at the output of the ASP for all channels combined (i.e. the entire target-clutter subspace), is similarly defined with the ASP matrix filter, W, included as

$$JNR_{out} \equiv \frac{tr[(LBW)^H R_j (LBW)]}{tr[(LBW)^H R_n (LBW)]}.$$

(2-46)

Also of interest is the JNR in the one-dimensional target subspace at the output of the ASP as well as the JNR in the one-dimensional subspaces comprising the rest of the target-clutter subspace. These subspaces can be thought of as basis vectors for the target-clutter subspace and are defined as the columns of the clutter Beamformer, B_c, after being transformed by the beamsteering matrix, L. The JNR for the nth clutter subspace basis (the first is chosen to be the target subspace) is defined as

$$JNR_{out}(n) \equiv \frac{(Lb_n)^H (LBW) (LBW)^H R_j (LBW) (LBW)^H (Lb_n)}{(Lb_n)^H (LBW) (LBW)^H R_n (LBW) (LBW)^H (Lb_n)}$$

(2-47)

where b_n is the nth column of the clutter Beamformer, B_c. In general, the sum of the individual $JNR_{out}(n)$

23

will not necessarily equal the JNR_{out}, because the clutter Beamformer columns are not constrained to be an orthonormal basis. Typically, JNR_{out} is used to investigate the total jammer suppression, while the individual $JNR_{out}(n)$ are used to determine jammer suppression along a given target-clutter basis vector. The jammer suppression along the target subspace is usually the most pertinent since it provides a measure of how much jammer residue needs to be suppressed by the STAP. The jammer cancellation ratio is simply defined as the ratio of output-to-input JNR. For the JNR definitions of Equation 2-45 and Equation 2-46 total JCR is given by

$$JCR \equiv JNR_{out}/JNR_{in},\qquad(2\text{-}48)$$

For the individual subspace JNR of Equation 2-47 a corresponding input JNR formula should be used to calculate the JCR for that subspace.

2.2.3 Extraneous Interference Considerations

The performance metrics considered so far have involved the detection of a target embedded within a particular class of interference (i.e. complex Gaussian distributed noise, clutter and jammer signals) and the corresponding control of false-alarms from these expressly characterized interference sources. Also of concern is the rejection of extraneous signals which are not included in the interference characterization. These types of interference are varied and difficult to analyze within a general framework. A possible classification of these sources, which is closely linked with the way the Gaussian processor of this study processes data, is to distinguish between those sources which affect the primary data only, those which affect the secondary data only, and those which contribute to both. The first type affects the processor only thru it's contribution to the primary data, thereby causing erroneous detections due to the additional power, or possibly degrading detection by combining destructively with the desired signal. The second extraneous source type can also degrade detection and cause erroneous detections through their influence on the estimated covariance matrices and the perturbation of the assumed probability distributions. The third type may be of less concern if it is correlated between primary and secondary data since the matched filter will tend to suppress such interference. On the other hand, if the primary and secondary contributions are uncorrelated for a type 3 source, then the effects attributed to both type 1 and 2 can be

present.

2.2.3.1 Filter Response Pattern Definitions

In this study, only the rejection of the first type of extraneous interference discussed in Section 2.2.3 is of interest. A common way investigating a processor's susceptibility to interference sources in the primary data, but not accounted for in the design of the filter, is to determine the processor's response to these signals relative to it's response to the desired signal. For the surveillance radar system being considered, it has been assumed that signal leakage between range bins is negligible. However, signals in the same range bin but with different AOA and/or Doppler than the desired signal (i.e. assumed target) can be present in the primary data and need to be suppressed. The figure-of-merit chosen for comparing the robustness of different systems against such interference will be referred to as the "System Response Pattern", $\underline{A}_T$, and is defined as

$$\underline{A}_T(f_t, f_s; f_{ts}, f_{ss}) \equiv \frac{\left| \underline{w}_{oT}^H \underline{T}^H (s_t \otimes s_s) \right|^2}{\underline{w}_{oT}^H s_T} \qquad \text{where } \underline{w}_{oT} \equiv \underline{R}_T^{-1} s_T. \qquad (2\text{-}49)$$

the steering vectors, s_t and s_s, of Equation 2-13 have been employed, and the "T" subscript emphasizes the dependence on the system's transformations/filters prior to the STAP detection algorithm block. Note the implied dependence on the assumed target normalized frequencies. The space-time weight vector, $\underline{w}_{oT}$, represents the optimum filter for the transformed data. It can also be related to the data filter in the numerator of the GLR test statistic of Equation 2-31 when the covariance matrix has been perfectly estimated (or equivalently when the number of i.i.d. secondaries increases without bound). In connection with this observation, $\underline{A}_T$ can be viewed as a normalized "asymptotic" filter magnitude response to sources different from the assumed target. Normalization by the matched target response allows a link to be developed between $\underline{A}_T$ and the extraneous-signal SNR handling capability of a particular system, as discussed below.

A more pertinent interpretation can be assigned to $\underline{A}_T$ by referring to Kelly's work in [18] which is related to the detection of mismatched signals using the GLR algorithm. Kelly's analysis utilized a decomposition of the "available SINR" (i.e. β_T of Equation 2-39 with s_T replaced by the steering vector of the dis-

25

placed source) into two components orthogonal with respect to the inverse of the covariance matrix, R_T. The component parallel to the desired steering vector he referred to as the SINR available for detection ($SINR_{det}$) and the other he called $SINR_{loss}$. He showed that detection performance is influenced by $SINR_{det}$ in the same way as β_T for the matched signal case, but the effect of $SINR_{loss}$ was substantially more complicated since it resulted in a modification of the distribution of the loss factor (i.e. it's pdf, which happens to be a Beta distribution for the matched case, is now a function of the $SINR_{loss}$ as well as other parameters). The detection of a mismatched signal was shown to be degraded by two effects related to the SINR components: (1) the reduction of $SINR_{det}$, and (2) the shift of the "loss factor pdf" towards greater loss as $SINR_{loss}$ is increased. It can be shown from Kelly's results that the effect of $SINR_{loss}$ is diminished as the number of secondaries increase. Kelly demonstrated that a significant shift in the "loss factor pdf" corresponded to substantial differences in the $SINR_{loss}$ (on the order of 5 dB or more), but it is expected for the systems considered here that the relative $SINR_{loss}$ levels would not differ that much between systems. However, because the $SINR_{det}$ will typically exhibit small values (in the sidelobe regions where extraneous signals are of concern), then the *relative* $SINR_{det}$ levels between systems can be substantial. For the system comparisons in this study, it is presumed that the reduction in $SINR_{det}$ will be the primary factor with respect to extraneous-signal rejection. From this point of view, two systems can be compared for their extraneous-signal rejection capability by determining the relative extraneous-signal SNR's which would result in the same probability of detection under target absent conditions. The ratio of $SINR_{det}$ for the two systems provides a good measure (which becomes better as the effects of $SINR_{loss}$ become less of an issue for system comparison). Using Kelly's formulas from [18] the ratio of detection SINR's can be written as

$$\frac{SINR_{det}(T_1)}{SINR_{det}(T_2)} = \frac{SNR_{T_1}}{SNR_{T_2}} \cdot \frac{A_{T_1}(f_t, f_s)}{A_{T_2}(f_t, f_s)}, \qquad (2\text{-}50)$$

and, therefore, the "asymptotic" system patterns from Equation 2-49 can be used as a measure of the relative extraneous-signal SNR's that can be tolerated by different systems. More precisely, for two systems differentiated by T_1 and T_2 with the same P_f and using the same number of secondaries, the ratio of the

26

SNR's corresponding equal extraneous-signal detection probability is determined by setting the ratio of Equation 2-50 to unity. Thus the difference in the System Response Pattern levels indicates the relative level of extraneous-signal rejection between the two systems. It should be mentioned that this measure does not include the aforementioned effects of $SINR_{loss}$ and also does not include the effect of data dimension. For the matched-signal case, a larger data vector dimension causes the detection performance to degrade. Thus, in comparing two systems for extraneous-signal rejection, it should be remembered that if one system has a substantially larger data vector dimension going into the GLR processor, it will incur an additional reduction in extraneous-signal rejection capability. The exact amount is not easily accessible, but using an estimate for the effective loss factor such as the mean of the beta distribution, it can be shown that this extra loss is less than 2 dB if the number of secondaries exceeds the data dimension by at least a factor of 3.

Another response pattern of interest is that of the ASP. Specifically, it is useful to be able to visualize the perturbation of the spatial target-clutter subspace response in the clutter channels due to the ASP filtering, as well as the depth, width, and placement of the jammer nulls. The ASP applies a matrix filter to the beamformer outputs, and it is desired to investigate the response in the entire ASP output subspace (i.e. the target-clutter subspace) as well as each output channel individually. For the combined subspace of all ASP output channels, the "ASP Response Pattern" is defined as

$$ASR(f_s; f_{ss}) \equiv \frac{\left| (LBW)^H s_s \right|^2}{tr[(LBW)^H R_n (LBW)]} , \tag{2-51}$$

where the response has been normalized to cancel any scale factor attributable to the ASP weight vectors, $w(n)$ and which gives the ASR an interpretation of SNR gain (or loss) for the direction corresponding to s_s. Sometimes it is useful to plot the response for each channel individually, therefore the "ASP Response Pattern" for the nth clutter channel is defined here as

27

$$ASR(n, f_s; f_{ss}) \equiv \frac{\left| (LBw(n))^H s_s \right|^2}{tr\left[(LBw(n))^H R_n (LBw(n)) \right]}.$$ (2-52)

Incidentally, the ASP weight vector is generally calculated by assuming enough secondary data vectors are available to perfectly estimate the jammer-plus-noise covariance matrix. In this case then, the "asymptotic" pattern is the desired result. Although not directly linked to detection performance, the ASP Response Pattern can provide assistance in assessing the effects of the ASP without the added complications of the space-time filtering of clutter and jammer residue.

2.2.3.2 Characterization of the System Pattern by a Scalar Performance Metric

The System Response Patterns given by Equation 2-49 are not always convenient to use and conclusions drawn from them are subjective in nature. In order to judge a systems' false detection performance more efficiently, a scalar metric is proposed (to be called the System Sidelobe Level or SSL) which is the average sidelobe level of the System Response Pattern. The average is performed for a specific target (i.e. fixed f_{ss} and f_{ts}) over a range of normalized spatial and Doppler frequencies which typically will not include the target region (i.e. the mainlobe). For uniform non-tapered sampling, (in space and time) an orthogonal set of bins generated from the original data all have equal size in normalized frequency coordinates. For this study, a source detected anywhere within the target bin is considered a valid detection. Thus, the target region is usually taken to be the bin centered on the assumed target. In this paper, the SSL is calculated for 1 or 2 simply connected rectangular regions in the space-Doppler plane. For instance, it is desired to calculate the SSL over a rectangular region which has an internal rectangular region excluded (e.g. the mainlobe). The SSL for a rectangular region with an excluded internal rectangular region can be calculated by taking the difference between the integrated System Responses for the two rectangular regions and dividing by the area of the included region. The integrated System Response for a rectangular region centered on the target's spatial-Doppler frequency pair is defined as

$$\overline{A_T}(\Delta f_t, \Delta f_s; f_{ts}, f_{ss}) \equiv \int_{f_{ts} - \Delta f_t / 2}^{f_{ts} + \Delta f_t / 2} \int_{f_{ss} - \Delta f_s / 2}^{f_{ss} + \Delta f_s / 2} A_T(f_t, f_s; f_{ts}, f_{ss}) \, df_s \, df_t.$$ (2-53)

Using this definition, the SSL for primary and excluded rectangular region is calculated from

$$SSL(\Delta f_t, \Delta f_s, \Delta f_{tx}, \Delta f_{sx}; f_{ts}, f_{ss}) \equiv \frac{\overline{A_T}(\Delta f_t, \Delta f_s; f_{ts}, f_{ss}) - \overline{A_T}(\Delta f_{tx}, \Delta f_{sx}; f_{ts}, f_{ss})}{\Delta f_t \cdot \Delta f_s - \Delta f_{sx} \cdot \Delta f_{tx}}. \qquad (2\text{-}54)$$

The first SSL metric uses the entire space-Doppler plane with the target mainlobe region excluded. The bin sizes for the primary region and the excluded target region between the halfpower points of the mainlobe for uniformly sampled untapered data are

$$\begin{aligned} \Delta f_t &= 1 & \Delta f_s &= 1 \\ \Delta f_{tx} &= 1/N_t & \Delta f_{sx} &= 1/N_c \end{aligned} \qquad (2\text{-}55)$$

Of course, the excluded region defined by Δf_{tx} and Δf_{sx} can be made larger if the outer sidelobe region is of more interest. A closed form expression for the integrated System Response, $\overline{A_T}$, (and therefore the SSL) can be obtained by performing the integrations indicated in Equation 2-54. For the application considered in this paper with uniform spatial and temporal sampling, a closed form expression for SSL is derived in Appendix C and repeated here,

$$\overline{A_T}(\Delta f_t, \Delta f_s; f_{ts}, f_{ss}) = \frac{\underline{w}_{oT}^H \underline{T}^H \{ (A_t \otimes A_s) \} \underline{T} \underline{w}_{oT}}{\underline{w}_{oT}^H \underline{S}_T}, \qquad (2\text{-}56)$$

where the matrices A_t and A_s defined in Equation C4 are functions of f_{ts}, f_{ss}, Δf_t, and Δf_s. A list of the SSL metrics used in this paper are given in Table 2-1. SSL1 is the average Sidelobe response for all spatial and

Table 2-1: Region Definitions for SSL Metrics

SSL Metric	Primary Region Spatial Dimension, Δf_s	Primary Region Doppler Dimension, Δf_t	Excluded Region Spatial Dimension, Δf_{sx}	Excluded Region Doppler Dimension, Δf_{tx}
SSL1	1	1	1/Nc	1/Nt

Table 2-1: Region Definitions for SSL Metrics

SSL Metric	Primary Region Spatial Dimension, Δf_s	Primary Region Doppler Dimension, Δf_t	Excluded Region Spatial Dimension, Δf_{sx}	Excluded Region Doppler Dimension, Δf_{tx}
SSL2	1	1/Nt	1/Nc	1/Nt
SSL3	1/Nc	1	1/Nc	1/Nt
SSL4	1	1/Nt	3/Nc	1/Nt
SSL5	1/Nc	1	1/Nc	3/Nt
SSL6	1	1/Nt	.5	1/Nt
SSL7	1/Nc	1	1/Nc	.5

Doppler frequencies excluding the target mainlobe (i.e. a single space-Doppler bin centered on (f_{ts}, f_{ss})).

SSL2 is the spatial sidelobe level for a doppler width of one bin and excluding the target mainlobe. SSL4&6 are the same as SSL2 except the excluded region is increased to determine the sidelobe levels farther away from the target. SSL3 is the Doppler sidelobe level for a spatial frequency width of one bin and excluding the target mainlobe. SSL5&7 are the same as SS3 except the excluded region is increased to determine the sidelobe levels farther away from the target. The SSL level are usually displayed together in order as a vector (or list).

2.2.4 Interference Scenarios for Numerical Analysis

The bulk of the numerical analysis in this study will be for the purpose of comparing the performance of various system architectures and processing algorithms. It is neither feasible, nor desirable to compare the systems for all types interference, but instead to focus on those scenarios most pertinent to the application being considered. Accordingly, the signal models detailed in Section 2.1 have been specialized to the case of a airborne surveillance radar utilizing a uniform linear array of sensors. The two types of interference considered in this study are ground clutter and WNJs. The spatial arrangement of jammers and their power levels will not be defined here, but will be specified as needed. This section is mainly concerned with the specification of the clutter signal statistics developed at the output of the sensors, and of the

Radar system parameters pertinent to the analyses. The Radar system parameters are listed in Table 2-2 and

Table 2-2: Radar System Parameters

Symbol	Parameter Definition	Default Value
f_0	Radar carrier center frequency	1250 MHz
λ_0	Radar carrier operating wavelength	.24 meters
P_t	peak transmit power	-
T_p	transmit pulsewidth	-
B	receiver equivalent noise bandwidth	1 MHz
PRF	pulse repetition frequency (PRF=$1/T_r$)	2 KHz
$G_t(\phi,\theta)$	array transmit power gain	-(uniform taper, no backlobe)
$g(\phi,\theta)$	receive sensor pattern (voltage)	omni
L_s	system losses on receive	-
N_0	receiver noise power spectral density	see Section 2.1.3
N_c	number of sensor outputs from array manifold	32
N_t	number of pulses per CPI	16
d	sensor spacing in wavelengths	.49
N_{el}	number of elements in a sensor column	8
d_{el}	element spacing along the column	.49

the clutter scenario parameters are given in Table 2-3 along with default values for those parameters required in the numerical analyses. The baseline system described by these parameters corresponds to a narrowband, medium PRF radar using a medium-sized uniform line array.

The scenarios to be discussed utilize the default values of the radar and scenario parameters except as noted. Scenario A uses all the default values. A substantial amount of ICM has been selected which roughly corresponds to a clutter velocity standard deviation of 1 m/s. Also, this scenario has the platform moving without velocity misalignment (i.e. velocity vector aligned with line array axis) which is one of the requirements for a system using "Displaced Phase Center Antenna" processing. In order to visualize the

Table 2-3: Clutter Scenario Parameters

Symbol	Parameter Definition	Default Value
CNR	total clutter-to-noise power ratio per element	40 dB
σ_{icm}	normalized rms clutter spectral standard deviation	.005
h_p	platform altitude	9 km
v_p	platform velocity vector, $[v_x, v_y, v_z]$, in m/s	[0., 120., 0.]
ϕ_p	platform velocity azimuth misalignment angle	0°
R_t	target range	50 km
$[\phi_t, \theta_t]$	target look direction, [az, el]	[0°, 10°]
N_{ac}	number of clutter scattering cells used in model	256

characteristics of Scenario A clutter-plus-noise, a 3D mesh plot of the power spectrum is provided in Figure
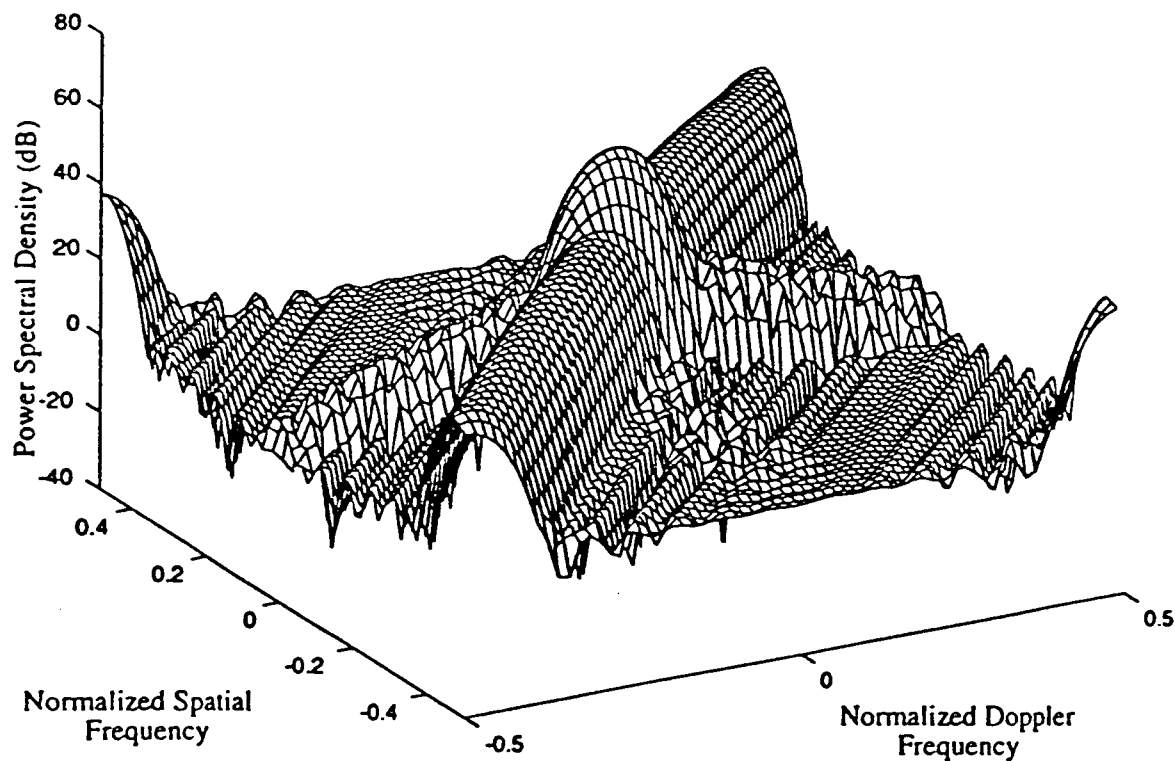
Figure 2-4: Power Spectrum for Clutter Scenario A

2-4. The power spectrums in this section were generated using the computed covariance matrices to create a truncated version of the discrete 2D correlation function. A Blackman window was applied to the correlation functions and a DFT was performed. Clutter Scenario B is the same as A except that the transmitter is steered 50° in azimuth. A gray-scale image plot of the clutter-plus-noise spectrum is given in Figure 2-5.
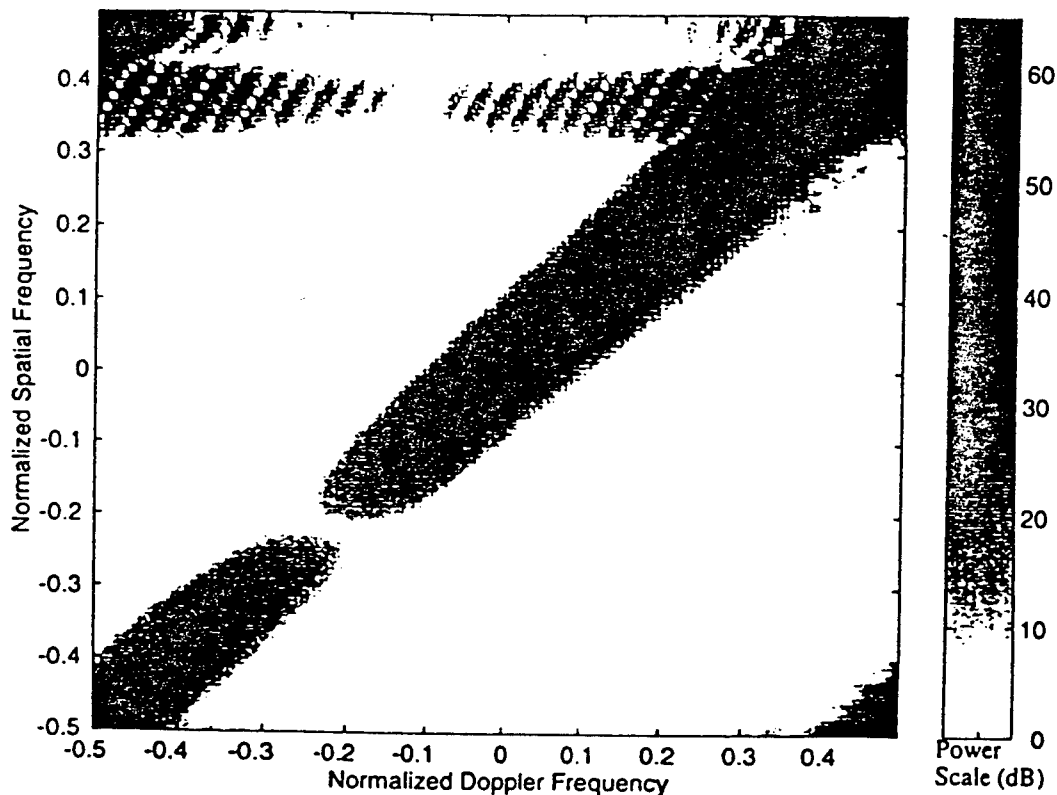
Figure 2-5: Power Spectrum for Clutter Scenario B

In Scenario C, the steering angle is broadside as in Scenario A, but a 25° azimuth velocity misalignment is introduced. Finally, Scenario D combines the effects of B and C with off-broadside steering of 50° and azimuth velocity misalignment of 25°. Gray-scale image plots of the clutter-plus-noise spectrums for Scenarios C and D are given in Figure 2-6 and Figure 2-7 respectively.

2.3 Baseline Systems Used for Comparative Analyses

This section is devoted to the definition and performance characterization of the selected baseline systems used for comparative analyses. As already discussed, cascaded ASP / STAP system architectures are of interest which utilize partially adaptive array techniques for the spatial pre-suppression of WNJ. From a practical viewpoint, fixed analog beamforming has been selected as the vehicle for implementing
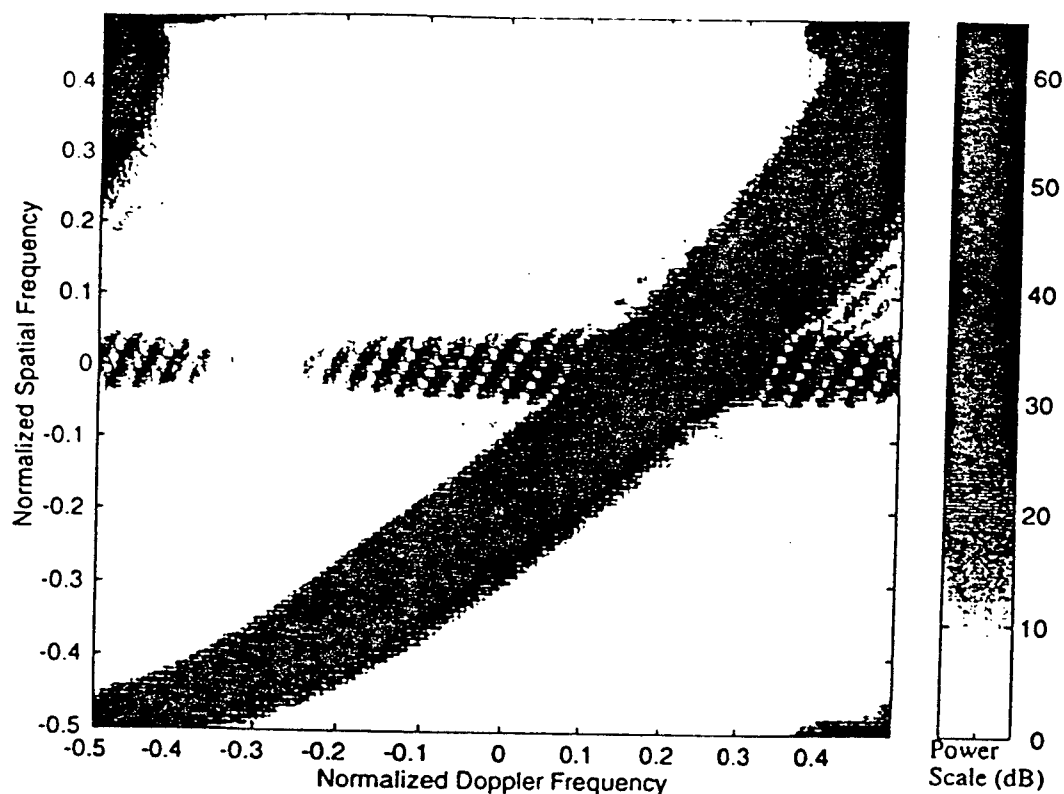
Figure 2-6: Power Spectrum for Clutter Scenario C

the partially adaptive arrays as opposed to digitizing every available spatial channel and performing some linear transformation digitally. System configurations will be distinguished primarily by the type of spatial DOF control and reduction employed. DOF control techniques refers to the type of fixed analog beamforming being used. The DOF reduction techniques considered here are of the adaptive spatial type and are designed specifically for suppression of WNJs by the ASP. Spatial DOF reduction is indicated in Figure 2-2 after the ASP function for the purposes of maintaining generality in the block diagram, although this type of processing will not be considered here. In this paper, temporal DOF reduction is accomplished using localized DFT bins (as in the Doppler Domain Localized, DDL, approach [8]) after the ASP. Five system configurations are described here which will serve to illustrate various benefits and/or deficiencies of the Cascaded Space- and Space-Time Adaptive Processing (CS-STAP) approach, they are:

- Fully-Adaptive STAP (FA),
- Joint Domain Localized (JDL),
- Cascaded Fixed Butler-JDL (CFB-JDL),

34
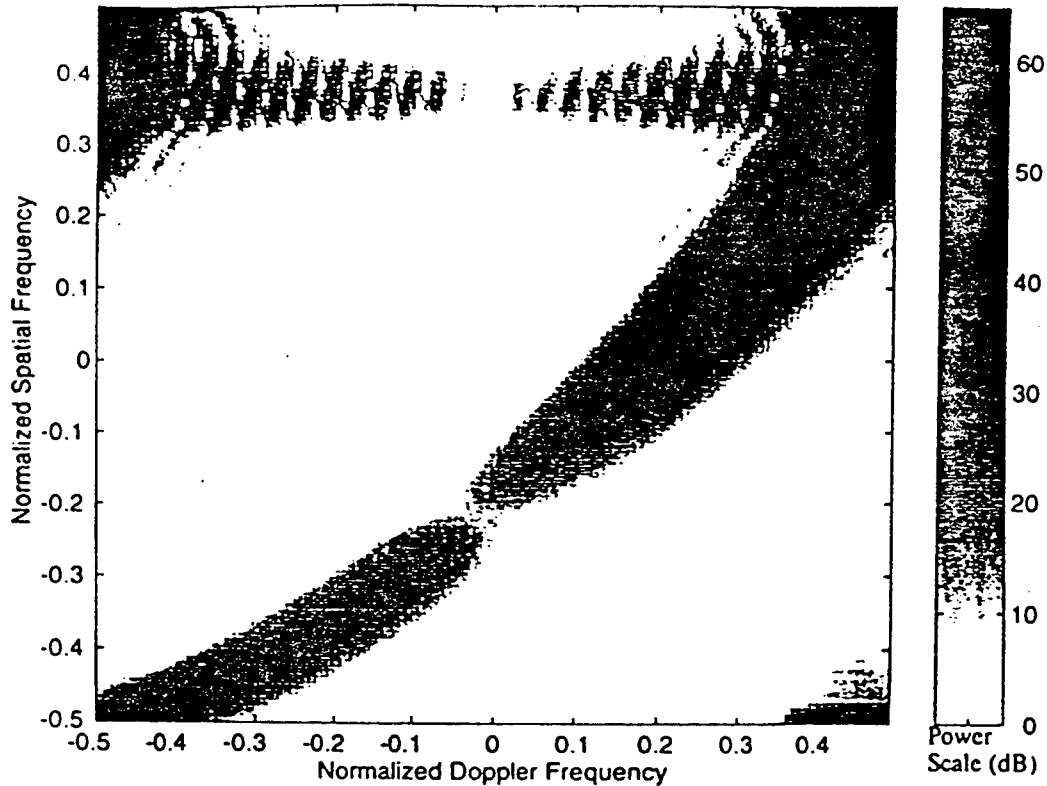
Figure 2-7: Power Spectrum for Clutter Scenario D

- Cascaded Symmetric Auxiliary-JDL (CSA-JDL),

- Cascaded Selective Butler-JDL (CSB-JDL).

Note that the word 'cascaded' distinguishes CS-STAP systems from those not employing spatial pre-suppression of jammers. The two non-cascaded systems (FA and JDL) are used as representative systems for the current approaches to simultaneous jammer-and-clutter suppression. The three cascaded systems were selected because of their potential to provide a high-performance practical solution. The FA system is a obvious starting point for any adaptive system which is required to handle interference with a complicated spectrum. The JDL architecture provides a natural link between the FA system and the selected cascaded systems as well as an excellent representative approach from the class of simultaneous partially adaptive STAP algorithms.

A block diagram of a generic Adaptive Spatial Processor (ASP) is given in Figure 2-8. In order to accentuate the distinction in functionality, the beamformer has been split into two parts, one intended for STAP processing, B_c, and the other for ASP WNJ processing, B_a, but of course, this is neither a require-
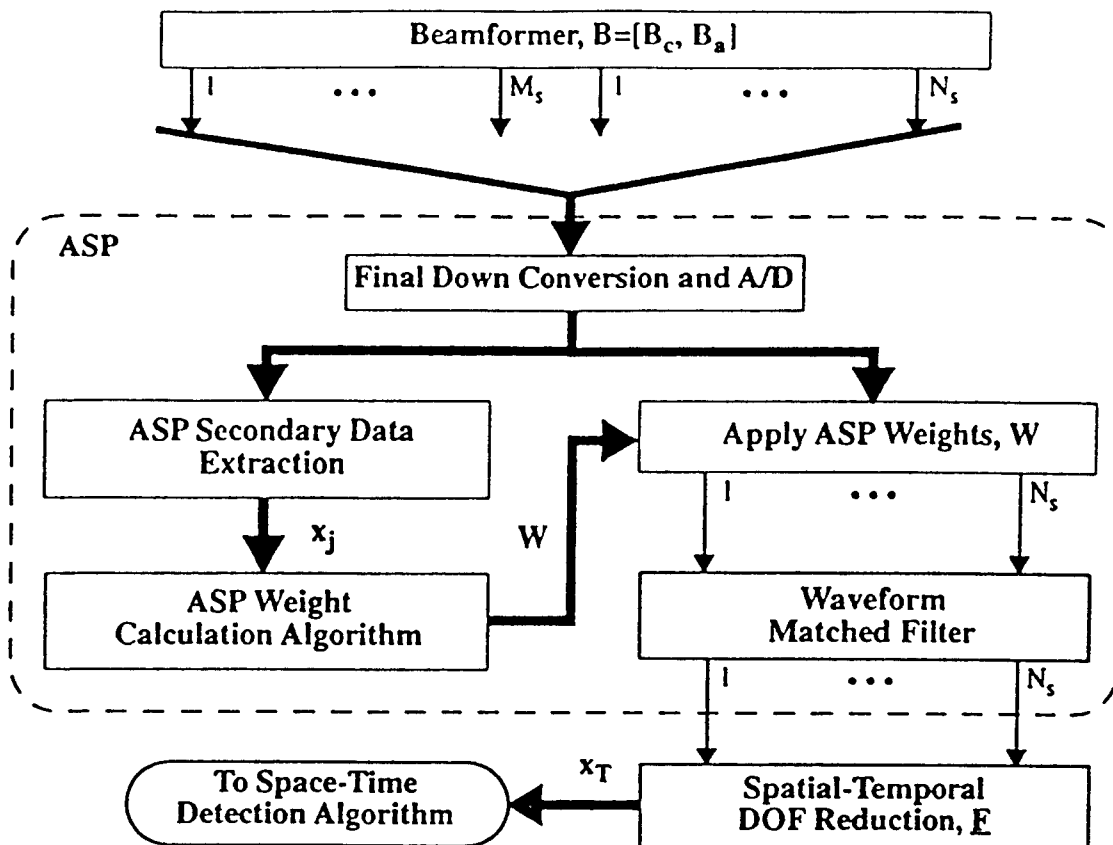
Figure 2-8: Generic Adaptive Spatial Processor Architecture

ment nor an implementation restriction. The set of M_s auxiliary channels (or beams) are sometimes referred to as jammer beams, because their primary purpose is to provide jammer suppression. The set of N_s channels are sometimes referred to as clutter beams for similar reasons. Among the clutter beams, usually at least one of them is highly directional and pointing at the desired target. Sometimes this beam is distinguished by referring to it as the target beam.

The ASP has several functions as indicated in Figure 2-8, three of which are of interest in this paper. These three are the 'Secondary Data Extraction', the 'ASP Weight Calculation' and the 'ASP Weight Application' functions. 'ASP Weight Calculation' generates a space-domain matrix filter whose function is to suppress jammers while leaving the target/clutter subspace unperturbed as much as possible, and which reduces the data dimension from M_s+N_s to N_s. 'ASP Weight Application' is merely a matrix filter operation. An important feature is that the weight matrix is held fixed during a CPI. The role of 'Secondary Data Extraction' is to obtain clutter-free jammer data to be used in ASP weight calculation. This function is dis-

cussed further in Section 3.1.

The detailed operation or performance of the other two ASP functions are not important for the purpose of this paper, but it is assumed that they are of high quality. The 'DownConversion and A/D' can be accomplished using a variety of techniques for digitization of a bandpass waveform (e.g. analog synchronous demodulation and digitization, direct IF sampling and digital demodulation, etc.). The 'Waveform Matched Filter' shown in Figure 2-8 is applied after digitization and ASP filtering in order to illustrate how receiver cost can be reduced by requiring fewer high quality pulse-compression channels, but this is not necessary. The 'Waveform Matched Filter' is a range-domain pulse-compression filter whose range sidelobes are assumed to be negligible. Since the ASP weights are fixed over a CPI, and therefore have flat spectral response in the range-domain, they will not interfere with pulse-compression. If the ASP weights were allowed to vary in the range-domain then the interactions with the matched-filter would need to be addressed. For those interested in adaptive canceller and pulse-compression interactions see [22] for example. The pertinent question here is the effect on the ASP weight calculation. Of importance is the effect on the secondary data covariance matrix if matched filtering is performed after as opposed to before the ASP weight calculation. It turns out that the difference in performance is negligible as long as the secondary data has been filtered to a bandwidth no larger than the receiver bandwidth which is typically established by the 'DownConversion and A/D' and/or 'Waveform Matched Filter' functions. Reasonable amounts of variation in spectral shape between the ASP primary and secondary data will have little impact on the system performance.

2.3.1 Baseline System Architectures

Referring to Figure 2-8, the FA system has no ASP and the clutter beamformer transformation is the identity matrix. There is no temporal DOF reduction either. That is, every column is digitized and every pulse sample from every column is used in the STAP detection algorithm (i.e. the GLRT). The FA system has enjoyed much attention in the literature (e.g. [14], [15], and [9]) due to it's flexibility and proclaimed robustness. However, a FA system for a medium sized array will typically require an impractical number of STAP secondary samples, particularly in a nonhomogenous environment. In reference to the loss metrics defined in Section 2.2.1, the FA processor incurs no SINR Loss, but will usually have substantial Estimation Loss (resulting in substantial Detection Loss) unless many STAP secondary samples are used.

37

There are several possible implementations of the JDL system. The one chosen here employs a Butler beamformer (i.e. an analog implementation of a DFT) to generate the adjacent orthogonal spatial DFT beams, while the temporal DFT bins are generated digitally so that a local region can be easily obtained for all Doppler bins. This implementation is used because of it's close relationship with many of the cascaded systems studied in this paper. Other JDL implementations are theoretically linked, and should have comparable performance under most circumstances. For an excellent description of the JDL concept refer to [7]. Of course, the JDL processor will incur both SINR and Estimation Losses, but the Estimation Loss will be substantially less than that for the FA system when the number of appropriate STAP secondary vectors available is limited.

The CFB-JDL system is a logical extension of the JDL to a cascaded processor. A fixed set of N_s Butler outputs are selected specifically for STAP clutter processing and another fixed set of M_s Butler outputs are selected for WNJ suppression. The jammer channels are used by the Adaptive Space Processor (ASP), while the clutter channels with jamming removed are used by the STAP. For the baseline processor, the WNJ beams are selected to be adjacent to the central JDL STAP beams. The number of jammer beams selected is determined by the number of WNJ's the system is required to handle.

The CSA-JDL system uses individual sensors (e.g. columns), symmetrically located about and close to the center of the array, to perform WNJ suppression. As indicated by the JDL appendage, central Butler beams are used for clutter suppression in the JDL STAP. This beamformer configuration is similar to a combination of two structures proposed in [1] (overlapping subgroups and symmetric auxiliaries), but with some important differences; (1) an orthogonal beamformer utilizing the whole aperture (i.e. a Butler beamformer) is used instead of overlapped subarrays, and (2) sensors used by the orthogonal beamformer are also used as auxiliaries for WNJ suppression.

The fifth baseline system, CSB-JDL, is a modification of a jammer suppression technique sometimes referred to as Adaptive-Adaptive Array Processing (e.g. see [4]). The basic concept is to locate discrete interferers (i.e. WNJ's in this paper) and then form beams pointed in those directions in addition to the target direction. The system studied here takes the following approach: (1) a Butler beamformer supplies all the necessary beams to cover the entire angle space, (2) the signal and clutter channels are preselected for JDL STAP, and (3) a direction of arrival algorithm (there are many to choose from) is used to locate dis-

38

crete interferers using clutter free data and the resulting DOA information is used to select the Butler chan-
nels closest to the interferer directions. In this paper, the DOA algorithms are not discussed in detail, and it
is assumed that all WNJs are located accurately enough to select the proper beam. A similar approach was
proposed in [5] for use in systems where *low antenna sidelobes* was a primary goal and *only spatially dis-
crete interference* was considered. The effects on clutter suppression were not investigated, nor was a prac-
tical implementation for a system combining this jammer suppression technique with a clutter suppression
algorithm.

2.3.2 Baseline System Algorithm

A discussion of the algorithms employed by the baseline systems is appropriate at this time. The
detection algorithm employed for all systems is the Generalized Likelihood Ratio Test (GLR) for which the
assumptions, test statistic definition, and theoretical detection performance are described in Section 2.2.1.

The adaptive spatial filter algorithm utilized in the ASP by the three baseline cascaded architec-
tures (the ASP is used in cascaded systems only) is the Sample Matrix Inverse (SMI). The SMI algorithm
(e.g. see [6]) has been chosen because it converges to the optimum filter (in the sense that SINR is maxi-
mized) when given an adequate amount of i.i.d. secondary data. Indeed, unless stated otherwise, it is
assumed that enough clutter-free secondary data is available to the ASP so that the 'true' jammer-plus-
noise covariance matrix can be used for analysis purposes. Just how 'enough' clutter-free secondary data is
obtained is the subject of Section 3.1. Since the ASP is a matrix filter with multiple inputs and outputs,
more needs to be said about the filter details. The matrix filter could be designed as a whole by determining
the output subspace for which the SINR is maximized subject to a set of predefined constraints. Alterna-
tively, a filter could be designed individually for each of the outputs each with it's own constraint set. A ver-
sion of the latter technique, referred to as the Decoupled Canceller, is used for the baseline systems. ASP
algorithm alternatives are explored in Section 3.2. In the baseline ASP, all the (N_s+M_s) spatial inputs (i.e.
clutter and jammer channels) are adaptively weighted and N_s separately calculated $(N_s+M_s)\times 1$ weight vec-
tors are applied to the input data. Making use of the ASP data notation of Figure 2-8, the baseline ASP filter
for the nth clutter channel (i.e. the nth column of the ASP weight matrix, W) is calculated as

$$w_n \equiv \upsilon_n \cdot R_{x_j}^{-1} (LB)^H (Lb_n) \text{ , for } n = 1, ..., N_s$$

$$\text{where} \qquad R_{x_j} \equiv E\{x_j x_j^H\} \ , \ \upsilon_n \equiv 1 / \left((Lb_n)^H (LB) R_{x_j}^{-1} (LB)^H (Lb_n) \right)' \qquad (2\text{-}57)$$

and where b_n is the nth column of the 'clutter-beam' portion of the beamformer matrix (i.e. B_c). The ASP secondary data is assumed to be clutter-free jammer-plus-noise data with the same jammer AOA and JNR characteristics as in the primary data. Thus, for the purpose of analysis the following relations are justified,

$$x_j = (LB)^H (j+n) \qquad \text{and} \qquad R_{x_j} = (LB)^H (R_j + R_n) (LB) . \qquad (2\text{-}58)$$

The Decoupled Canceler operates as a set of independent cancelers each with it's own constraint based on a distortionless response for the nth clutter beam when calculating the nth weight vector. An alternative interpretation is that each filter maximizes SINR where the target's spatial characteristic for the nth filter is understood to correspond to the nth clutter beam. The intent here is to minimize the WNJ power in each STAP subspace basis vector (i.e. clutter beam) while keeping the STAP subspace unperturbed.

2.4 Baseline Performance Studies and Degree-of-Freedom Selection

It is in this section that the system configuration parameters and performance levels are established which will be used in latter sections for quantitative comparisons. In addition, this section intends to enhance the motivation for using cascaded systems from a performance viewpoint. The cascaded systems can also have implementation benefits, but due to their dependence on many external factors (e.g. available technology, finances, overall platform goals, etc.) these additional benefits are not explored.

The remaining step in the specification of the baseline systems is selecting the number of spatial and temporal channels. Of course, this selection process is a function of the interference characteristics that the system is expected to handle, as well as other practical considerations such as system cost (which is particularly associated with spatial DOF). In this section, performance in the clutter scenarios of Section 2.2.4 with assumed WNJ environment requirements is the primary consideration. By definition, the fully adaptive system uses all sensor outputs and all pulses within a CPI so that channel number selection is not an

issue.

In selecting the number of temporal channels for systems employing DOF reduction, the reader is reminded that the primary consideration in this paper is the control and reduction of *spatial* DOF. Thus the number of temporal channels at the output of the Spatial-Temporal DOF Reduction function is chosen large enough to adequately handle the temporal spread of the clutter without limiting SINR performance, but small enough so that the estimation loss is kept to a reasonable level. All systems (except the FA or as specifically noted otherwise) will use five temporal channels, which provides a good compromise for the cases studied.

The number of spatial channels is selected by adding the number needed for clutter processing to the number needed to handle the maximum number of WNJs specified in the assumed system requirement. The number of spatial channels needed for clutter processing is chosen as small as possible to minimize estimation loss and control susceptibility to extraneous signals, but large enough to provide 'adequate' SINR so that clutter rejection is not a limiting factor in detection performance. To accomplish these goals is not always easy, as will be seen. Another reason to avoid too many 'extra' spatial DOF in the STAP for this study is that it is desired to be able to determine if the ASP is providing satisfactory jammer rejection. Additional spatial STAP DOF can mask ASP deficiencies by having the STAP compensate for inadequate jammer suppression.

Two WNJ system specifications are considered here. One system is required to handle a few (i.e. 4) jammers. This system, identified by the '4-Aux' appendage, is exposed to a WNJ environment containing the maximum required. The other system, identified by the '12-Aux' appendage, is required to handle a more considerable number of WNJs (i.e. 12), but it is exposed to fewer jammers than required. It is the latter situation for which the cascaded systems are expected to provide substantial benefits against sidelobe jammers (from a performance as well as implementation viewpoint) since they can greatly reduce the computational load and secondary data requirement for the STAP.

The parameters for the baseline systems (i.e. number of channels and secondary data samples) have been selected based on some preliminary numerical performance studies with deference to the considerations discussed above. The number of spatial and temporal channels used by the processing blocks for

41

Table 2-4: Number of Channels for Baseline Systems Processing Blocks

System / WNJ Capability	ASP Jammer Channels, M_s	STAP Spatial Channels, $N_s=N_{ps}$	STAP Temporal Channels, N_{pt}
FA	0	N_c	N_t
JDL / 4-Aux	0	7	5
CFB-JDL / 4-Aux	4	3	5
CSA-JDL / 4-Aux	4	3	5
CSB-JDL / 4-Aux	adapted as needed up to 4	3	5
JDL / 12-Aux	0	15	5
CFB-JDL / 12-Aux	12	3	5
CSA-JDL / 12-Aux	12	3	5
CSB-JDL / 12-Aux	adapted as needed up to 12	3	5

Loss comparisons is discussed in Section 2.4.1 in conjunction with Estimation Loss.

2.4.1 STAP Estimation Loss and Secondary Data Support

To determine the Estimation Loss (as well as the Detection Loss), the number of secondary samples (i.e. i.i.d. range bins) assumed available for STAP covariance estimation must be selected. This number can vary drastically in practice, but it has already been mentioned that a (severely) nonhomogenous clutter environment is of interest. Thus a relatively small number of secondaries is implied. In Figure 2-9, the Estimation Loss is plotted versus the number of secondaries used and parameterized with respect to the data vector dimensions corresponding to the systems considered in this study. Estimation Loss is a weak function of P_d, and these curves are useful over a wide range of detection probabilities (at least for $.05 < P_d < .95$). Due to the factorization of Detection Loss into SINR Loss and Estimation Loss, the system engineer can study the effects of different system architectures and algorithms on each loss term independently. For the purpose of illustrating Detection Loss in a nonhomogenous environment, the number of secondary data samples used for STAP covariance estimation is selected to be 120 (unless indicated otherwise). Note that
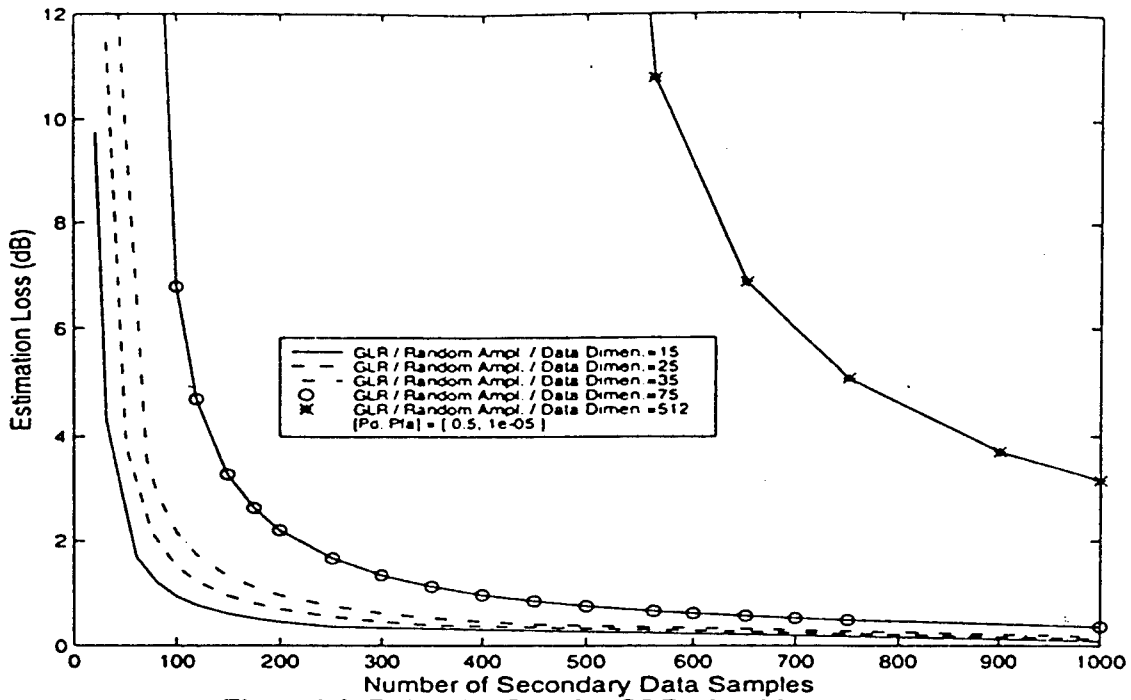
Figure 2-9: Estimation Loss for GLR Algorithm

this number is insufficient to generate an invertible covariance matrix for the FA systems considered here. Therefore, Detection Loss of the FA systems will be based on using a secondary data sample set 10% larger than the space-time FA data vector dimension (i.e. $K=1.1*N_c*N_t$). The FA results are meant for reference only; as an indication of the FA system capability if the number of 'adequately i.i.d.' range bins available is minimally sufficient to perform FA processing.

2.4.2 Performance for Systems Required to Handle a Few WNJs

The '4-Auxiliary' system is required to handle up to 4 WNJs for each of the clutter scenarios, and therefore the number of auxiliary channels is $M_s=4$. Through numerical analyses, it has surfaced that for most of the scenarios investigated, 3 spatial STAP DOF are sufficient for clutter suppression, and therefore $N_s=3$ spatial DOF is chosen for the Baseline systems. However, for the case with 2 clutter-region jammers, 5 spatial STAP DOF are needed to obtain good performance and hence this number is sometimes used. Some results for the '4-Auxiliary' case are given in the following subsections.

43

2.4.2.1 Performance in the Absence of Jammers

The first step in the analysis of the cascaded configurations is to determine if they will degrade system performance when presented with a scenario for which they are not needed (i.e. WNJ free interference). Using the clutter-only scenarios of Section 2.2.4 the five baseline systems are compared. Representative Detection Loss results are given in Figure 2-10 and Figure 2-11. The cascaded systems per-
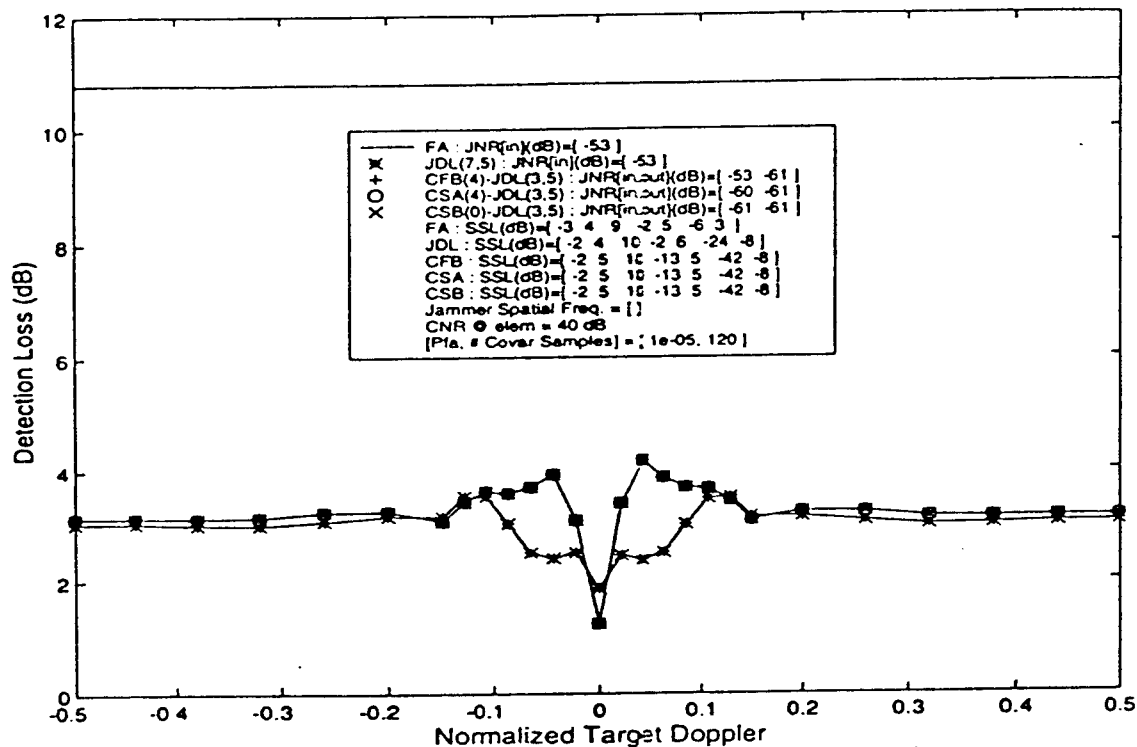

Figure 2-10: Detection Loss without Jammers: 4-Aux/Scenario A

form at least as well as reference systems (i.e. the FA and JDL systems) and exhibit no detrimental effects for clutter-only scenarios. Note that all the reduced DOF systems exhibit significantly lower spatial SSL levels (response plots not shown) away from the mainlobe as indicated by SSL4&6 shown in the figure legends. Also note that the Detection Loss for the FA system is not a function of target Doppler, because it incurs no SINR Loss and Estimation Loss is independent of s, R, and T.

2.4.2.2 Performance Studies for Sidelobe WNJ Environments

WNJs located in the "sidelobe region" facilitate the analysis of jammer suppression without the added complication of clutter suppression degradation. Stated another way, sidelobe jammer suppression

Detection Loss (dB)

12

10

8

6

4

2

0
-0.5 -0.4 -0.3 -0.2 -0.1 0 0.1 0.2 0.3 0.4 0.5

Normalized Target Doppler

Legend:
```
——    FA : JNR[in](dB)=[ -53 ]
 ✱    JDL(7,5) : JNR[in](dB)=[ -70 ]
 +    CFB(4)-JDL(3,5) : JNR[in,out](dB)=[ -70  -71 ]
 O    CSA(4)-JDL(3,5) : JNR[in,out](dB)=[ -66  -71 ]
 X    CSB(0)-JDL(3,5) : JNR[in,out](dB)=[ -71  -71 ]
      FA : SSL(dB)=[ -3  3  10  -2  6  -7  4 ]
      JDL : SSL(dB)=[ -2  3  11  -3  6  -36  -8 ]
      CFB : SSL(dB)=[ -2  5  10  -14  5  -40  -8 ]
      CSA : SSL(dB)=[ -2  5  10  -14  5  -40  -8 ]
      CSB : SSL(dB)=[ -2  5  10  -14  5  -40  -8 ]
      Jammer Spatial Freq. = [ ]
      CNR @ elem = 40 dB
      [Pfa, # Covar Samples] = [ 1e-05, 120 ]
```
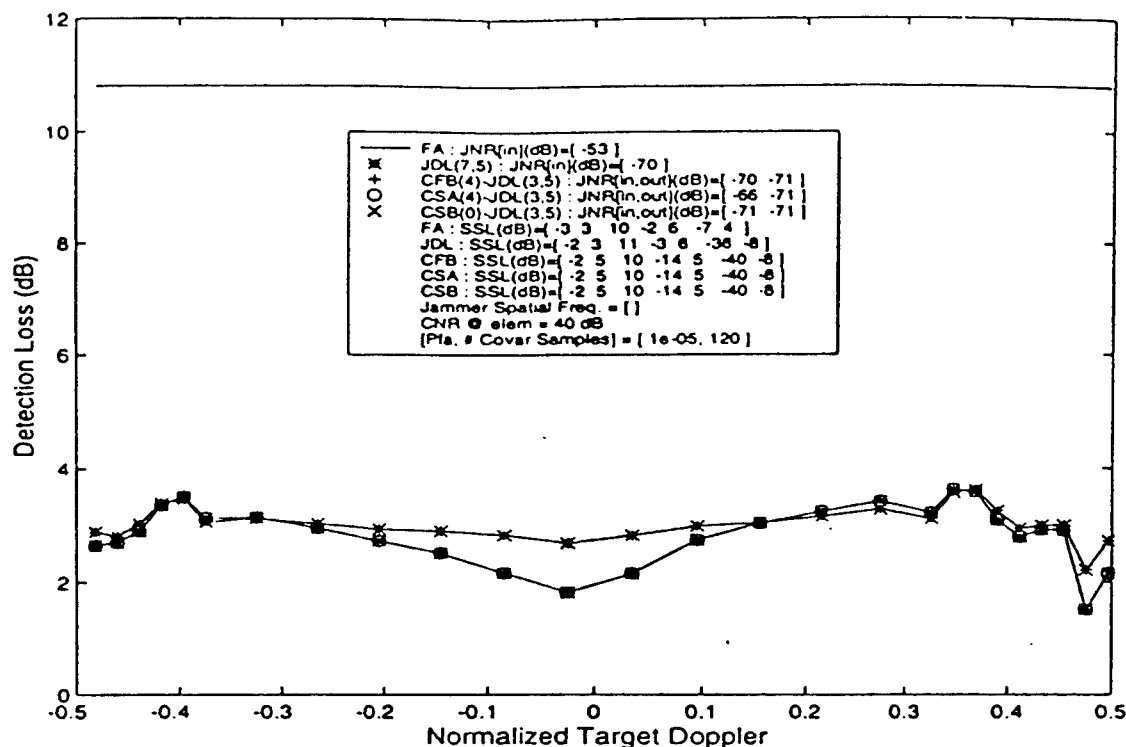
Figure 2-11: Detection Loss without Jammers: 4-Aux/Scenario D

will have much less effect on STAP performance than clutter region jammers as long as the number of jammers does not exceed the number of auxiliary channels. The clutter scenarios used in Section 2.2.4 are used along with sidelobe WNJs to compare the five baseline systems. The JNRs for each jammer will always be the same (unless stated otherwise) and for these results are set to 60dB. Detection Loss results are given in Figure 2-12 and Figure 2-13 for clutter scenarios A and D respectively. System Response spatial patterns are given in Figure 2-14 and Figure 2-15 for a system tuned to a target with the spatial and Doppler frequencies specified in the plot legend. The System Response spatial pattern plot is a spatial cut from the two-dimensional System Response at the specified target Doppler. Note that the CSA system produces SSL levels in-between that of the FA system and the other systems and also exhibits more detection loss than the other cascaded systems for target Dopplers approaching the mainlobe clutter. So far Detection Loss has been used for performance comparisons. From this point on it is desirable to focus in on SINR Loss since the system architecture and algorithm differences will be primarily a function of s, R, and T. If Detection Loss is of interest for a particular level of secondary sample support then the appropriate Estimation Loss from Figure 2-9 can be added to the SINR Loss results. Thus, in Figure 2-16 and Figure 2-17 SINR Loss
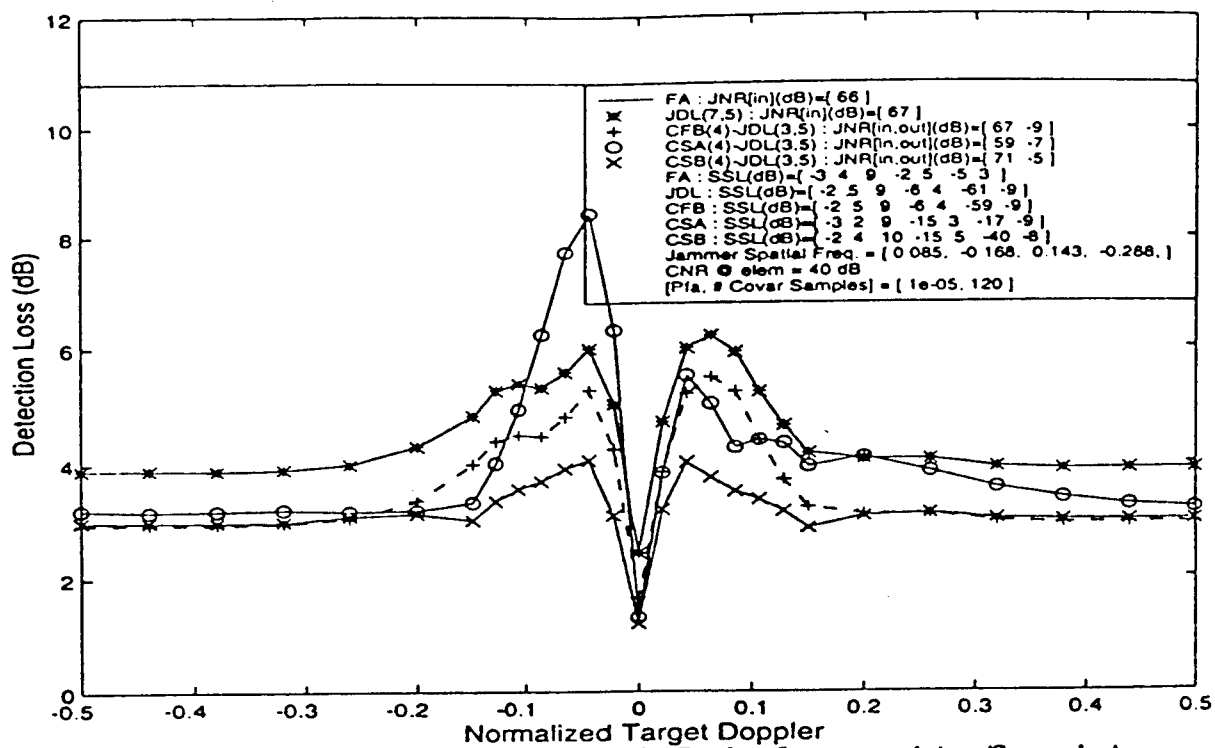
45

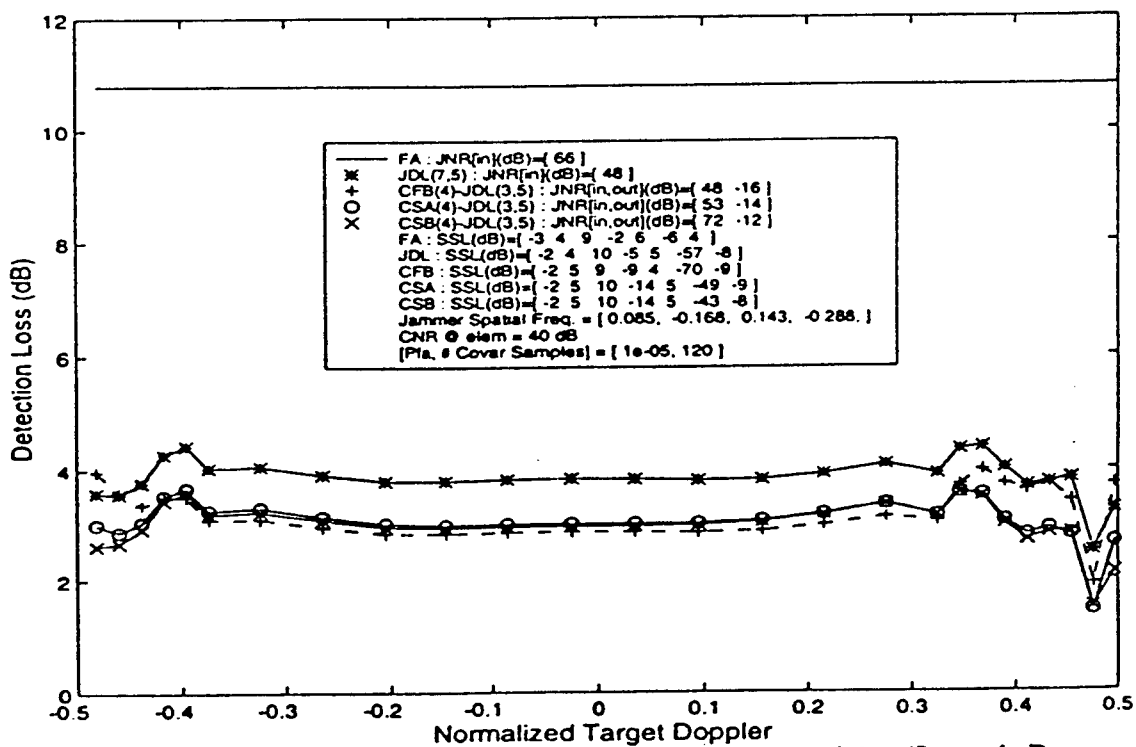Figure 2-12: Detection Loss with Sidelobe Region Jammers: 4-Aux/Scenario A

Figure 2-13: Detection Loss with Sidelobe Region Jammers: 4-Aux/Scenario D
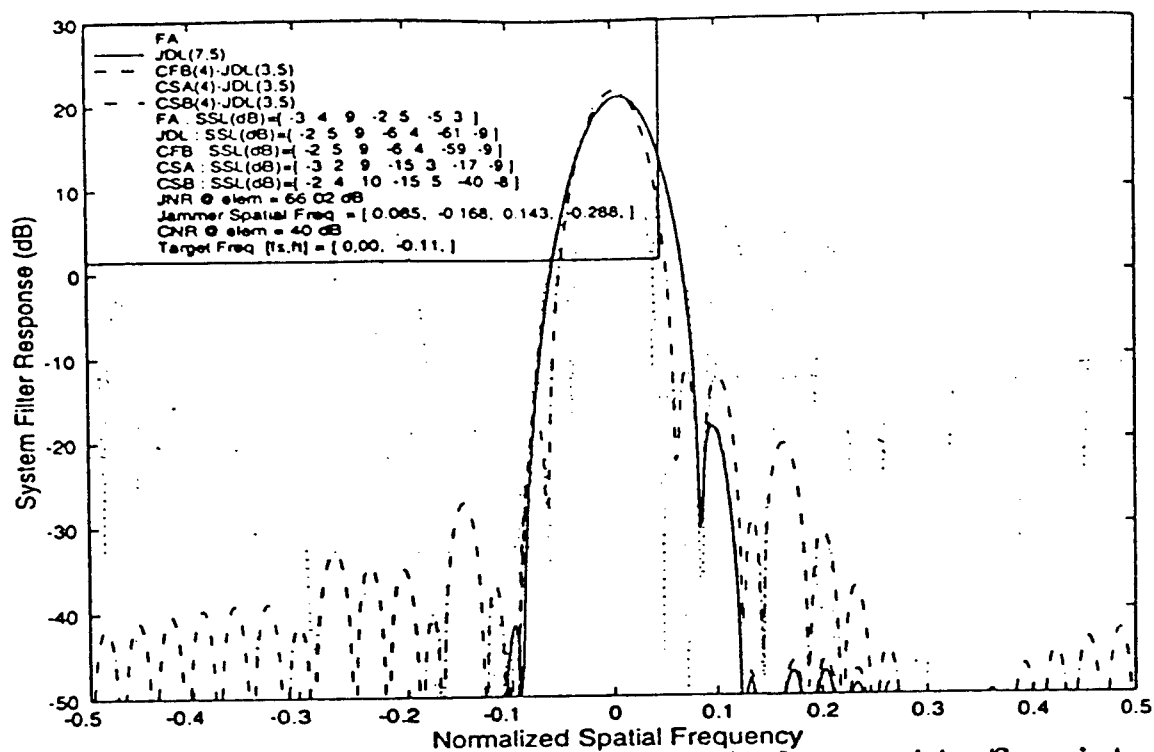
46

Figure 2-14: Spatial System Response with Sidelobe Region Jammers: 4-Aux/Scenario A
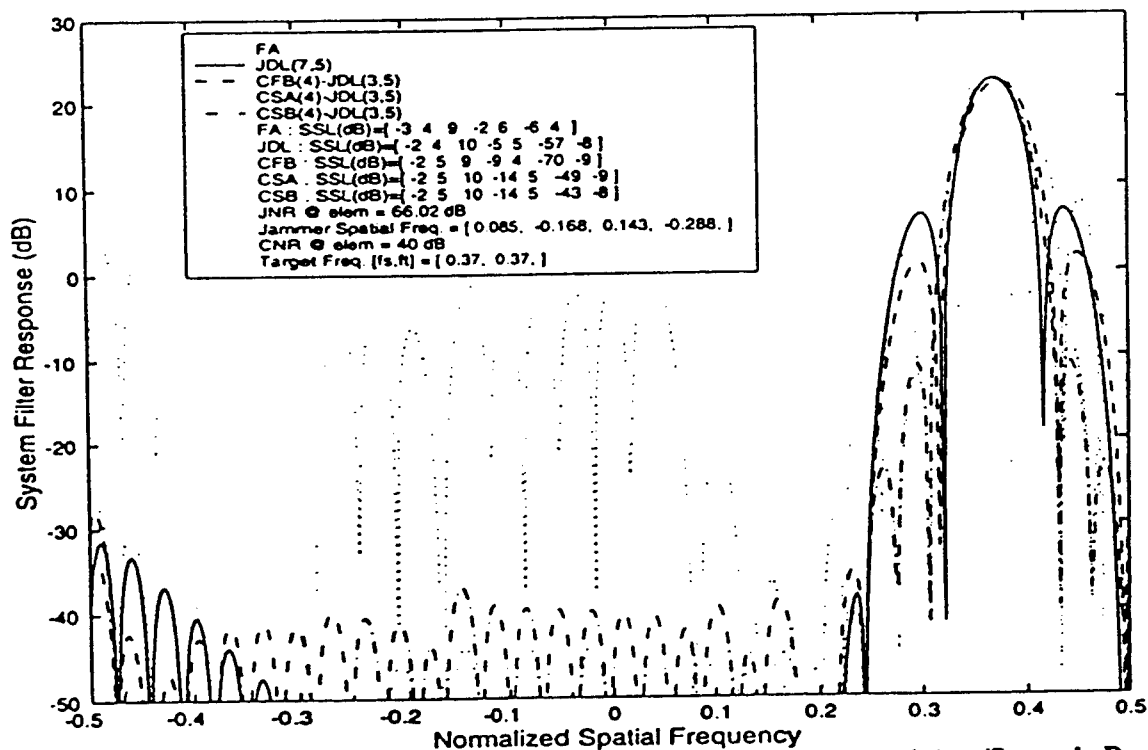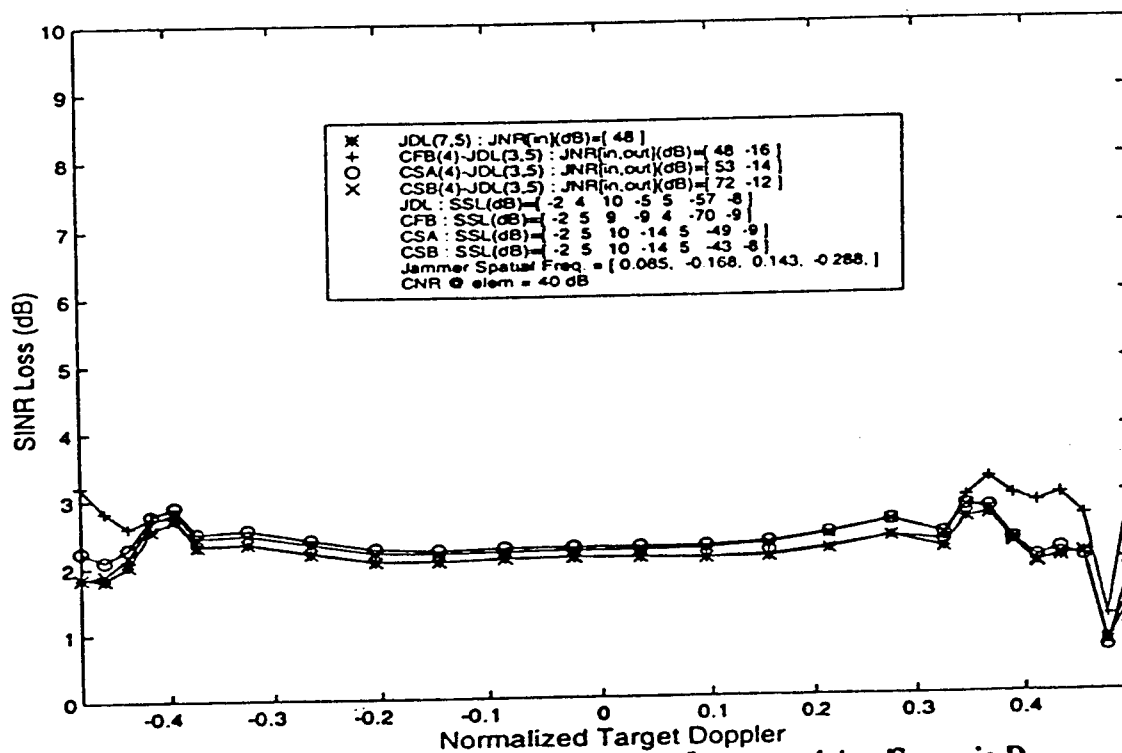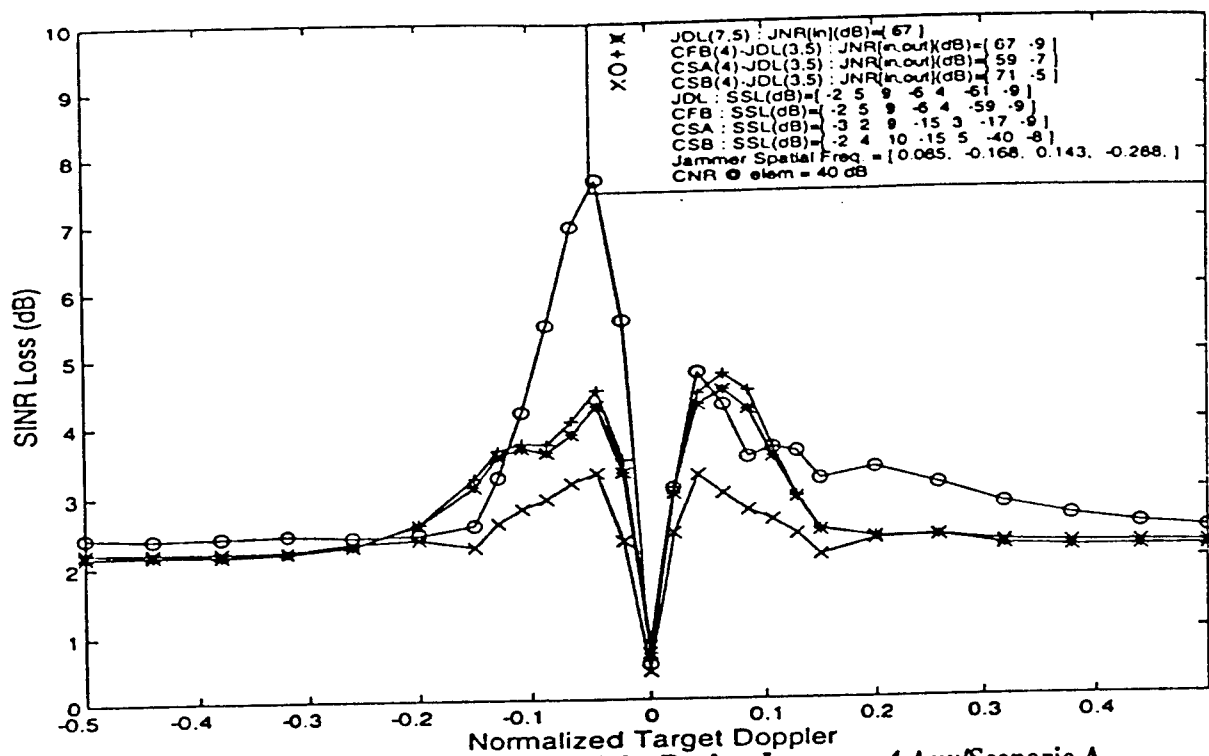

Figure 2-15: Spatial System Response with Sidelobe Region Jammers: 4-Aux/Scenario D

Figure 2-16: SINR Loss with Sidelobe Region Jammers: 4-Aux/Scenario A

Figure 2-17: SINR Loss with Sidelobe Region Jammers: 4-Aux/Scenario D

results are included for completeness and ease of comparison with future results.

2.4.2.3 Performance Studies with WNJ's in the Clutter Region

As mentioned previously, it is presumed that the clutter subspace defined by the N_s spatial STAP

channels has been designed in order to provide good clutter suppression. It is desirable to minimize perturbation of this subspace while rejecting WNJ power. However, when a jammer angle is located within the clutter region noticeable perturbation is inevitable. Hence, it is of interest to determine which system architectures are robust under these circumstances. Scenario A results are given in Figure 2-18 and Figure 2-19
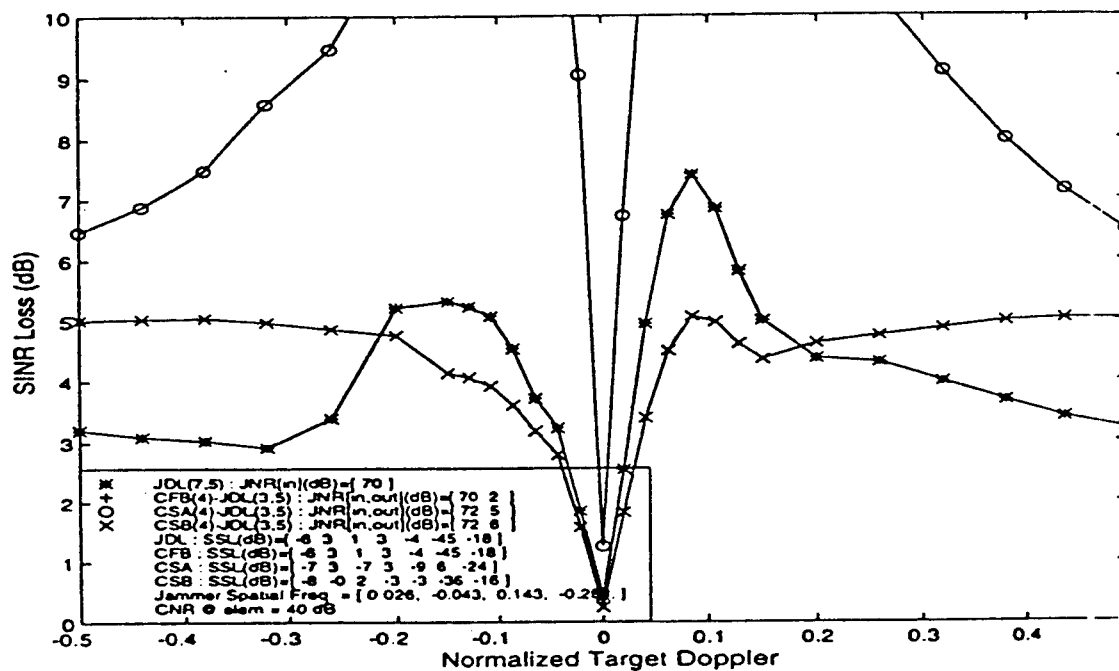
Figure 2-18: SINR Loss with Clutter Region Jammers: 4-Aux/Scenario A

with two of the four jammers located within the clutter region, but not in the mainlobe (i.e. target region).

Significant SINR loss is evident for the CSA-JDL system possibly indicating a fundamental problem with

this approach for clutter region jammers. The other two cascaded systems showing performance comparable to the JDL. Reduction in SINR for all systems (including the maximum attainable given by the FA system) is evident by comparing the System Response of Figure 2-19 to Figure 2-14 at $f_s=0$. Note that all the

reduced DOF systems exhibit more SINR Loss than in the sidelobe jammer case. Also note that the output

Figure 2-19: Spatial System Response with Clutter Region Jammers: 4-Aux/Scenario A

jammer levels (shown in terms of JNR in the plot legends) are not suppressed to the noise floor as in previous results. Scenario D performance results with two clutter region jammers are given in Figure 2-20. The results are similar to those for Scenario A except that the CSB-JDL system is showing slightly poorer performance. Substantial performance improvement can be achieved by increasing the number of spatial STAP channels to $N_s=5$ as shown in Figure 2-21 and Figure 2-22. Evidently, having two jammers in the clutter region requires more STAP DOF in order to maintain a low SINR loss. Increasing the number of ASP DOF (i.e. M_s), however, does not provide the same performance improvement.

2.4.2.4 Performance Studies with WNJ's in the Target Region

The most severe angular location for a jammer is near the desired signal. In this case it is of interest to determine if the cascaded approach to WNJ cancellation is still viable, or if the jammer now needs to be handled at the same time as the clutter. Said another way, when the jammer resides within the target subspace it may be advisable to supply the STAP filter with all the interference information. Performance results for the case with one jammer in the target region and three sidelobe jammers is shown in Figure 2-23 for Scenario A and Figure 2-24 for Scenario D. The SINR Loss for the JDL and CFB-JDL are very

50

Figure 2-20: SINR Loss with Clutter Region Jammers: 4-Aux/Scenario D

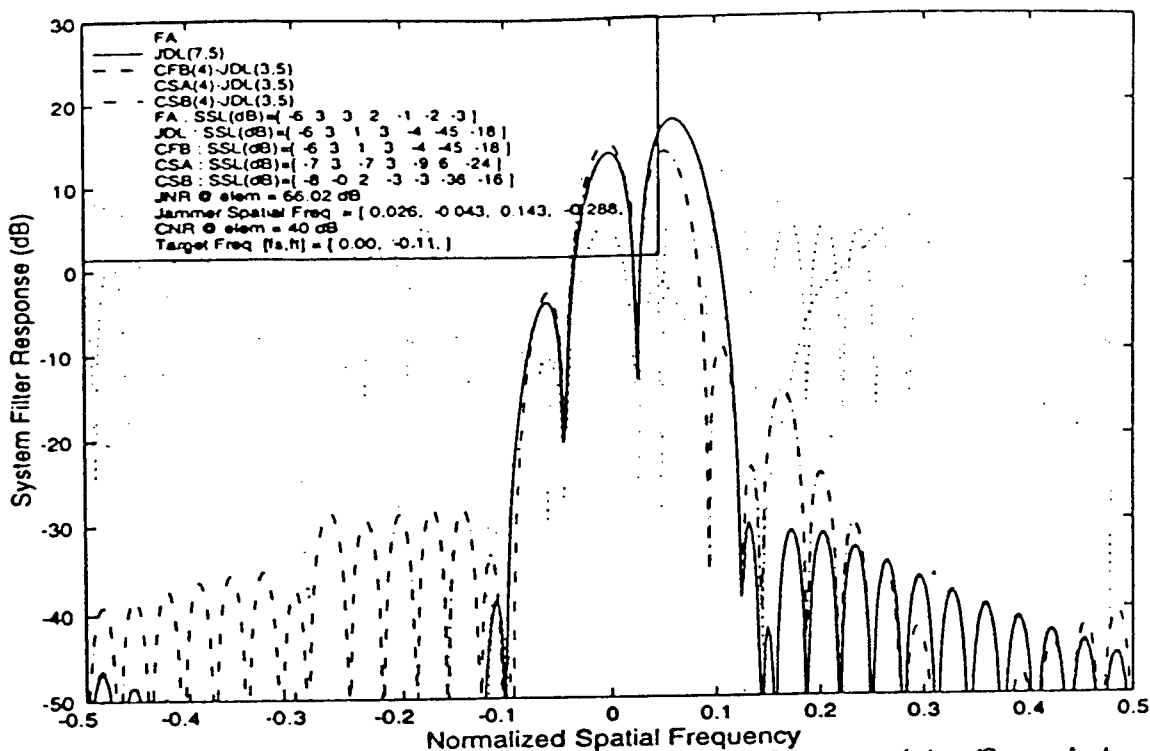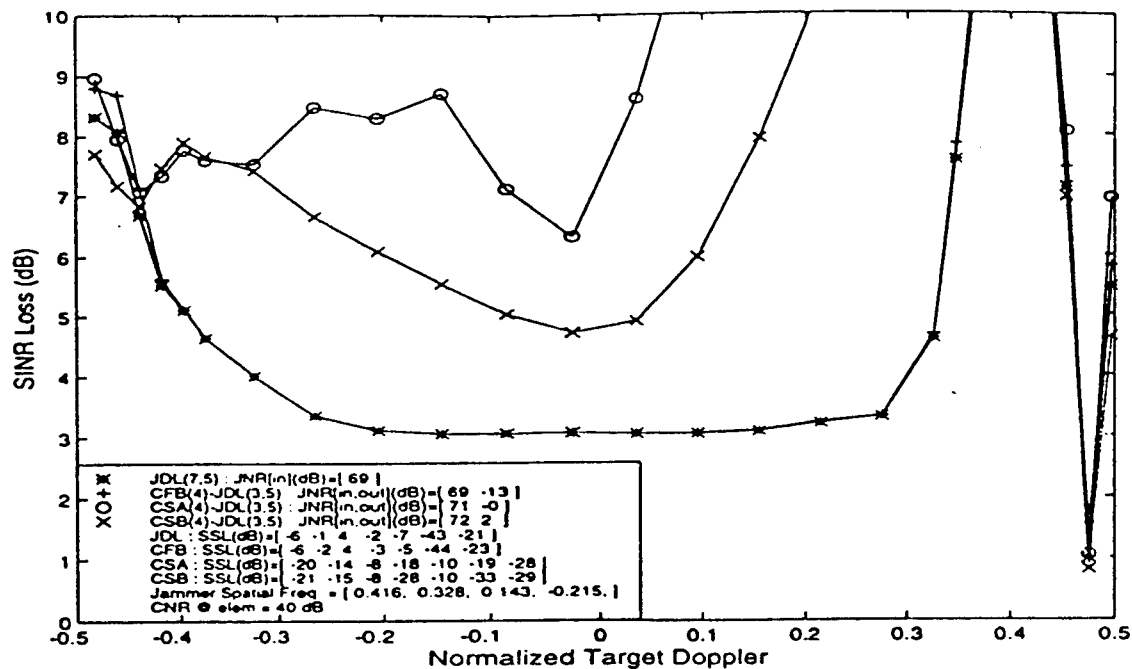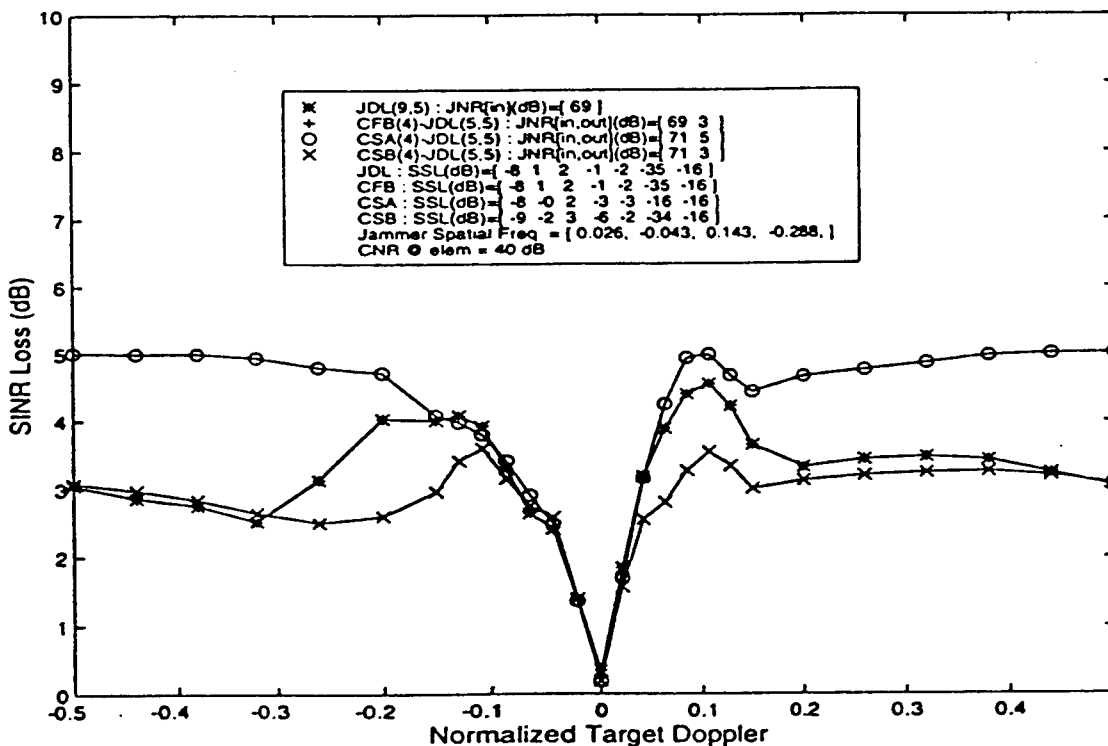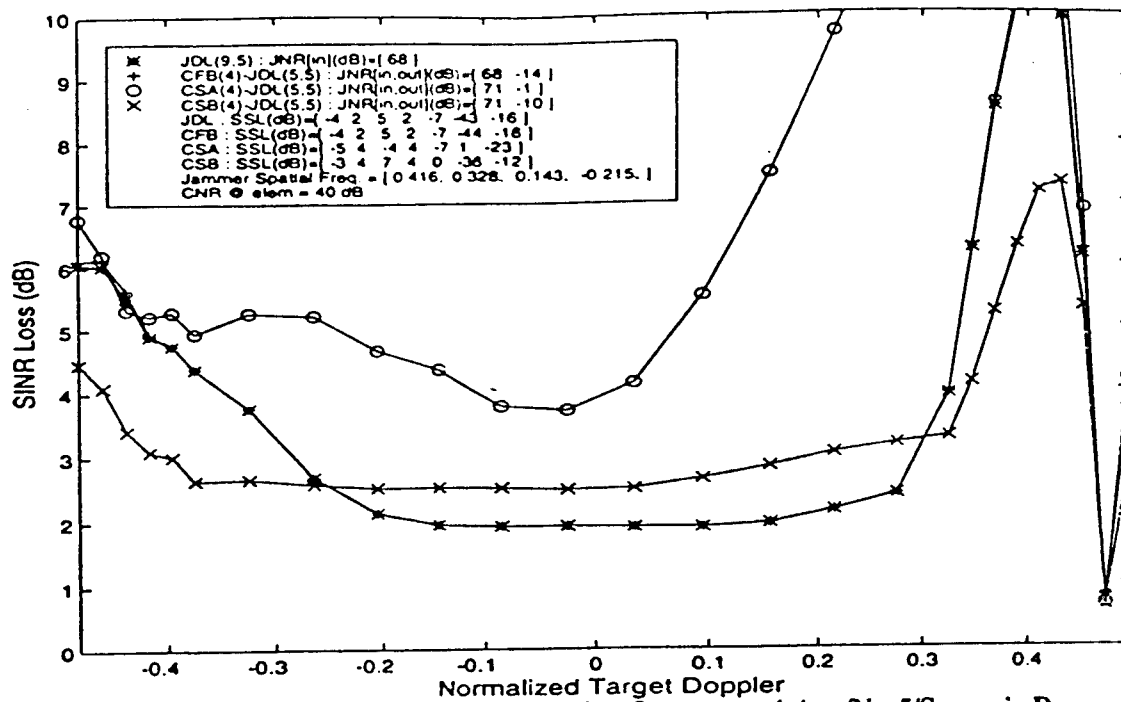**Figure 2-21: SINR Loss with Clutter Region Jammers: 4-Aux/N$_s$=5/Scenario A**

Figure 2-22: SINR Loss with Clutter Region Jammers: 4-Aux/N_s=5/Scenario D
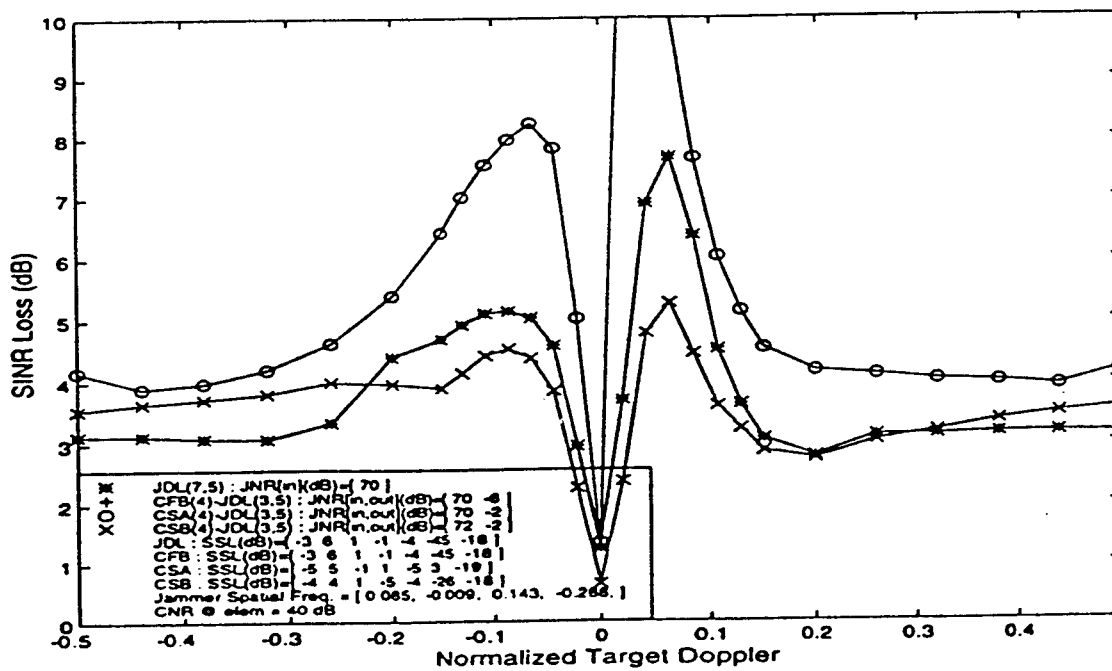
Figure 2-23: SINR Loss with Target Region Jammer: 4-Aux/Scenario A
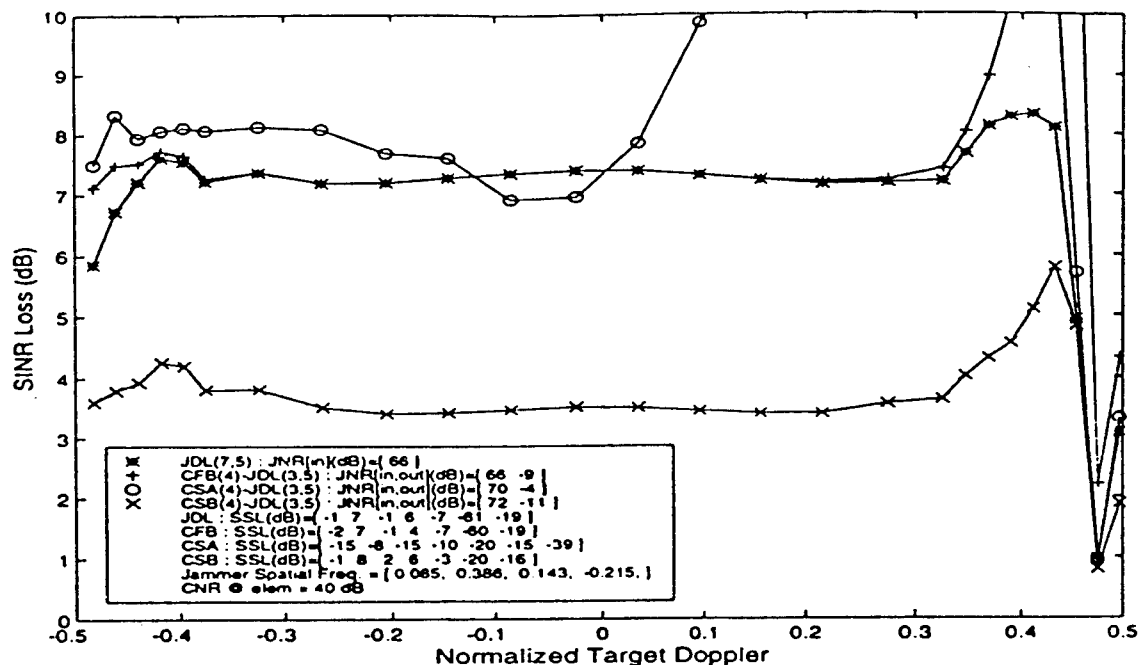
Figure 2-24: SINR Loss with Target Region Jammer: 4-Aux/Scenario D

close, while the CSB-JDL system exhibits quite robust behavior for this case. A spatial cut of the System

Response for Scenario A is given in Figure 2-25. As expected, the SINR's at $f_s=0$ are greatly reduced for all

the systems including the SINR Bound (or FA system).

2.4.3 Performance for Systems Required to Handle Many WNJs

The '12-Auxiliary' system is required to handle up to 12 WNJs for each of the clutter scenarios.

Accordingly, the number of auxiliary channels is set to $M_s=12$. The WNJ scenarios will contain four jam-

mers as in Section 2.4.2, but this time the number of auxiliary channels exceeds the number of jammers by

a factor of three. The number of spatial STAP channels is selected as $N_s=3$ as in Section 2.4.2. Selected

results for the '12-Auxiliary' case are given in the following subsections.

2.4.3.1 Performance Studies for Sidelobe WNJ Environments

The cascaded systems show better detection performance than the JDL and FA systems for the

sidelobe jammer case shown in Figure 2-26 for scenario A and Figure 2-27 for Scenario D. They also

exhibit better SSL levels as indicated in the plot legends and as demonstrated in the System Response spa-

53

Figure 2-25: Spatial System Response with Target Region Jammer: 4-Aux/Scenario A

Figure 2-26: Detection Loss with Sidelobe Jammers: 12-Aux/Scenario A
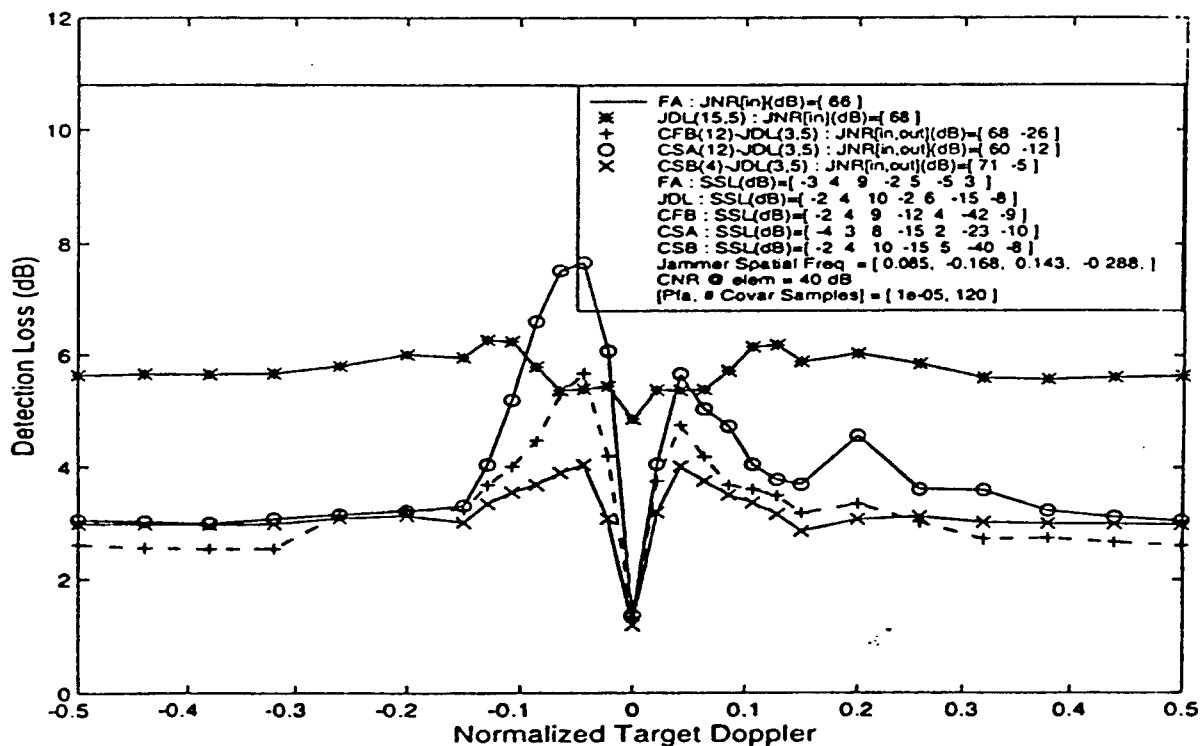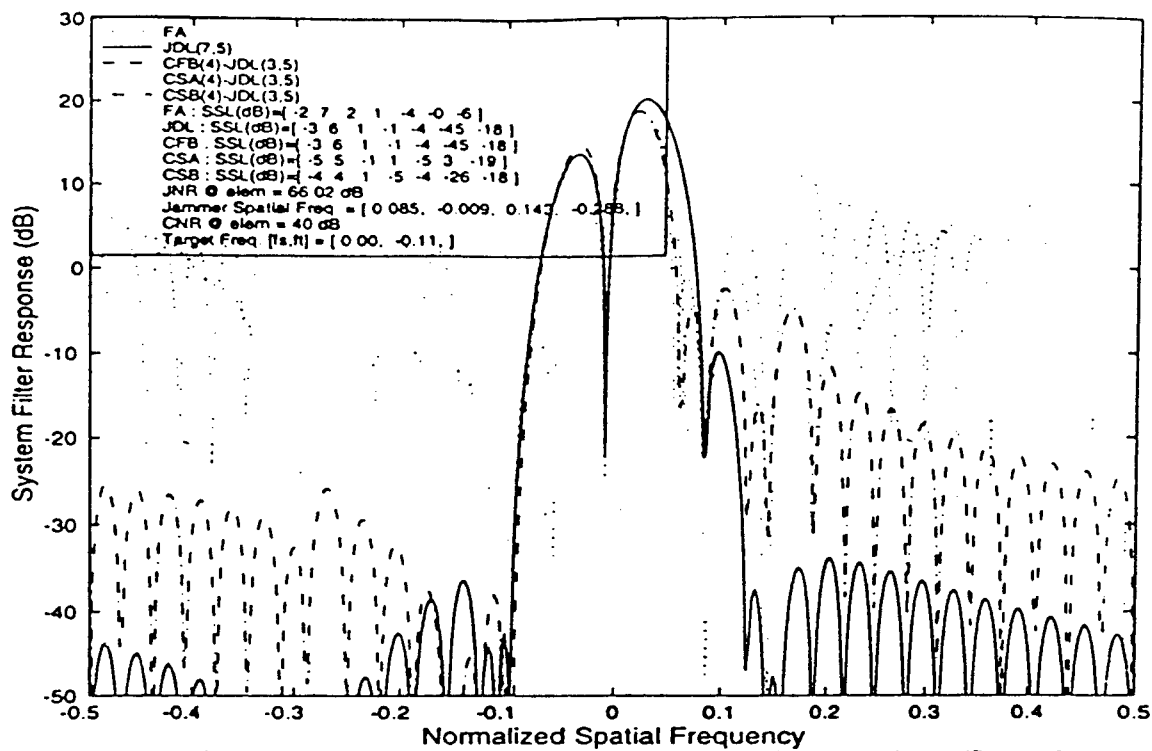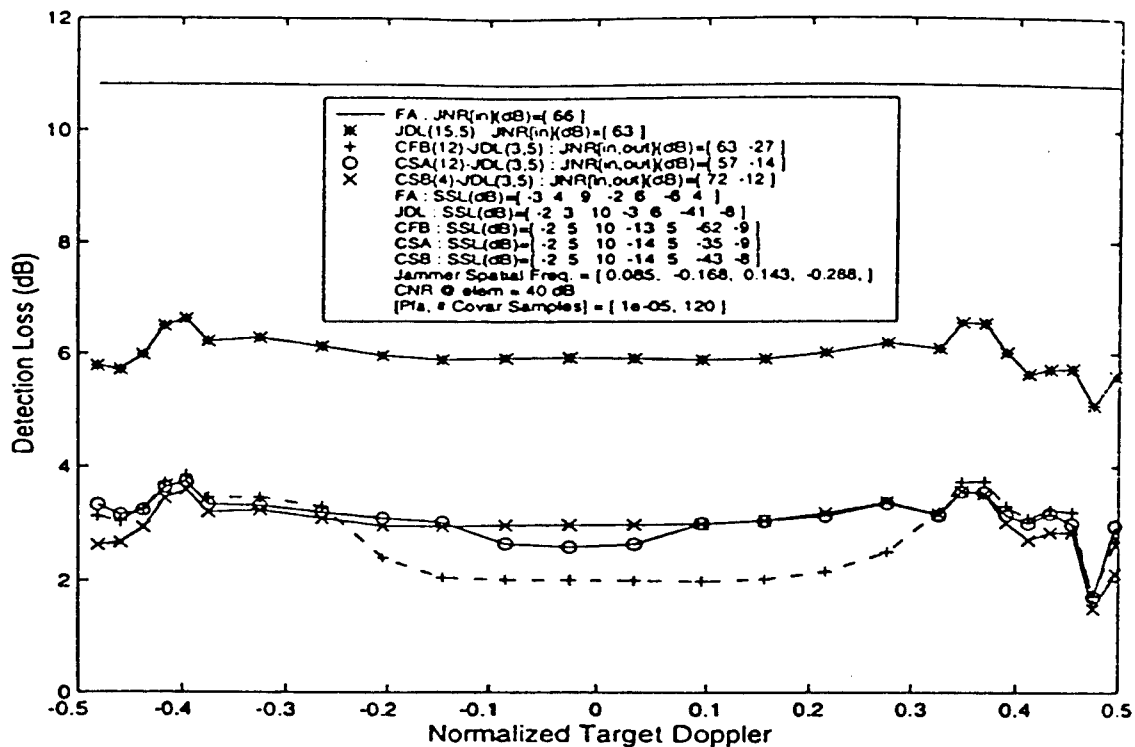
Figure 2-27: Detection Loss with Sidelobe Jammers: 12-Aux/Scenario D

tial cut of Figure 2-28 for Scenario A. Similar results are obtained for Scenario D. Thus, the cascaded systems have better detection performance as well as more protection against extraneous signals in the test range cell. Since SINR Loss is used for comparative analyses, it is shown here in Figure 2-29 and Figure 2-30. Comparing the SINR Loss with the Detection Loss reveals a substantial Estimation Loss for the JDL system of about 5 dB for the case where 120 secondary samples are used.

2.4.3.2 Performance Studies with WNJ's in the Clutter Region

As in Section 2.4.2.3 with clutter region jammers, it is expected that the cascaded systems will show some performance degradation, but now the JDL should not degrade as much since it has many extra DOF to use. These expectations are realized as shown in Figure 2-31 for Scenario A and in Figure 2-32 for Scenario D. Note that the CFB-JDL system in particular maintains relatively good SINR performance. Although the performance degradation for WNJs in the clutter is not as pronounced as in the '4-Aux' case, the performance of all the cascaded systems can be still be noticeably improved if the number of STAP spatial channels is allowed to increase to $N_s=5$ as evidenced by Figure 2-33 for Scenario A.

Figure 2-28: Spatial System Response with Sidelobe Jammers: 12-Aux/Scenario A

Figure 2-29: SINR Loss with Sidelobe Jammers: 12-Aux/Scenario A

56

Figure 2-30: SINR Loss with Sidelobe Jammers: 12-Aux/Scenario D

Figure 2-31: SINR Loss with Clutter Region Jammers: 12-Aux/Scenario A
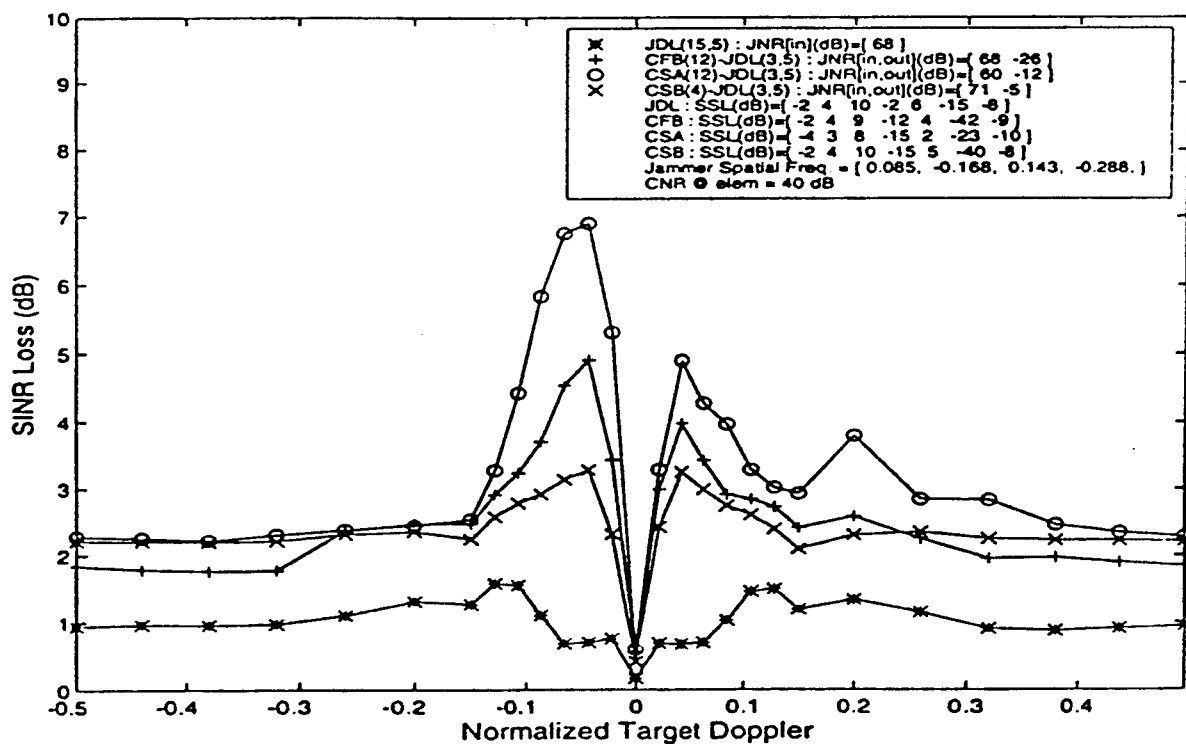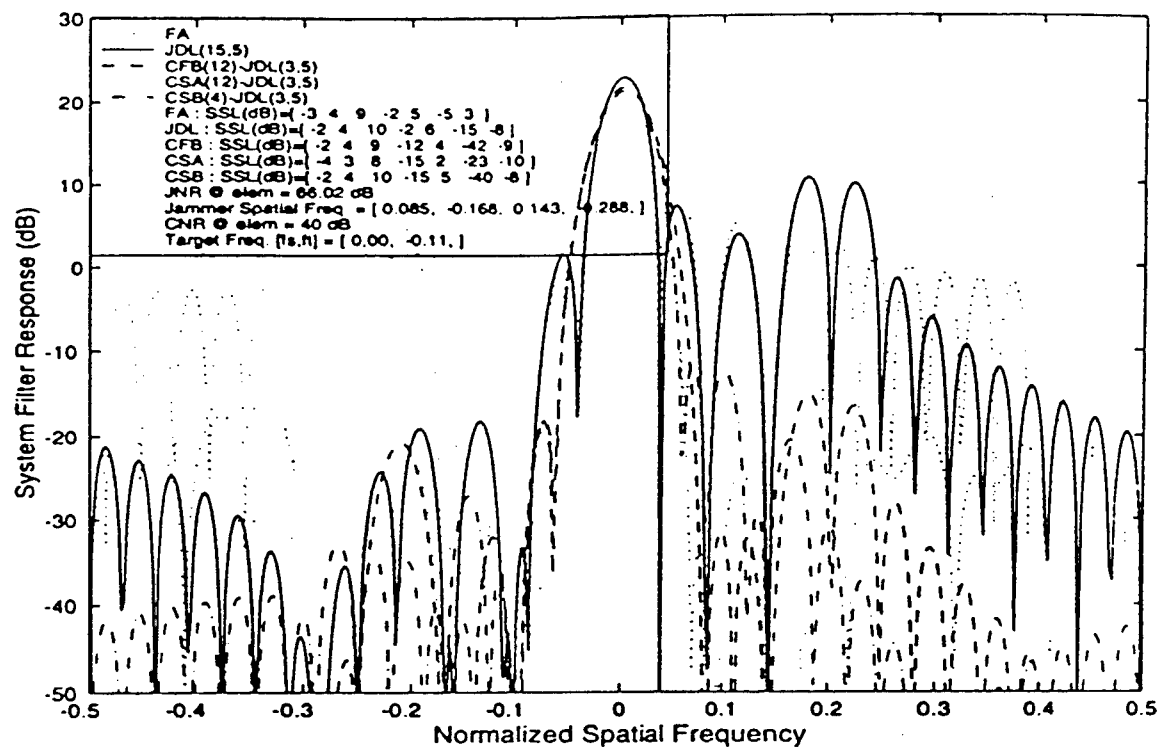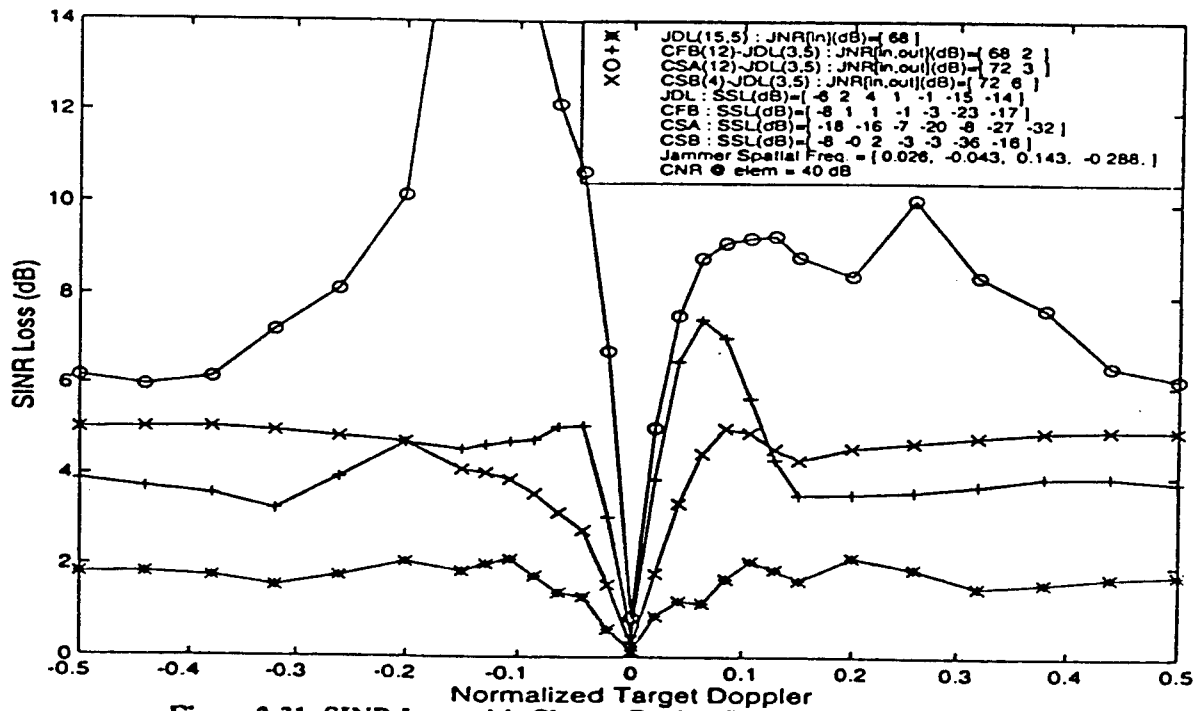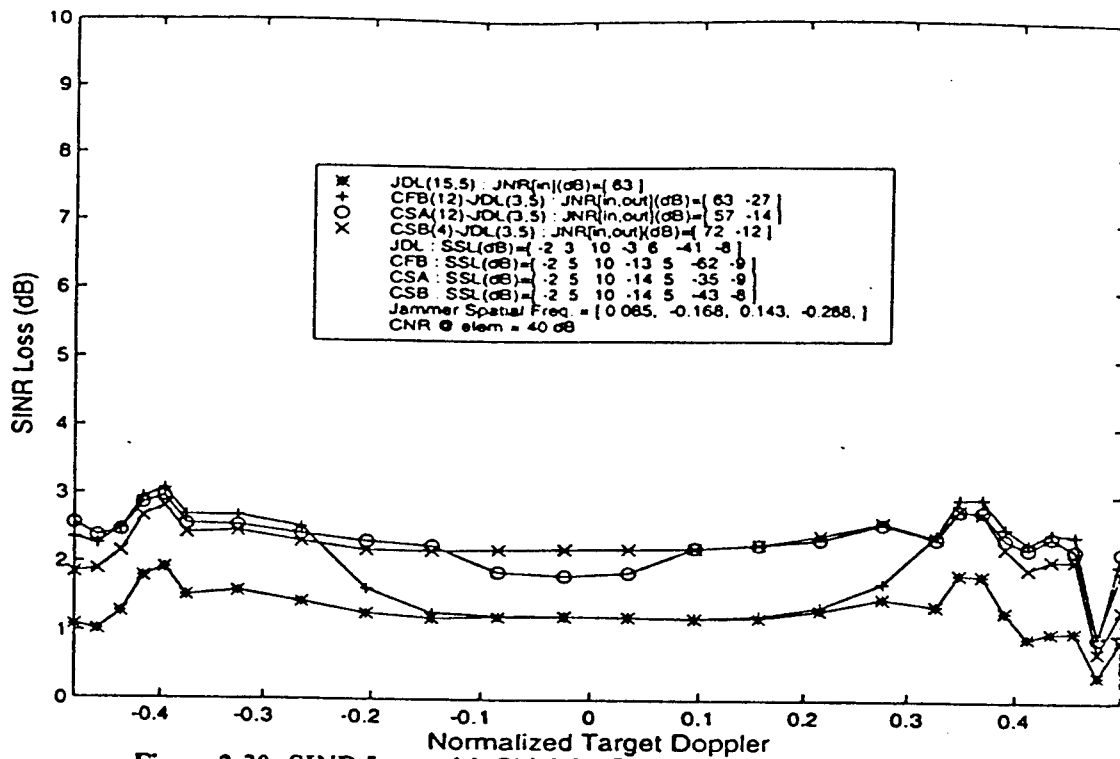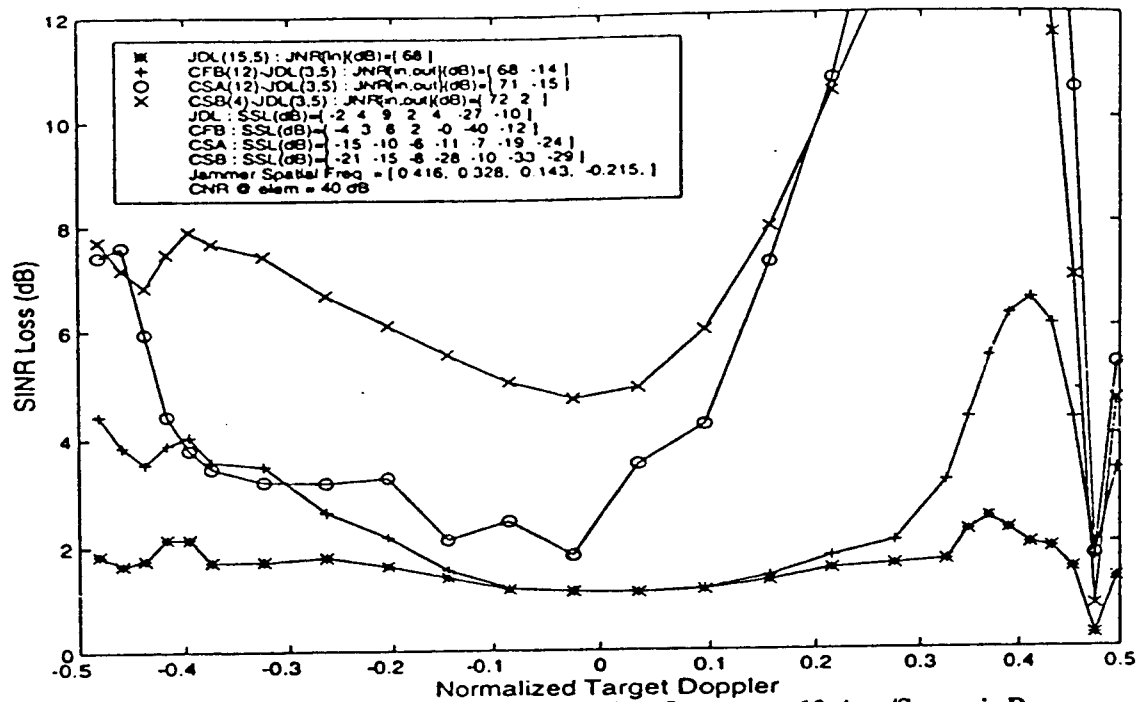
Figure 2-32: SINR Loss with Clutter Region Jammers: 12-Aux/Scenario D
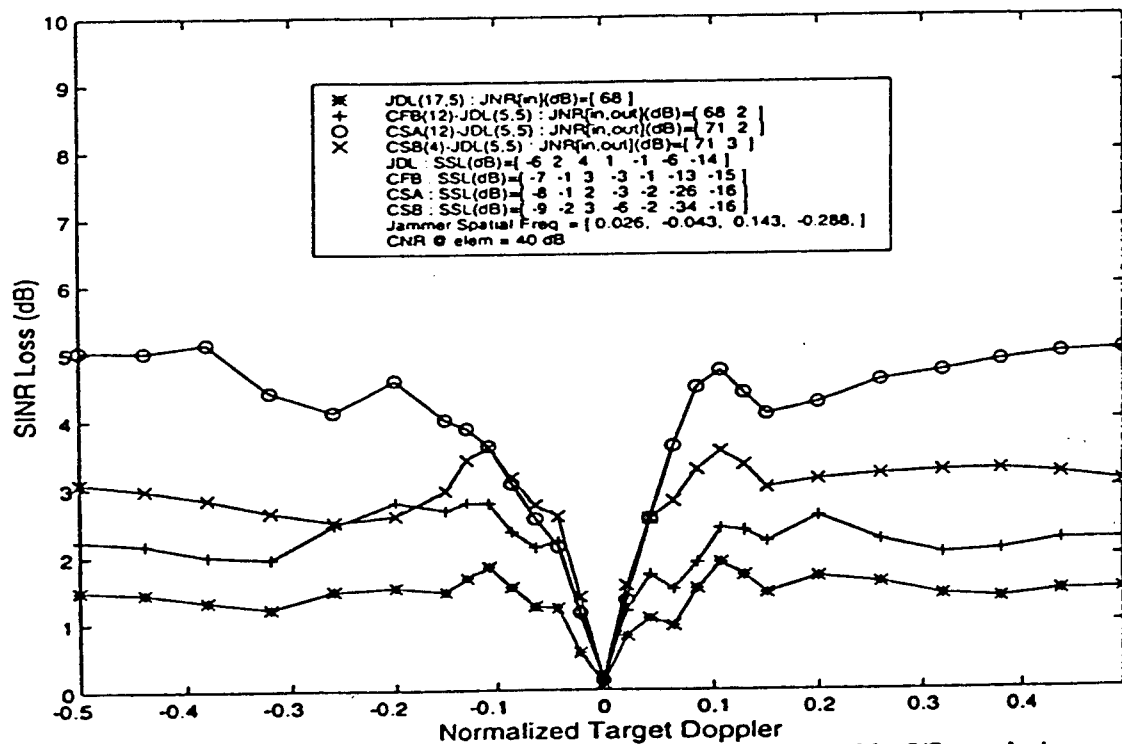
Figure 2-33: SINR Loss with Clutter Region Jammers: 12-Aux/N_s=5/Scenario A

2.4.3.3 Performance Studies with WNJ's in the Target Region

The performance of the CFB-JDL and CSB-JDL systems remain competitive with the JDL for the case with one jammer in the target region and three sidelobe jammers for both Scenario A and D as evidenced by the SINR Loss results in Figure 2-34 and Figure 2-35. However, the CSA-JDL system shows
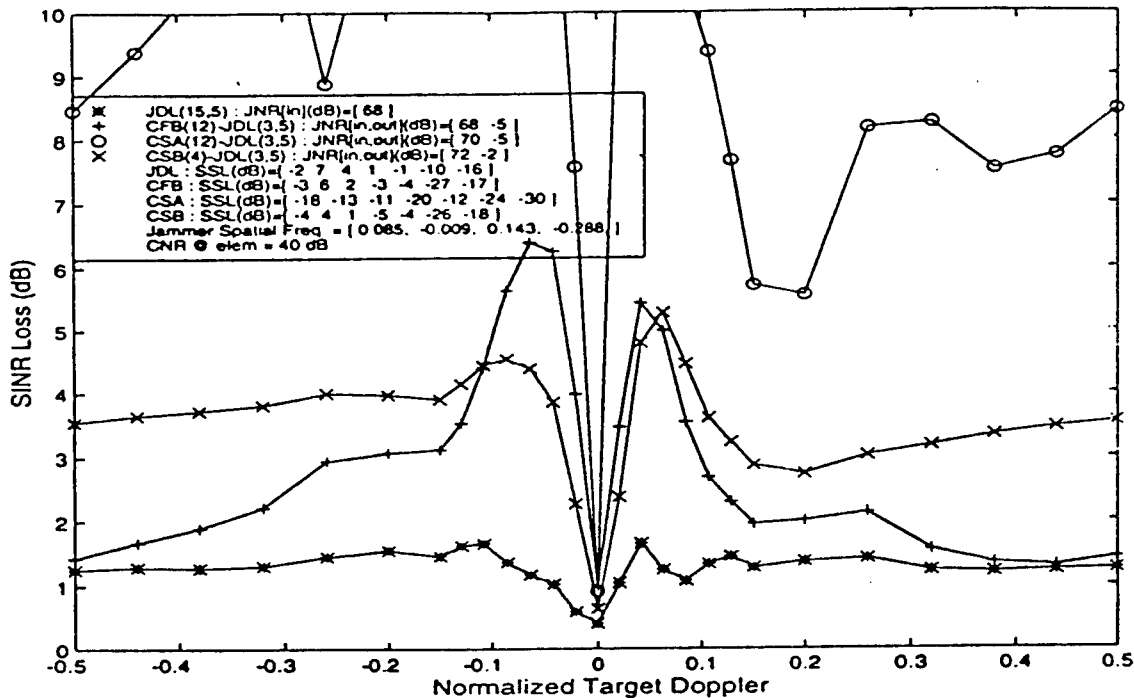
Figure 2-34: SINR Loss with Target Region Jammers: 12-Aux/Scenario A

considerable SINR degradation as was the case for the '4-Aux' systems.

2.4.4 Discussion of Baseline Performance Results

The preceding performance studies have shown that cascaded systems are a viable alternative to the combined clutter and WNJ suppression problem, and are the preferred approach in circumstances with limited secondary support in terms of Detection Loss as well as extraneous signal protection. Even under circumstances with jammers within the clutter and/or signal subspace, for which the cascaded approach is at a disadvantage (since clutter information is unavailable to the ASP), the cascaded systems exhibit competitive results. In addition, very little was said of the implementation benefits. It is easy to see that reducing the number of channels that must be well matched and digitized can greatly improve system

SINR Loss (dB)

10
9
8
7
6
5
4
3
2
1
0

-0.4   -0.3   -0.2   -0.1   0   0.1   0.2   0.3   0.4

Normalized Target Doppler

JDL(15,5) : JNR(in)(dB)=[66]
CFB(12)-JDL(3,5) : JNR(in,out)(dB)=[66 -14]
CSA(12)-JDL(3,5) : JNR(in,out)(dB)=[69 -10]
CSB(4)-JDL(3,5) : JNR(in,out)(dB)=[72 -11]
JDL : SSL(dB)=[-1 8 3 6 -2 -20 -15]
CFB : SSL(dB)=[-1 7 2 4 -3 -29 -16]
CSA : SSL(dB)=[-10 -3 -9 -5 -18 -16 -27]
CSB : SSL(dB)=[-1 8 2 6 -3 -20 -16]
Jammer Spatial Freq. = [0.085. 0.386. 0.143. -0.215.]
CNR @ elem = 40 dB
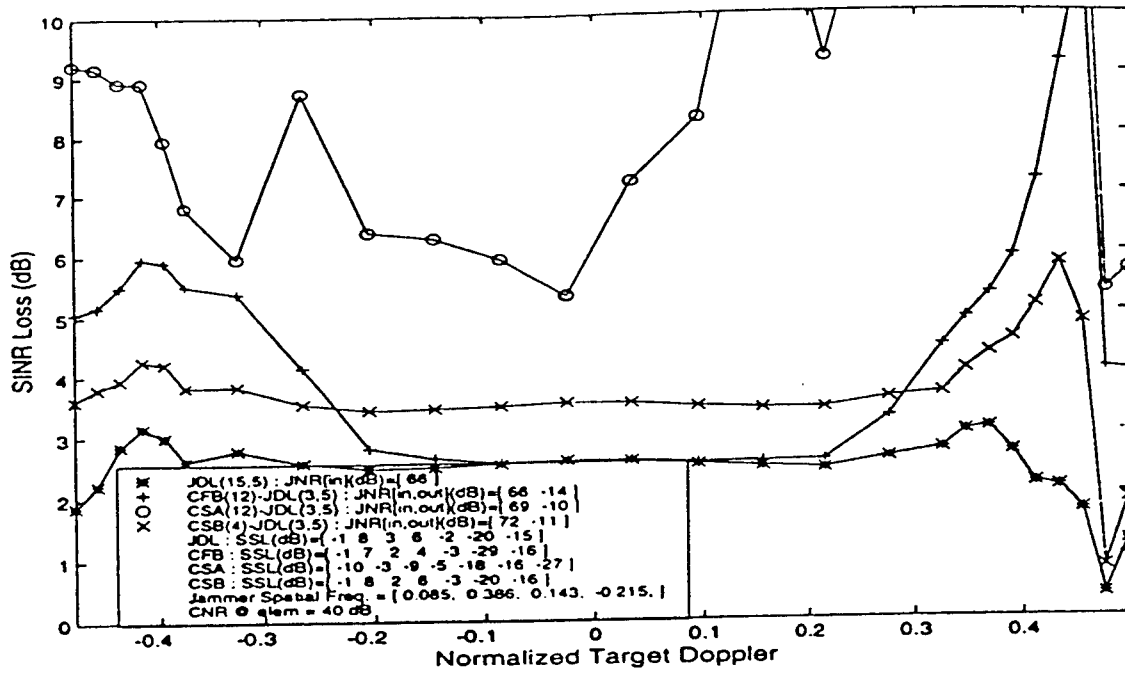
Figure 2-35: SINR Loss with Target Region Jammers: 12-Aux/Scenario D

affordability and reliability. The cascaded systems can also; (1) reduce the number of waveform matched filters (i.e. pulse compressors) which lessens the computational load, (2) reduce the number of STAP channels thereby preserving the performance of adaptive systems in severely nonhomogenous interference environments, and (3) diminish System Response sidelobe levels by eliminating superfluous DOF in the STAP.

3 Implementations and Alternatives for the Adaptive Space Processor

In this section, attention is focused on the implementation of the ASP baseline approaches. The primary topic is how to obtain adequate clutter-free secondary data for WNJ suppression. In the past, clutter-free secondary data extraction has been performed by using data which is known to have none or little amounts of clutter power. Three mainstream techniques are mentioned here. Low-clutter range cells can sometimes be collected during a Low PRF mode, but are restricted to only a portion of a PRI. Low-clutter Doppler regions can be obtained during a high PRF mode, but require special Doppler filtering to isolate low-clutter regions. This technique is usable primarily for circumstances resulting in an uncomplicated space-time clutter spectrum. Clutter-free collection during a passive mode (i.e. non-transmitting) of the Radar is possible, but severely restricts the time period for collection. These techniques all have restrictions on when and how much clutter-free data is available. It is desired to have little or no restrictions on WNJ data collection so that an entire RPI data set can be used if necessary. In this way, Estimation Loss for WNJ covariance estimation can be made negligible. Additional benefits to unrestricted secondary collection are (1) robustness against blinking jammers, (2) very fast adaptation possible (even sub-PRI in some cases), and (3) provides a system foundation amenable to handling the jammer multipath (i.e. hot clutter) problem. Section 3.1 presents an approach which can realize these advantages.

3.1 Sideband Canceller (SBC) Concept

This section develops a new technique for generating the adaptive spatial weights used to suppress WNJ for a general CS-STAP system architecture. The central idea is to obtain clutter free WNJ data using a narrow RF sideband which is adjacent to, but disjoint from, the Radar receiver mainband. The assumption is that the spectrum of a WNJ contributing to the Radar receiver signal will also encompass a non-zero bandwidth surrounding the receiver band. An additional assumption is that an IF or baseband filter can provide a narrow WNJ passband adjacent to the Radar band, but free from any Radar effected signals (i.e. clutter and targets). A conceptual block diagram of the SBC is shown in Figure 3-1. Note that the beamsteering and beamforming transformations are now considered to be functions of the mainband and sideband center frequencies. Thus, where applicable, the response of the sideband channels for different carrier frequencies is accounted for in the analyses. The design of the sideband canceler involves the definition of the Sideband
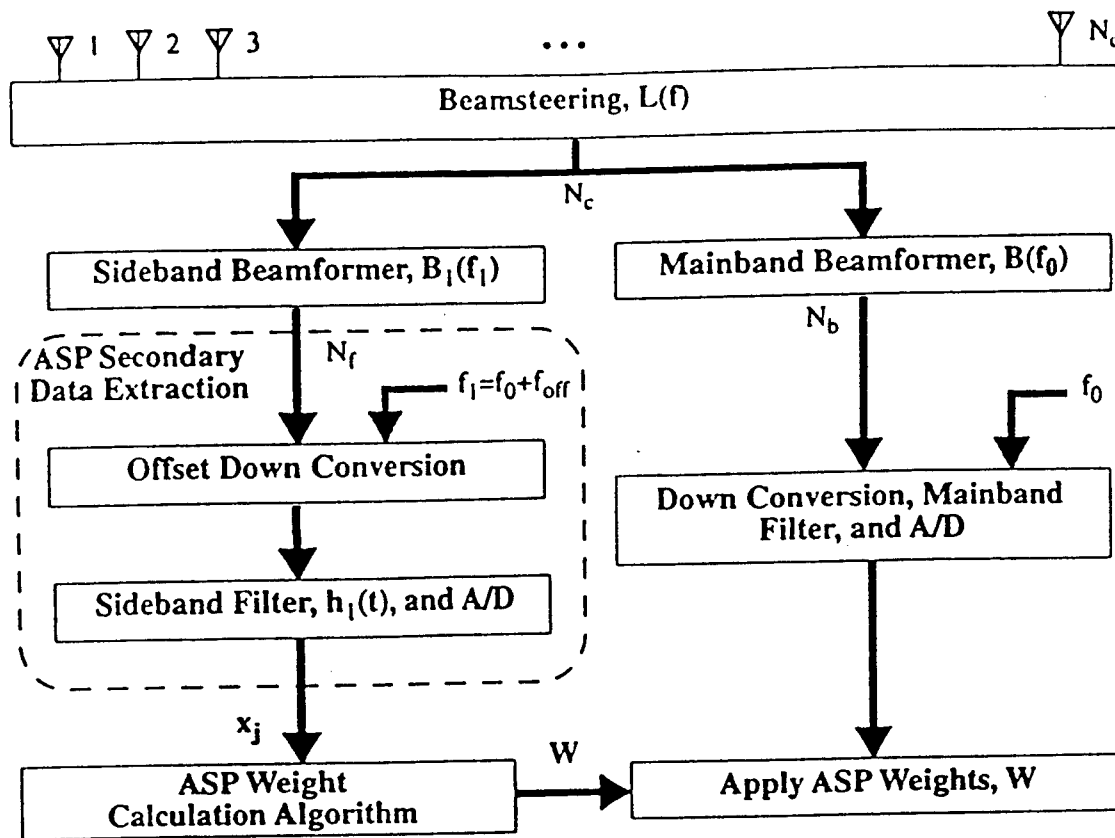
∇ 1 ∇ 2 ∇ 3   · · ·   ∇ N_c

```
┌─────────────────────────────────────────────────────────────┐
│                    Beamsteering, L(f)                         │
└─────────────────────────────────────────────────────────────┘
                              $N_c$
```

| Sideband Beamformer, $B_1(f_1)$ | Mainband Beamformer, $B(f_0)$ |

N_b

┌ ─ ─ ─ ─ ─ ─ ─ ─ ─ ─ ─ ─ ┐
/ASP Secondary N_f
| Data Extraction
| ← $f_1 = f_0 + f_{off}$ ← f_0

| Offset Down Conversion | | Down Conversion, Mainband Filter, and A/D |

| Sideband Filter, $h_1(t)$, and A/D |

x_j

W

| ASP Weight Calculation Algorithm | → | Apply ASP Weights, W |

Figure 3-1: Sideband Canceler Conceptual Block Diagram

Beamsteering, $L_1(f_1)$, and Sideband Beamformer, $B_1(f_1)$, which may or may not be the same type as the mainband beamformer $B(f_0)$, the specification of the Sideband Filter, h_1, and the design of the ASP Weight Calculation Algorithm.

The beamsteering transformation response, $L(f)$, for the different carrier frequencies can be a factor in the performance of the SBC concept, particularly when the Radar look direction is other than broadside. Since a phased-array is considered here, beamsteering takes the form of progressive sensor-to-sensor phase shifts. Array calibration can be included in the beamsteering transformation model, but will not be included here. Hence, $L(f)$ is taken to be a unitary diagonal matrix whose diagonal elements may be functions of the carrier frequencies. However, sensor response variations over the bandwidth of the receiver's mainband (or sideband) will be assumed negligible for all system components as discussed in the System Model descriptions of Section 2.1.

Several SBC approaches will be considered in this section. Although it is important to keep in mind

the dependence of performance, processing complexity, and cost on the type of Sideband Beamformer selected, performance is the primary focus of this investigation. The specific Sideband Beamformer definition for each approach is discussed as needed. Note that the number of beams at the output of the Sideband Beamformer is not necessarily the same as for the mainband, N_b. Some sideband compensation techniques will require more beams in order to obtain satisfactory performance, and in general for this study $N_f \geq N_b$. With regard to system cost it is desirable to minimize the number of receiver channels. However, as will be pointed out later, the bandwidth of a sideband channel is kept quite narrow, and therefore the cost can be substantially less than that of a mainband channel. Therefore a large number of sideband channels does not necessarily preclude the use of such an approach. The ASP weight matrix will always have N_b columns (and N_s rows) in order to be compatible with the mainband data for which it is intended. Thus, for sideband systems with $N_f > N_b$ the ASP Weight Calculation block will, as part of the algorithm, provide the necessary dimension reduction.

The sideband filter is assumed to be the principal factor in determining the frequency response for the sideband channels, as is the mainband filter for the mainband channels. As discussed in Section 2.1.4 and Section 2.1.5, the frequency response of the channels from the sensors to the input of the STAP are modeled as having a Gaussian shaped bandpass for the purposes of calculating the data covariance matrices. Thus, the exact specification of the sideband and mainband filters is not necessary for the analyses of this study; instead, the parameters which need to be specified are the center (or equivalently carrier) frequencies, f_0 and f_1, and the corresponding bandwidths. The sideband frequency offset, f_{off}, is chosen as small as possible while allowing the sideband filter to sufficiently suppress radar generated signals. The bandwidths are used in characterizing the sensor-to-sensor decorrelation of the WNJ signals as discussed in Section 2.1.5. The mainband bandwidth specified in Table 2-2 is used for the majority of the results with any exceptions specifically noted. The sideband bandwidth is chosen considerably smaller than the mainband bandwidth for two reasons: (1) minimize the cost of the sideband channels, and (2) restrict the ASP to respond to the narrowband spatial characteristics of the jammers without consuming spatial DOF to attempt to handle bandwidth effects. Bandwidth effects are better handled using joint space-time processing and therefore are left for the STAP.

The baseline ASP weight calculation algorithm of Equation 2-57 needs to be adapted for use in the SBC concept, in order to account for the characteristics of the sideband data. Further, the particular adaptation technique used will have ramifications on performance, cost, and the type of sideband beamformer (and beamsteering) used. This topic is addressed mainly in Section 3.3, but is also considered as necessary in other sections.

3.2 Sideband Data Modeling

A complete description of the target, clutter and WNJ data models for the Radar mainband was given in Section 2.1. Here, the appropriate model for the sideband data is developed in order to form a mathematical basis for further developments and analyses. In Section 2.1, space-time data was arranged by stacking spatial snapshots for a given range bin, producing an angle-Doppler transform domain. In this section, Doppler processing is not utilized. Instead, the data is described in terms of spatial snapshots as functions of time (discrete, m, or continuous, t) without any special regard to PRI boundaries. CPI boundaries, however, are still important, because the ASP weight matrix is allowed to change at CPI boundaries only (i.e. not during a CPI) for a particular range bin. However, the ASP filter may be different for different range bins. This constraint on the ASP weights is convenient for analysis and should be useful for many practical situations, but should not be considered as a general restriction on the SBC approach.

The Sideband filter is assumed to have sufficiently narrow bandwidth that the narrowband approximations used in Section 2.1 are applicable, and the data at the output of the Sideband filter can be expressed in terms of complex envelopes. Using Equation 2-16 and Equation 2-23 with appropriate modifications, the spatial snapshot data model as a function of continuous time at the output of the Sideband filter is given as

$$
x_l(t) = (L_l B_l)^H \left[(\alpha(t) \odot h_l(t)) s_s(f_{ss}(f_l)) + \sum_{l=1}^{N_r} \sum_{q=1}^{N_{ac}} (c_{lq}(t) \odot h_l(t)) s_s(f_{sc}(f_l)) \\ + \sum_{k=1}^{N_j} s_s(f_{sjk}(f_l)) \cdot (j_k(t) \odot h_l(t)) + n(t) \odot h_l(t) \right] , \quad (3\text{-}1)
$$

where $\odot$ denotes convolution, the dependence on carrier frequency is indicated, and notation has been

64

slightly modified to incorporate time functions. As is customary, convolution of a scalar function with a vector implies convolution with each element individually. As mentioned earlier, it is assumed that the sideband is separated far enough from the mainband that the Sideband filter can reduce Radar generated signals to negligible levels. Thus after sampling (at greater than the Nyquist rate), the discrete sideband data can be modeled as

$$x_1(m) = (L_1 B_1)^H \left[\sum_{k=1}^{N_J} s_s(f_{sjk}(f_1)) \bullet a_{jk}(m) + n(m) \right],$$ (3-2)

where $n(m)$ is the discrete filtered noise sequence and $a_{jk}(m)$ is the discrete filtered jammer sequence for the kth jammer. The reader is reminded that the beamsteering and beamformer transformations, L and B, are in general, functions of the carrier frequency. The sideband data is assumed to be wide-sense stationary and a spatial snapshot at any given sample has zero-mean and covariance matrix given by

$$R_{x_1} \equiv E\{x_1 x_1^H\} =$$

$$(L_1 B_1)^H \left[\sum_{k=1}^{N_J} \frac{B_1}{B} \sigma_{jk}^2 A_{jk}(B_1) \bullet s_s(f_{sjk}(f_1)) s_s(f_{sjk}(f_1))^H + \frac{B_1}{B} \sigma_n^2 I_{N_c} \right] (L_1 B_1)$$ (3-3)

where the jammer sequence correlation matrix, A_{jk}, has the same form as that given by Equation 2-25, except that the correlation function of Equation 2-22 requires the sideband bandwidth, B_1. The derivation of Equation 3-3 made use of the jammers' flat spectrum and that the mainband and sideband channel spectrums are assumed to have the same shape but different bandwidths. As expected, the jammer's JNR and AOA information is left unchanged from the mainband, although the covariance matrix is modified due to the change in carrier frequency and, to a lesser degree, due to the different bandwidths. If the mainband and sideband channel spectrum shapes are different, then Equation 3-3 would remain the same except that A_{jk} would require modification to account for the different correlation functions.

3.3 Sideband-to-Mainband Adaptive Weight Compatibility and Compensation

Calculation of the ASP weights via the Decoupled Canceler algorithm of Equation 2-57 using the sideband data covariance matrix of Equation 3-3 can result in performance degradation, because DOA information is encoded based on different carrier frequencies resulting in different normalized spatial frequencies for the jammers. To illustrate this degradation, the SINR Loss for a system employing the sideband data directly with the Decoupled Canceler algorithm is shown in Figure 3-2 and Figure 3-3. For this
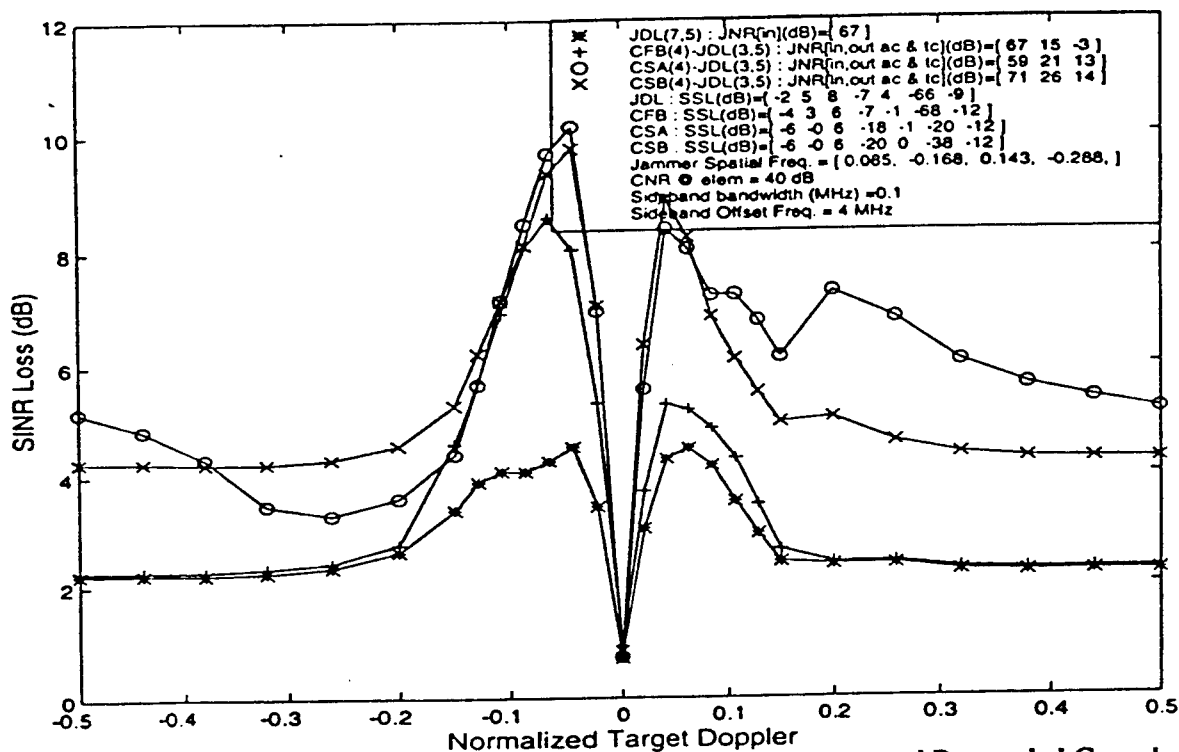

Figure 3-2: SINR Loss with Sidelobe Region Jammers using Uncompensated Decoupled Canceler: 4-Aux/Scenario A

example, steering and beamforming is accomplished using components which have the same response in the sideband as the mainband. This is not an unreasonable assumption since the beamformer being used is the Butler matrix, which is commonly implemented using wideband components, and the steering is accomplished using RF phase-shifters which can also be relatively wideband. A narrow sideband bandwidth was chosen (i.e. 0.1 MHz) and a sideband offset of 4 MHz was used. It is evident that the ASP weights generated using the sideband data directly are incompatible for jammer suppression in the mainband. The problem can be visualized by plotting the mainband ASR pattern nulls. The ASR nulls are
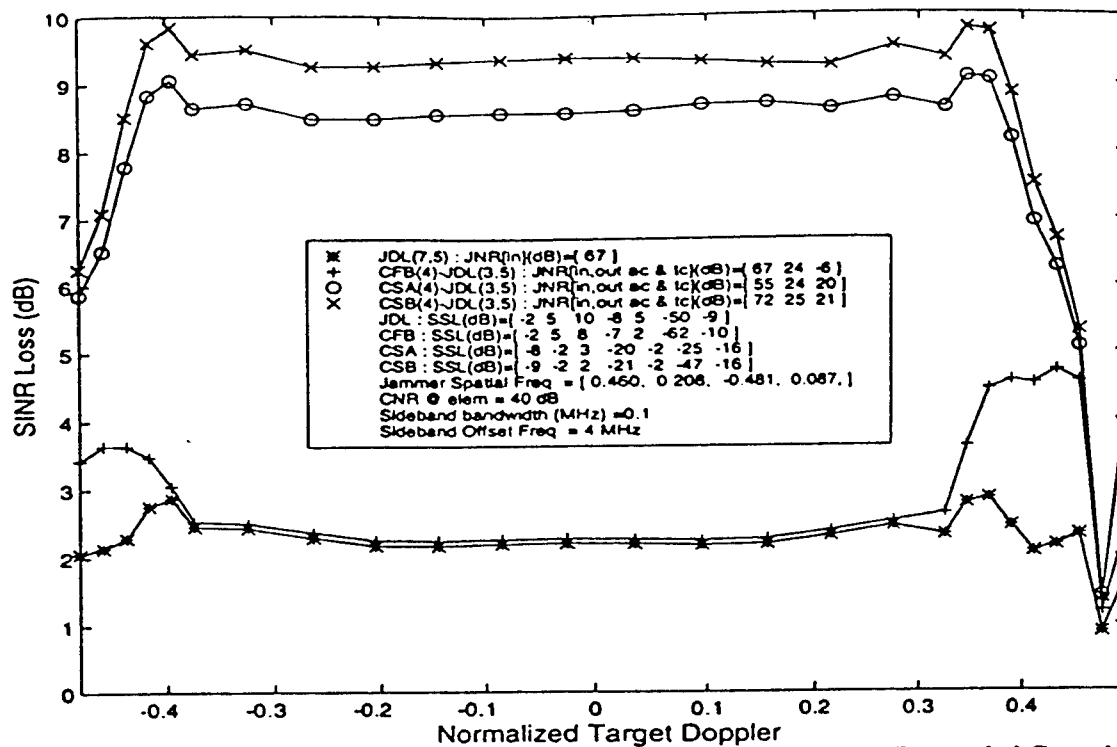
66

Figure 3-3: SINR Loss with Sidelobe Region Jammers using Uncompensated Decoupled Canceler: 4-Aux/Scenario D

located at spatial frequency locations corresponding to the jammer locations for the sideband carrier. However, for mainband data, these spatial frequencies do not correspond to the jammer locations. Therefore, the resulting nulls in the mainband are slightly shifted away from the jammer locations, and because the nulls are relatively narrow, a significant loss in jammer suppression can result. Note that the loss is small in the case of the CFB system which uses sidelobe responses to cancel the sidelobe jammers. This can be attributed to the well matched sidelobe structure of the Butler matrix resulting in wide-angle jammer suppression. This feature can be shown to disappear for even small beamformer channel errors, and therefore cannot easily be maintained in practice. The results for the CSB and CSA systems are more indicative of practical performance. In Section 3.3.1 through Section 3.3.4 various compensation techniques are described, and performance comparisons for the case of sidelobe jammers are provided.

3.3.1 Beamsteering Matrix Design

As a first step in the compensation of the sideband data, an advantageous beamsteering transformation is selected. Note that when the array is steered off broadside, the mainband and sideband beams will

shift different amounts if the phase shifters have the same response at both carriers. It is desirable to have

the mainbeam peaks at the different carriers line up as, will be demonstrated. Thus, the diagonal beamsteer-

ing transformation is chosen to be different for the two carriers (i.e. $L_1 \neq L_0$), and instead the phase shifts

at the sideband carrier are designed to provide the same steering angle as the mainband. Since the sideband

bandwidth for practical systems will typically be very narrow, it is not expected that this will cause a prob-

lem in the phase-shifter implementation. The performance improvement for a system employing this steer-

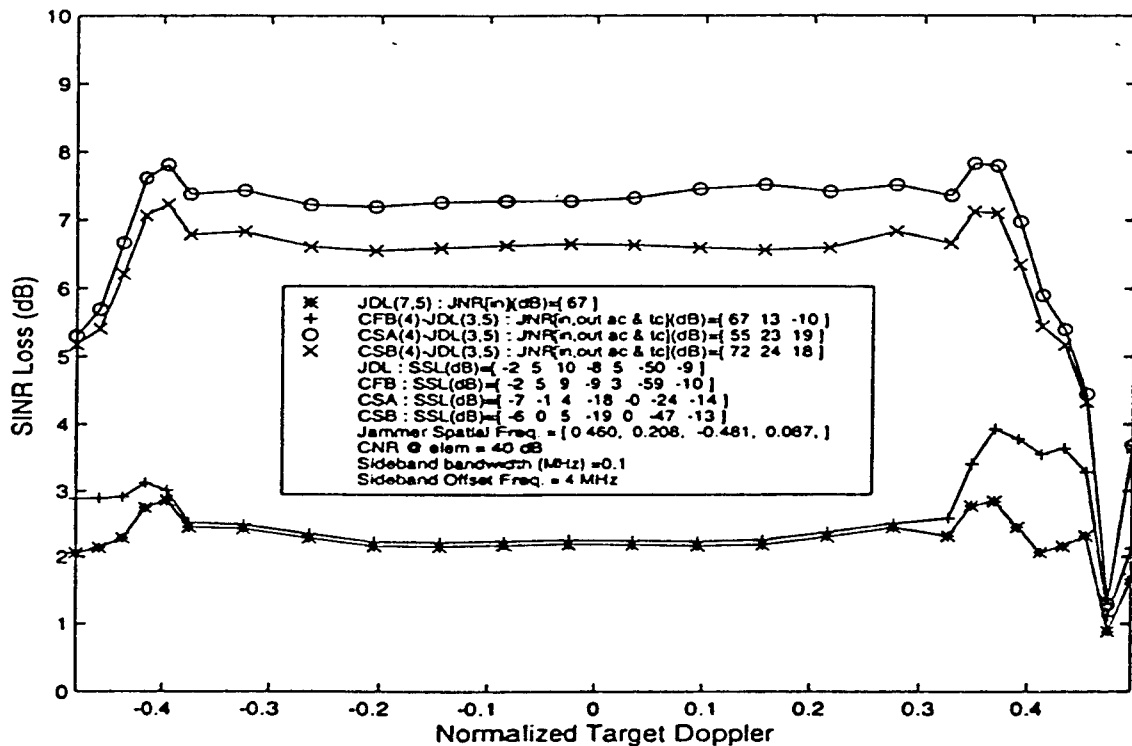ing method is demonstrated in Figure 3-4. This initial performance improvement is compounded in the

Figure 3-4: SINR Loss with Sidelobe Region Jammers using Steering Compensated Decoupled Canceler: 4-Aux/Scenario D

compensation techniques yet to be discussed since they can benefit from the use of this beamsteering

method.

3.3.2 Data Domain Compensation via Focussing Matrices

Compensation in the data domain refers to applying a transformation to the digitized sideband data

in order that the covariance matrix of the transformed jammer data approximates the mainband jammer

covariance matrix. This investigation will concentrate on using a linear transformation, F, to accomplish

68

the desired compensation. Referring to Equation 3-3, Equation 2-58, and Equation 2-24, an F is sought which satisfies

$$F^H (L_1 B_1)^H s_s(f_{sjk}(f_1)) = (L_0 B_0)^H s_s(f_{sjk}(f_0)) \qquad \text{for } k = 1, ..., N_j$$

$$\text{or} \qquad F^H (L_1 B_1)^H S_1 = (L_0 B_0)^H S_0$$

(3-4)

where the columns of the matrices, S_0 and S_1, are the spatial steering vectors for each jammer at the appropriate carrier. For simplicity, the bandwidth decorrelation effects, represented by A_{jk} in the jammer covariance matrices, have been ignored in this equation. It is easy to show that if Equation 3-4 is satisfied, then the jammer covariance matrix for the compensated sideband data will be the same as for the mainband jammer covariance (to within a scale factor) if the bandwidth decorrelation effects are neglected. This procedure of using a linear transformation to modify data from one band in order to be used for processing data from a different band is closely related to coherent signal-subspace processing which has been applied to the AOA estimation problem for wideband sources. The resulting linear transformations have been called 'focussing matrices' and this terminology is used here. Detailed information on this topic can be found in [23] and [24].

In this section, data compensation will be performed with the jammer locations, power, and number being unknown. Since a jammer can presumably be located at any angle, the focussing matrix is designed for a set of prespecified angles evenly distributed in spatial frequency (of the mainband) over the entire field of view. Thus the S_0 matrix will not correspond to the unknown jammer locations, but will instead reflect the preselected locations of calibration sources. Accordingly, the S_1 matrix corresponds to the same source angles, but will have a structure reflecting the sideband carrier. In this way, the focussing matrices are precalculated using receiver calibration data. The measurements would allow the matrix product $(LB)^H D$ to be determined for the mainband and sideband receivers. The approach used here is to use as many focussing angles, N_a, as possible while allowing Equation 3-4 to have an exact solution. Note that the matrices S_1 ($N_c x N_a$), L_1 ($N_c x N_c$), and B_1 ($N_c x N_f$) are all full rank for any practical system design. If we require $N_a \leq N_f$, then it is straight forward to show that an exact solution to Equation 3-4 is

$$F^H = (L_0B_0)^H S_0 [(L_1B_1)^H S_1]^+ . \qquad (3\text{-}5)$$

where the superscript '+' denotes Pseudo-Inverse (i.e. Moore-Penrose inverse). The solution of Equation 3-5 is exact whenever the term in '[]' brackets is full column rank. For the results of this section, the number of focussing angles, N_a, and focussing channels, N_f, are chosen to be equal to the number of sensor channels (i.e. $N_a = N_f = N_c$). If it is desired to focus at more angles than N_f (i.e. $N_a > N_f$), then it can be shown that the solution given in Equation 3-5 is also the solution to the more general problem of finding the matrix, F, which minimizes the Frobenius norm of the error matrix (i.e. the matrix difference of the two sides of Equation 3-4).

Although the matrices B_0, L_0, and L_1 have already been specified, there is some room for selecting the sideband beamformers, B_1, for each system. In order to keep the effects of sideband-to-mainband channel mismatch to a minimum, it is desirable to have the beamformers matched. Also to keep system cost down, the sideband beamformer should use as much of the mainband hardware as possible. Hence, for the CFB-JDL and the CSB-JDL systems the sideband beamformer is chosen to be a full Butler matrix, whereas for the CSA-JDL the same auxiliary channels are used as well as the JDL beams, plus enough additional Butler beams (adjacent to the JDL beams) in order to attain N_c sideband channels. Performance results for this technique using a fixed set of calibration source locations is given in Figure 3-5. Note that although the CSB-JDL and CSA-JDL systems show improvement, the CFB-JDL suffers some degradation in the central doppler region. The degradation can be attributed to the calibration source locations not being aligned with the Butler beam peaks when the array is steered off broadside and not aligned with a calibration angle. Another troublesome feature of this technique is that the focussing matrices are functions of the array steering angle, and therefore a set of focussing matrices are needed to cover a range of steering angles. Both of these undesirable attributes can be abrogated by modifying the calibration method as explained below.

As an alternative to the Focussing calibration discussed above, consider the following. Instead of requiring a fixed set of calibration angles, the angle locations are shifted in unison as the array steering angle changes such that the central source is kept aligned with the central target beam (i.e. mainbeam). For broadside steering the sources are chosen as before, which are aligned with the peaks of the Butler beams
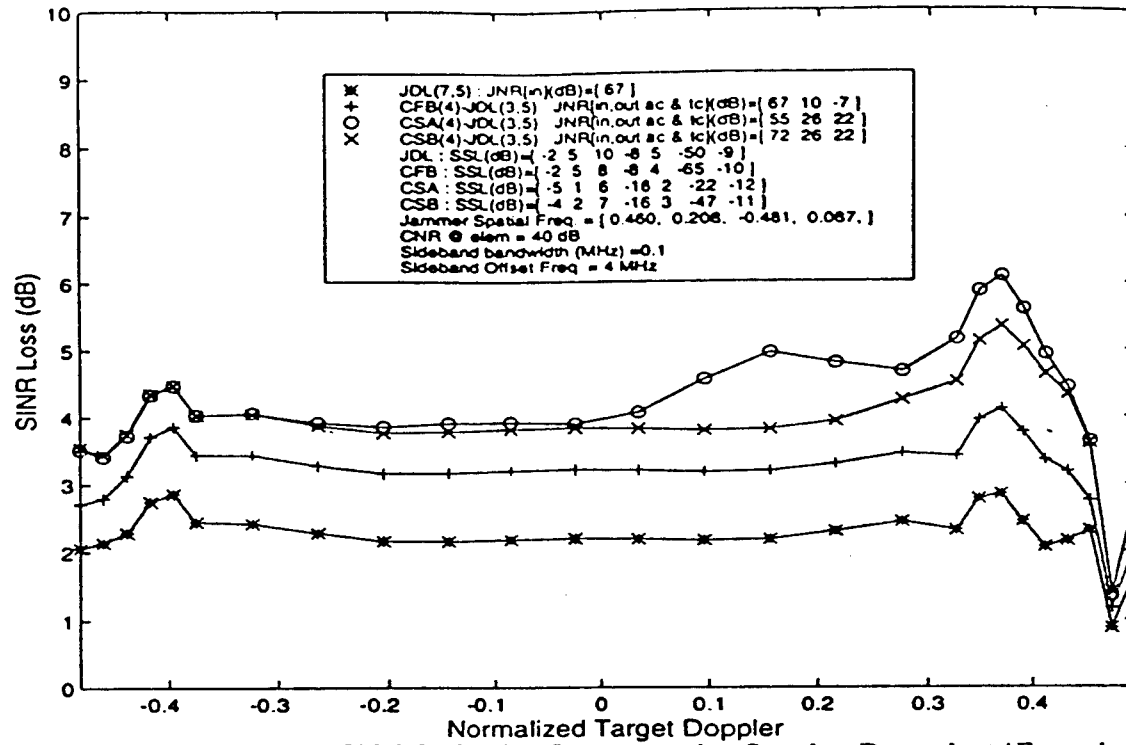
70

Figure 3-5: SINR Loss with Sidelobe Region Jammers using Steering-Dependent / Focussing-Compensated Decoupled Canceler: 4-Aux/Scenario D

with $N_a=N_c=N_f$. Now making use of the beamsteering definition of Section 3.3.1, the fixed steering matrices of Equation 3-4, S_0 and S_1, are replaced by steering matrices which are a function of the steering angle,

$$D_0 = L_0 S_0 \qquad \text{and} \qquad D_1 = L_1 S_1.$$ (3-6)

and which keep the mainband and sideband mainbeams aligned. Substituting these steering matrices, D_0 and D_1, for S_0 and S_1 in Equation 3-4, and using the unitary feature of the beamsteering matrix, the focussing matrix equation to be solved becomes

$$F^H B_1^H S_1 = B_0^H S_0.$$ (3-7)

which is now independent of the array steering angle and reflects a broadside steering condition. Clearly, the solution to Equation 3-7 has the same form as Equation 3-5, but with the beamsteering matrices absent.

The implication is that as long as the beamsteering definition of Section 3.3.1 can be implemented accurately, only a single focussing matrix needs to be calculated using only the fixed broadside set of calibration sources. Performance results given in Figure 3-6 using this method for calculation of the focussing matrix
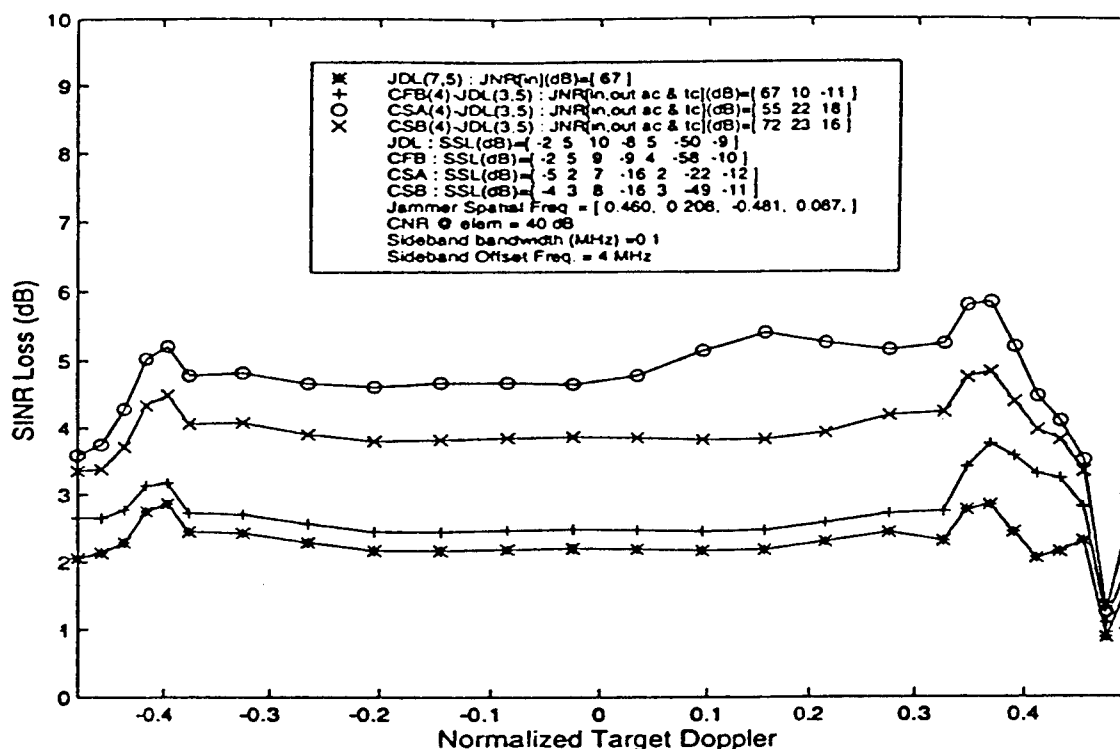

Figure 3-6: SINR Loss with Sidelobe Region Jammers using Steering-Independent / Focussing-Compensated Decoupled Canceler: 4-Aux/Scenario D

shows an improved performance for the CFB-JDL alluded to above. The CSB-JDL system also shows slight improvement, whereas the CSA-JDL system shows minor degradation at some dopplers. Focussing at the Butler peaks evidently is beneficial to systems employing butler beams for jammer suppression, while a system using omni-directional auxiliaries does not appear to benefit.

3.3.3 Spectral Analysis Aided Focussing Compensation

It is of interest to determine how much the data domain focussing method can be improved if the focussing matrix is calculated adaptively, after spatial spectral analysis has located the jammers. There are many good techniques available in the literature for AOA processing of narrowband data (e.g. see [25] for element space and [26] for beamspace techniques), and it is assumed here that perfect estimates are available. The focussing matrix is designed using the steering-independent method and focusing at the peaks of

the clutter/target beams and at the jammer locations. Thus, the S_0 used in Equation 3-7 is generated using a steering matrix, D_0, which has N_s columns corresponding to the clutter beams, and N_j additional columns corresponding to the jammer locations transforming according to Equation 3-6. As expected, the performance results are quite good as shown in Figure 3-7 and Figure 3-8. It should be noted that in the literature,
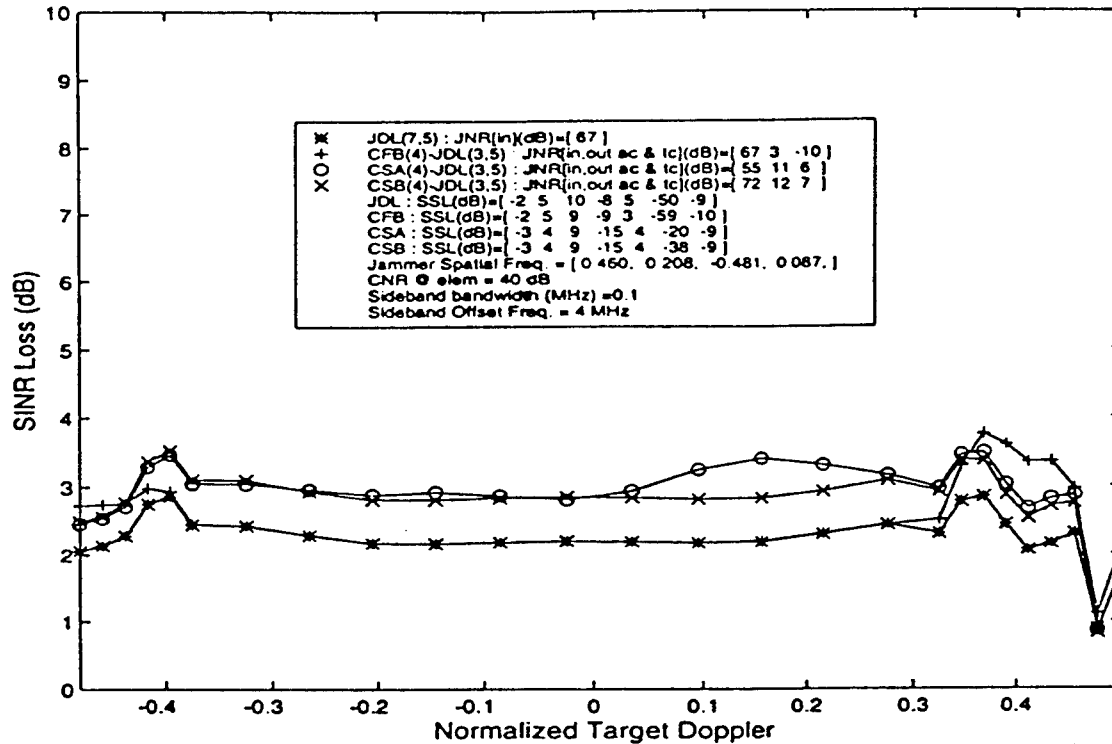

Figure 3-7: SINR Loss with Sidelobe Region Jammers using Spectrally-Assisted Focussing-Compensated Decoupled Canceler: 4-Aux/Scenario D

when a transformation precedes the AOA algorithm it often is required to be unitary in order to leave the noise subspace unperturbed. This is not a problem for the CFB-JDL and CSB-JDL, but an alternative sideband beamformer (e.g. the Identity implying no beamforming) may be needed for the CSA-JDL system.

Some apparent drawbacks of AOA assisted focussing are (1) significant amount of additional computation for the AOA processing, and (2) many more calibration points are required to achieve full potential. However, once the AOA information is obtained, new opportunities for performance improvement are available. For instance, AOA information can identify clutter and signal region jammers, thereby allowing dynamic allocation of spatial DOF for those interferers (e.g. force the ASP to ignore them and increase the spatial DOF out of the ASP in order to process these jammers in the STAP).
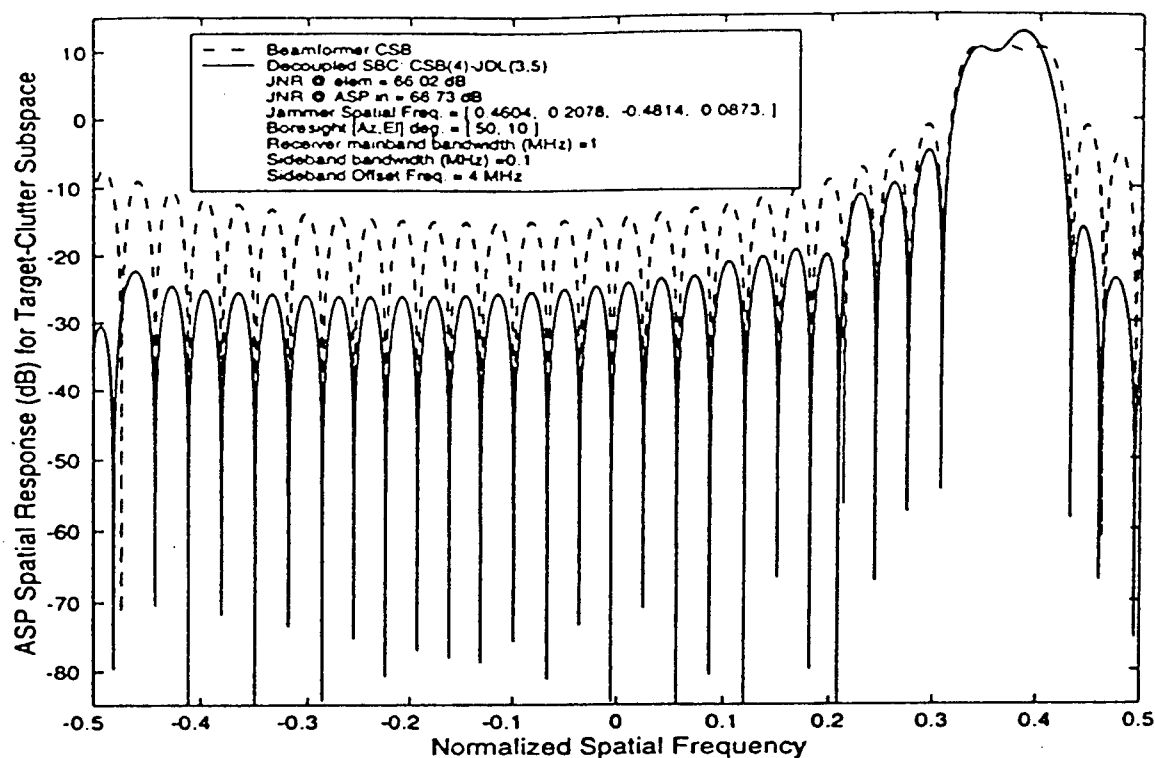
Figure 3-8: CSB-JDL ASR Pattern with Sidelobe Region Jammers using Spectrally-Assisted Focussing-Compensated Decoupled Canceler: 4-Aux/Scenario D

3.3.4 Data Domain Compensation via Dual-Sideband Combining

The next form of compensation to be discussed attempts to shift and/or widen the ASP null by combining two symmetrically located sidebands (with respect to the mainband) prior to weight calculation. The approach used here is to have both sideband channels designed the same way with regard to their respective carrier frequencies and to minimize the duplication of hardware. The beamsteering unit is designed as in Section 3.3.1, but now having an additional phase shift specification for the added sideband. The beamformers are assumed wideband enough to have the same response for both sidebands. A simple modification to the SBC block diagram of Figure 3-1 can be used to obtain the combined sideband WNJ signals using a single sideband filter / down-conversion / A/D chain. Prior to the sideband filter, the signals are down-converted so that the mainband is at baseband. Note, this is tantamount to using the mainband data just prior to the Mainband Filter block, because the beamformers are designed to be the same. Then a passband sideband filter is applied, followed by down-conversion using the sideband carrier offset frequency, f_{off}, and finally A/D conversion. The beamformers do not need to be the same to use this technique,

however, more hardware will be required, and the system will be more susceptible to mismatch between the sideband and mainband jammer data.

The dual-sideband data covariance matrix that is being generated is seen to be the summation of two covariance matrices which have the same form given in Equation 3-3, but corresponding to different carrier frequencies. In general then, it is assumed the data from each sideband is uncorrelated, and the resulting covariance matrix is

$$R_{x_d} \equiv E\{x_d x_d^H\} = R_{x_1} + R_{x_2}$$

$$= (L_1 B_1)^H \left[\sum_{k=1}^{N_j} \frac{B_1}{B} \sigma_{jk}^2 A_{jk}(B_1) \bullet s_s(f_{sjk}(f_1)) s_s(f_{sjk}(f_1))^H + \frac{B_1}{B} \sigma_n^2 I_{N_c} \right] (L_1 B_1) +$$

$$(L_2 B_2)^H \left[\sum_{k=1}^{N_j} \frac{B_2}{B} \sigma_{jk}^2 A_{jk}(B_2) \bullet s_s(f_{sjk}(f_2)) s_s(f_{sjk}(f_2))^H + \frac{B_2}{B} \sigma_n^2 I_{N_c} \right] (L_2 B_2)$$

(3-8)

However for the specific systems considered here, by design the sideband bandwidths, beamformers and carrier frequencies are given by

$$B_1 = B_2, \qquad B_1 = B_2, \qquad f_1 = f_0 + f_{off}, \qquad \text{and} \qquad f_2 = f_0 - f_{off}. \qquad (3-9)$$

Performance results after applying this dual sideband model to each of the baseline systems is given in Figure 3-9. Comparing these results with those of Figure 3-7 show that the Spectrally-Assisted Focussing Matrix produces slightly better SINR performance for the CSB-JDL and CSA-JDL systems even though the Dual-Sideband approach provides better jammer suppression as indicated by the JNR levels given in the plot legends. This difference is pointed out to illustrate that in addition to the jammer suppression, STAP performance is also dictated by the clutter subspace at the output of the ASP. The Dual-Sideband approach causes more perturbation to the clutter subspace in an effort to generate a wide null as can be seen by comparing the ASR patterns in Figure 3-10 and Figure 3-8 for example. Note that the clutter subspace width has been decreased. For systems where the sidebands are close together this may not be a problem. However, as the sidebands move apart the clutter subspace will continue to degrade. In this case a tech-
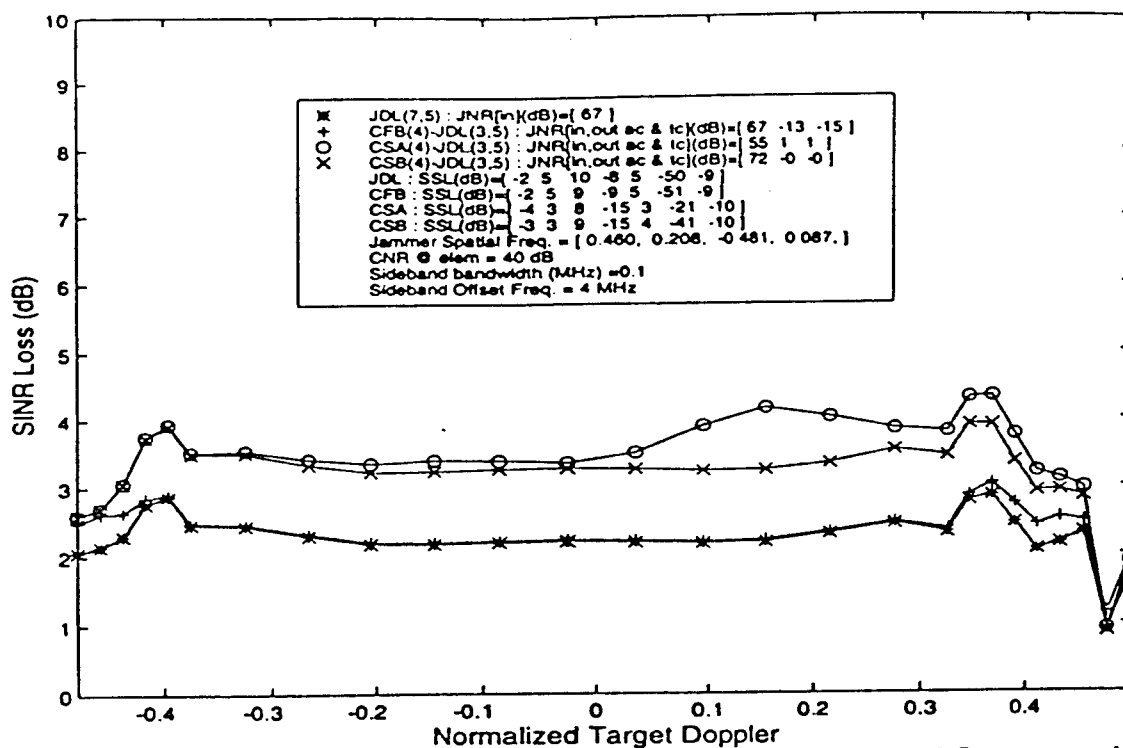
75

Figure 3-9: SINR Loss with Sidelobe Region Jammers using Dual-Sideband Compensated Decoupled Canceler: 4-Aux/Scenario D

nique such as Space-Range processing (comparable to the so-called Frost array which uses tapped-delay lines, see e.g. [27]) may be used in order to generate a wide null without degrading the clutter subspace. This topic is left for future investigation.

3.3.5 Weight Domain Compensation via Double-Sideband Weight Averaging

In this section a different compensation technique utilizing two sidebands, called Double-Sideband Weight Average Compensation (DWAC), is discussed. The fundamental concept is to generate ASP weight vectors separately for each sideband and then combine them to produce a weight vector appropriate for jammer cancellation in the mainband. Digitized data sets for two sidebands located symmetrically about the radar mainband are generated. ASP weights for each sideband produce nulls on opposing sides of the desired mainband location. The intent is to combine them in a way such that the spatial responses combine to place the null at the desired location as in the Dual-Sideband compensation method of Section 3.3.4, but without the additional bandwidth effects inherent in that approach. Of course, the data sets could be generated by using two separate sideband receivers constructed as in Figure 3-1, but more efficient ways which
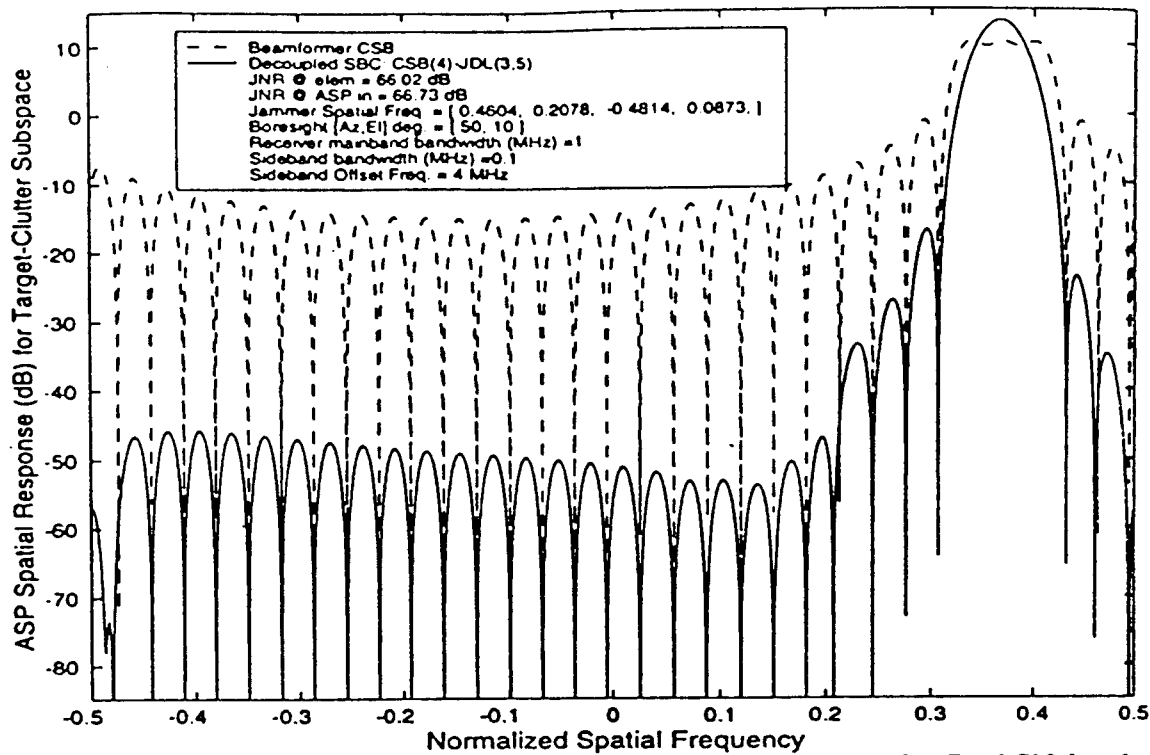
Figure 3-10: CSB-JDL ASR Pattern with Sidelobe Region Jammers using Dual-Sideband Compensated Decoupled Canceler: 4-Aux/Scenario D

use the same hardware for both channels can easily be developed. For instance, the down-conversion stage before the Sideband Filter can alternately use two opposing sideband offset frequencies, $\pm f_{off}$, thereby generating digitized data from alternating sidebands. Thus the DWAC method averages the weight vectors generated from the two sideband data sets using the same cancelation algorithms. Thus in the case of the Decoupled Canceler of Equation 2-57, sample covariance matrix estimates (corresponding to Equation 3-3) for each data set are calculated and the DWAC compensated weight matrix is given by

$$ W = \frac{1}{2} \cdot (W_1 + W_2) . \tag{3-10} $$

Note that the gain constraint of the DC is preserved since both W_1 and W_2 satisfy the same constraint. In general, one should verify that the weight vector averaging makes sense for the cancelation algorithm being used in terms of satisfying any constraints and interference suppression. For the cancelation algorithms considered in this investigation, it is found that the desired null-shift is indeed obtained by this averaging

77

technique. Clearly, the scale factor of 1/2 is superfluous, but left here to illustrate the weight balancing being proposed. Very acceptable performance is obtained from this simple technique as evidenced by the JNR and SINR Loss results given in and Figure 3-11. It is also instructive to look at the JNR residual as a
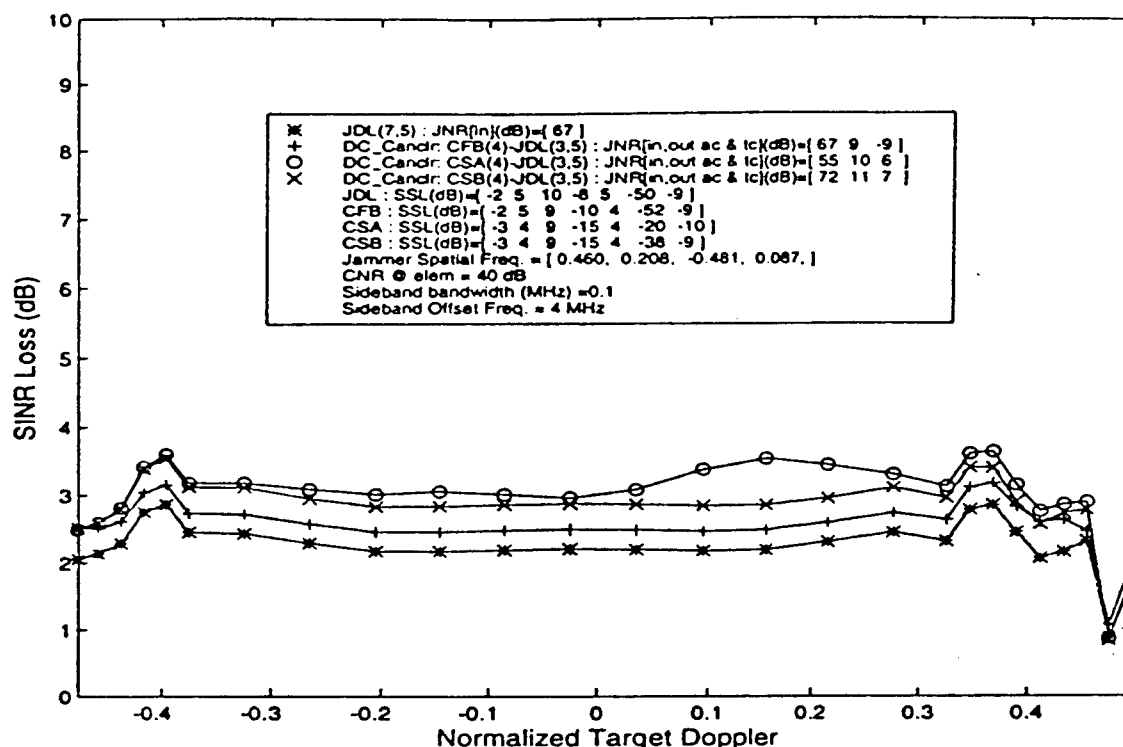

Figure 3-11: SINR Loss for Sidelobe Region Jammers using Double-Sideband Average Compensated Decoupled Canceler: 4-Aux/Scenario D

function of sideband offset frequency given in Figure 3-12. The Double-Sideband Averaging provides fairly uniform performance over a ±5 MHz offset range. Although not shown here, the Focussing matrix approaches (with the exception of the spectrally-assisted version) do not exhibit this uniform JNR performance, but rather have a minimum at zero offset frequency, and can degrade rather quickly away from zero offset. In a sense then, the double-sideband method can be regarded as having larger "compensation bandwidth".

3.3.6 Summary of Sideband Compensation Techniques

In this section, a sideband method was described for acquisition of jammer-only secondary data, along with several methods for using the sideband data to adaptively generate spatial weights for the suppression of mainband jamming. The compensation techniques considered belong to two general categories:
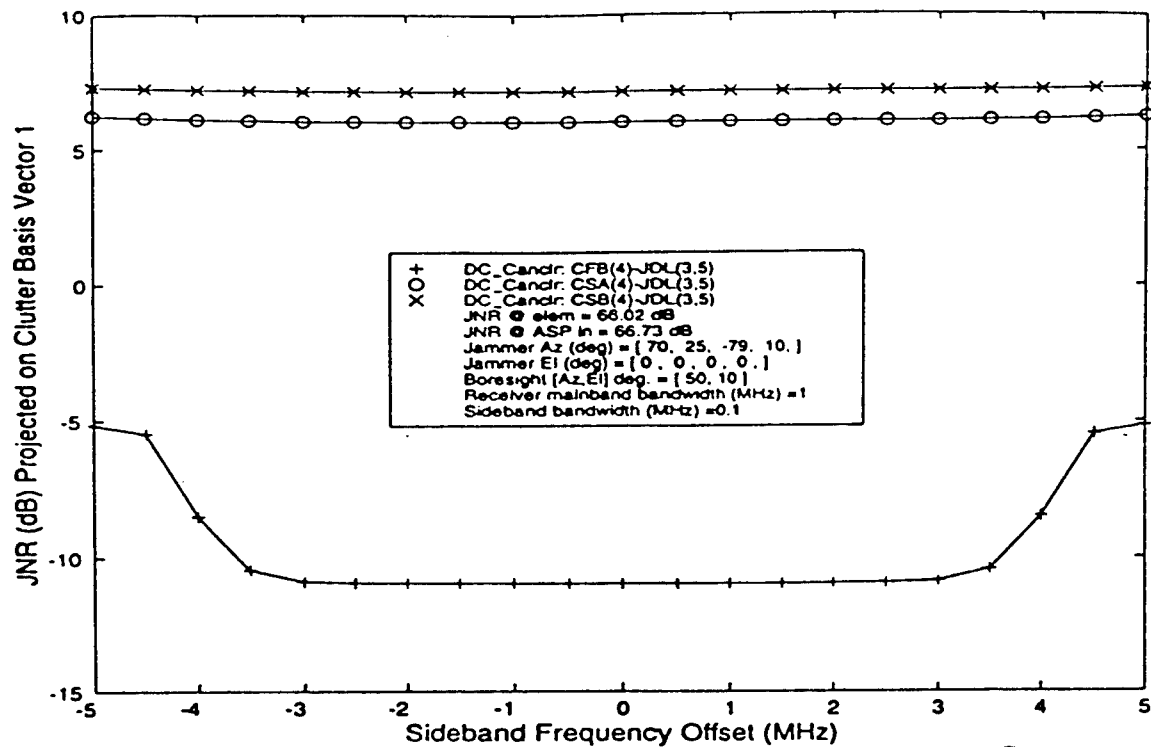
Figure 3-12: JNR for Sidelobe Region Jammers using Double-Sideband Average Compensated Decoupled Canceler: 4-Aux/Scenario D

(1) data domain compensation whereby the sideband data is transformed to take on the characteristics indicative of the mainband interference prior to weight calculation, and (2) weight domain compensation where spatial weight vectors generated from uncompensated sideband data are modified to provide the desired interference cancelation in the mainband. Among the data domain techniques, the spectrally-assisted focussing matrix approach shows the best performance potential. However, because of it's additional requirement for pre-location of the jammers, the steering independent focussing matrix approach with minor additional SINR Loss may be preferred. The Dual-Sideband approach also shows acceptable performance, but in systems employing two sidebands the Double-Sideband Averaging method may be preferred since it exhibits slightly better performance and does not consume spatial DOF to generate wide spatial nulls. However, it should be noted that wide spatial nulls can provide protection against mainband-to-sideband channel mismatch, but this presupposes the use of space-range processing, which is beyond the scope of this report.

4 Summary

4.1 Conclusions

Several cascaded architectures have been proposed as an implementation of the SAPS concept. The performance results for these cascaded systems compare favorably with the simultaneous STAP approaches, and verify their viability in future radar designs. A key component of the WNJ pre-suppression concept is the acquisition of jammer-only secondary data. The sideband technique described herein has the unique advantage over other techniques that it allows collection of secondary data during any portion of an RPI. Sideband compensation methods were proposed and analyzed showing that ample jammer suppression can be achieved in the mainband while using the sideband secondary data for weight calculation.

4.2 Further Work

The work done so far in the area of jammer pre-suppression in conjunction with STAP has only scratched the surface. More investigation into dealing with jammers in the clutter and target regions as well as other sideband compensation methods is prudent. Also, studying the effects of imperfect beamformers (i.e. channel errors) and mainband-to-sideband channel mismatch is of great practical interest. A well defined wholistic approach to the design of "optimal" beamformer transformations is another possible area to improve the proposed systems. Perhaps more importantly, is the expansion of the divide-and-conquer concept for handling interference generated by sources with dissimilar characteristics. When faced with real-world problems which can often present multiple forms of interference, being able to focus ones resources on each separately can be very advantageous. One example, for which the sideband concept described here may provide a skillful solution, is the problem of jammer multipath (also known as "hot" clutter). Sideband data could be used to supply a Space-Range Processor (SRP) with a sufficient amount of secondary data to allow the application of a sizeable adaptive space-range algorithm.

Appendices

Appendix A: Optimum Receiver for Random Target Amplitude Model

In this appendix, a sufficient statistic for the binary hypothesis test of Section 2.2.1 is generated by algebraic manipulation of the likelihood ratio. The resultant statistic is the optimal Neyman-Pearson receiver under the assumed Gaussian data distribution models. The data model for the $p \times 1$ vector, x, is given by

$$x = \alpha s + n \quad \text{where} \quad n \sim CN(0, R) \quad \text{and under each hypothesis}$$
$$H_0 : \alpha = 0 \quad \text{and} \quad H_1 : \alpha \sim CN(0, \sigma^2) \tag{A1}$$

where "$\sim$" is read "is distributed as" and "CN" represents the complex normal distribution with probability density function (see e.g. [19])

$$p(x | m, R) = \pi^{-p} |R|^{-1} \exp\left[-(x - m)^H R^{-1} (x - m) \right]. \tag{A2}$$

It is composed of a target vector with random complex amplitude, α, and specified structure, s, embedded in additive zero-mean (circularly) complex Gaussian interference. It is assumed that the interference, n, and the target amplitude are independently distributed. The data has zero-mean under both hypotheses, but the covariance matrix is different with

$$H_0 : E\{x x^H\} = R \quad \text{and} \quad H_1 : E\{x x^H\} = R + \sigma^2 s s^H \equiv R_1. \tag{A3}$$

Under hypothesis H_0, the data obviously has the same distribution as the interference. Under H_1 it is easy to show that the data is also CN distributed as follows. Since the interference is CN, any linear combination is also CN (see [19] p. 375). Therefore, by the independence of α and n, for any $p \times 1$ vector, a, by Proposition 9.15 of [19]

$$a^H x \sim CN(0, a^H R_1 a).$$

(A4)

Thus by Definition 9.2 of [19] the data is distributed as

$$H_1 : x \sim CN(0, R_1).$$

(A5)

Now the likelihood ratio statistic is given by

$$l \equiv \frac{P_{x|H_1}}{P_{x|H_0}} = \frac{|R| \exp [-x^H R_1^{-1} x]}{|R_1| \exp [-x^H R^{-1} x]}.$$

(A6)

By taking the logarithm of l and ignoring terms which do not depend on the data, an equivalent statistic is

$$\eta' = x^H (R^{-1} - R_1^{-1}) x.$$

(A7)

Using the matrix inversion lemma (a general form can be found in [20]) and Equation A3 it is found that

$$R_1^{-1} = R^{-1} - \frac{R^{-1} s s^H R^{-1}}{\sigma^2 + s^H R^{-1} s}$$

(A8)

from which the statistic can be written as

$$\eta' = \frac{x^H R^{-1} s s^H R^{-1} x}{\sigma^2 + s^H R^{-1} s}.$$

(A9)

Now the likelihood ratio decision rule can be written as

$$\eta = \left| s^H R^{-1} x \right|^2 \underset{H_0}{\overset{H_1}{\gtrless}} \eta_0$$

(A10)

which is seen to involve colored-noise matched filtering of the input data.

Appendix B: Simplification of the GLR Conditional Detection Probability

In this appendix, the conditional detection probability formula for the GLR detector given by Equation 2-37 is simplified. The formula for $P_{d|\rho}$ is rewritten here as

$$P_{d|\rho} = 1 - P_f \cdot \sum_{j=1}^{M} \binom{M}{j} r^j \cdot \sum_{m=0}^{j-1} \frac{q^m}{[q+1]^{m+1}} \tag{B1}$$

where the following substitutions have been used;

$$q = \rho \beta_T (1 - \eta_{oT}) \ , \ r = \frac{\eta_{oT}}{1 - \eta_{oT}} \ , \text{ and } M = K - N_T + 1 \ . \tag{B2}$$

The second summation in Equation B1 can be put in the form of a geometric progression. Then using the closed form expression given in [21] p. 1 yields

$$\sum_{m=0}^{j-1} \frac{q^m}{[q+1]^{m+1}} = \left(\frac{1}{q+1}\right) \sum_{m=1}^{j} \left(\frac{q}{q+1}\right)^{m-1} = \left(\frac{1}{q+1}\right) \cdot \frac{\left(\frac{q}{q+1}\right)^j - 1}{\left(\frac{q}{q+1}\right) - 1} = 1 - \left(\frac{q}{q+1}\right)^j \ . \tag{B3}$$

Substituting the result of Equation B3 into Equation B1 it is seen that $P_{d|\rho}$ can be written as the sum of two finite binomial power series. Using the closed form expression for a binomial power series given by [21] p. 21 produces the formula

$$\sum_{j=1}^{M} \binom{M}{j} r^j = \sum_{j=0}^{M} \binom{M}{j} r^j - 1 = (1+r)^M - 1 \ . \tag{B4}$$

Substituting Equation B3 and Equation B4 into Equation B1 results in the following simplification for $P_{d|\rho}$

$$P_{d|\rho} = 1 - P_f \cdot \sum_{j=1}^{M} \binom{M}{j} r^j \cdot \left[1 - \left(\frac{q}{q+1} \right)^j \right]$$

$$= 1 - P_f \cdot \left\{ (1+r)^M - 1 - \left[\left(1 + \frac{rq}{q+1} \right)^M - 1 \right] \right\} \cdot \tag{B5}$$

$$= P_f \cdot \left[\frac{\rho \beta_T + 1}{\rho \beta_T (1 - \eta_{oT}) + 1} \right]^M$$

Now, using the relationship between the threshold and P_f given by Equation 2-35 produces the desired final form for the conditional detection probability

$$P_{d|\rho} = \left[\frac{\rho \beta_T + 1}{\rho \beta_T + P_f^{-1/M}} \right]^M . \tag{B6}$$

Appendix C: Closed Form Expression for the Integrated System Response

A closed form expression for the integrated System Response, $\overline{A}_T$ defined by Equation 2-54 is derived for the case of data uniformly sampled in space and time. Under these conditions, the expressions for the spatial and temporal steering vectors, s_t and s_s, of Equation 3-11 are appropriate. Using Equation 2-49, Equation 2-54 can be written as

$$\overline{A}_T(\Delta f_t, \Delta f_s; f_{ts}, f_{ss}) = \frac{\underline{w}_{oT}^H T^H \left\{ \displaystyle\int_{f_{ts} - \Delta f_t/2}^{f_{ts} + \Delta f_t/2} \int_{f_{ss} - \Delta f_s/2}^{f_{ss} + \Delta f_s/2} (s_t s_t^H) \otimes (s_s s_s^H) \, df_s df_t \right\} T \underline{w}_{oT}}{\underline{w}_{oT}^H T^S_T} . \tag{C1}$$

where the terms which are not a function of the spatial or Doppler frequencies can be taken outside the integral. Furthermore, using the properties of the Kronecker product and separating sole functions of spatial and Doppler frequencies yields the following formula

$$\overline{\underline{A}_T}(\Delta f_t, \Delta f_s; f_{ts}, f_{ss}) = \cfrac{\underline{w}_{oT}^H \underline{T}^H \left\{ \int\limits_{f_{ts} - \Delta f_t/2}^{f_{ts} + \Delta f_t/2} (s_t s_t^H)\, df_t \otimes \int\limits_{f_{ss} - \Delta f_s/2}^{f_{ss} + \Delta f_s/2} (s_s s_s^H)\, df_s \right\} \underline{T}\,\underline{w}_{oT}}{\underline{w}_{oT}^H \underline{S}_T} . \tag{C2}$$

Notice that each integral is of the same form with differences only in the parameters of the integrand and the limits of integration. Also note that the integrands are Hermitian-Toeplitz matrices so that only the elements of the first column need to be integrated. For convenience, rewrite Equation C2 as

$$\overline{\underline{A}_T}(\Delta f_t, \Delta f_s; f_{ts}, f_{ss}) = \frac{\underline{w}_{oT}^H \underline{T}^H \left\{ A_t \otimes A_s \right\} \underline{T}\,\underline{w}_{oT}}{\underline{w}_{oT}^H \underline{S}_T} \tag{C3}$$

where the corresponding definitions for the matrix integrals, A_t and A_s, are obvious. The elements of A_t and A_s can be evaluated using elementary integration formulas. The resulting expressions are

$$A_s = \text{Toeplitz}\,(s_{ss} \bullet d_s) \text{ and } A_t = \text{Toeplitz}\,(s_{st} \bullet d_t)$$
where the elements of d_s are $d_s(n) = (\Delta f_s)\,\text{sinc}\,(n\Delta f_s) \qquad, n = 0, ..., N_c - 1 .$ \hfill (C4)
and similarly for d_t, $d_t(n) = (\Delta f_t)\,\text{sinc}\,(n\Delta f_t) \qquad, n = 0, ..., N_t - 1$

The function Toeplitz() represents a Hermitian-Toeplitz matrix with the first column given by it's argument, and the sinc() function is defined in the usual manner as

$$\text{sinc}\,(x) \equiv \sin\,(\pi x)\,/\,\pi x . \tag{C5}$$

The heavy dot, '$\bullet$', represents a matrix Hadamard product (i.e. element-by-element product).

References

[1] R. Klemm, "Antenna design for adaptive airborne MTI", Proceedings of the IEE International Radar Conference, pp. 296-299, Brighton Conference Centre, UK, October 12-13, 1992.

[2] R. Klemm, "Adaptive air- and spaceborne MTI under jamming conditions", Proc. of IEEE National Radar Conference, pp. 167-172, Boston, MA, April 1993.

[3] D.F. Marshall, "A two step adaptive interference nulling algorithm for use with airborne sensor arrays", Proc. 7th SP Workshop on SSAP, Quebec City, Canada, June 26-29, 1994.

[4] E. Brookner and J. Howell, "Adaptive-adaptive array processing", Proceedings of the IEEE, vol. 74, no. 4, April 1986.

[5] W.F. Gabriel, "Using spectral estimation techniques in adaptive processing antenna systems", IEEE Trans. on Antennas and Propagation, vol. AP-34, no. 3, March 1986.

[6] I.S. Reed, J. D. Mallet, and L. E. Brennan, "Rapid convergence rate in adaptive arrays", IEEE Trans. on Aerospace and Electronic Systems, vol. AES-10, no. 6, pp. 853-863, November 1974.

[7] H. Wang and L. Cai, "On adaptive spatial-temporal processing for airborne surveillance radar systems", IEEE Trans. on Aerospace and Electronic Systems, vol. AES-30, no. 3, pp. 660-670, July 1994.

[8] H. Wang and L. Cai, "A localized adaptive MTD processor", IEEE Trans. on Aerospace and Electronic Systems, vol. AES-27, no. 3, pp. 532-538, May 1991.

[9] J. Ward, *Space-Time Adaptive Processing for Airborne Radar*, MIT/LL Internal Technical Report #1015, Dec. 1994.

[10] L. C. Godara and A. Cantoni, "Uniqueness and linear independence of steering vectors in array space", Journal of the Acoustical Society of America, 70(2), Aug. 1981.

[11] D. K. Barton, "Land clutter models for radar design and analysis", Proc. IEEE, vol. 73, no. 3, pp. 198-204.

[12] H. L. VanTrees, Detection, Estimation, and Modulation Theory - Part I, John Wiley & Sons, Inc., New York, 1968.

[13] J. Butler, *Multiple Beam Antennas*, Sanders Assoc. Internal Memo RF 3849, Jan. 1960.

[14] L.E. Brennan and I.S. Reed, "Theory of adaptive radar", IEEE Trans. on Aerospace and Electronic Systems, vol. AES-9, no. 2, pp. 237-252, March 1973.

[15] E.J.Kelly, "An adaptive detection algorithm", IEEE Trans. on Aerospace and Electronic Systems, vol. AES-22, no. 1, pp.115-127, March 1986.

[16] H. Park, *Adaptive Radar Target Detection Algorithms in Space-Time and Polarization Domains*, Syracuse University Ph.D. Dissertation, pp. 16-24, Dec. 1993.

[17] R.A. Johnson and D.W. Wichern, Applied Multivariate Statistical Analysis, 3rd Ed., Prentice Hall, Inc., 1992.

[18] E.J.Kelly, "Performance of an adaptive detection algorithm; rejection of unwanted signals", IEEE Trans. on Aerospace and Electronic Systems, vol. AES-25, no. 2, pp.122-133, March 1989.

[19] M. L. Eaton, Multivariate Statistics: A Vector Space Approach, John Wiley & Sons, Inc., 1983.

[20] W. L. Brogan, Modern Control Theory, 3rd Ed., Prentice Hall, Inc., 1991.

[21] I.S. Gradshteyn and I.M. Ryzhik, Table of Integrals, Series, and Products, ed. by Alan Jeffrey, Academic Press, Inc., 1980.

[22] K. Gerlach, "Further considerations of Adaptive canceller and pulse compression interactions", IEEE Trans. on Aerospace and Electronic Systems, vol. AES-31, no. 1, pp.310-319, January 1995.

[23] H. Wang and M. Kaveh. "Coherent Signal-Subspace Processing for the detection and Estimation of Angles of Arrival of Multiple Wide-Band Sources", IEEE Trans. on Acoustics, Speech, and Signal Processing, vol. 33, No. 4, August 1985.

[24] H. Hung and M. Kaveh. "Focussing Matrices for Coherent Signal-Subspace Processing", IEEE Trans. on Acoustics, Speech, and Signal Processing, vol. 36, No. 8, August 1988.

[25] R.O. Schmidt, "Multiple Emitter Location and Signal Parameter Estimation", IEEE Trans. on Antennas and Propagation, vol. AP-34, no. 3, March 1986.

[26] M.D. Zoltowski, et. al., "Beamspace Root-MUSIC", IEEE Trans. on Signal Processing, vol. 41, no. 1, January 1993.

[27] L.J. Griffiths and C.W. Jim, "An Alternative Approach to Linearly Constrained Adaptive Beamforming", IEEE Trans. on Antennas and Propagation, vol. AP-30, no. 1, January 1982.

AIR FORCE RESEARCH LABORATORY
ATTN: DAVID FERRIS
32 BROOKS ROAD
ROME, NEW YORK 13441-4114

RESEARCH ASSOC FOR DEFENSE CONV INC
10002 HILLSIDE TERRACE
MARCY, NEW YORK 13403

AFRL/IFOIL
TECHNICAL LIBRARY
26 ELECTRONIC PKY
ROME NY 13441-4514

ATTENTION: DTIC-OCC
DEFENSE TECHNICAL INFO CENTER
8725 JOHN J. KINGMAN ROAD, STE 0944
FT. BELVOIR, VA 22060-6218

MISSION
OF
AFRL/INFORMATION DIRECTORATE (IF)

The advancement and application of information systems science and
technology for aerospace command and control and its transition to air,
space, and ground systems to meet customer needs in the areas of Global
Awareness, Dynamic Planning and Execution, and Global Information
Exchange is the focus of this AFRL organization. The directorate's areas
of investigation include a broad spectrum of information and fusion,
communication, collaborative environment and modeling and simulation,
defensive information warfare, and intelligent information systems
technologies.